A Study of the Aqueous Phase Processing of Organic Aerosols through Stable Isotope Analysis

by

Denise Napolitano

A Dissertation Presented in Partial Fulfillment
of the Requirements for the Degree
Doctor of Philosophy

Approved June 2018 by the
Graduate Supervisory Committee:

Pierre Herckes, Chair
Matthew Fraser
Everett Shock

ARIZONA STATE UNIVERSITY

August 2018

ABSTRACT

Atmospheric particulate matter (PM) has a pronounced effect on our climate, and exposure to PM causes negative health outcomes and elevated mortality rates in urban populations. Reactions that occur in fog can form new secondary organic aerosol material from gas-phase species or primary organic aerosols. It is important to understand these reactions, as well as how organic material is scavenged and deposited, so that climate and health effects can be fully assessed. Stable carbon isotopes have been used widely in studying gas- and particle-phase atmospheric chemistry. However, the processing of organic matter by fog has not yet been studied, even though stable isotopes can be used to track all aspects of atmospheric processing, from particle formation, particle scavenging, reactions that form secondary organic aerosol material, and particle deposition. Here, carbon isotope analysis is used for the first time to assess the processing of carbonaceous particles by fog.

This work first compares carbon isotope measurements ($\delta^{13}C$) of particulate matter and fog from locations across the globe to assess how different primary aerosol sources are reflected in the atmosphere. Three field campaigns are then discussed that highlight different aspects of PM formation, composition, and processing. In Tempe, AZ, seasonal and size-dependent differences in the $\delta^{13}C$ of total carbon and *n*-alkanes in PM were studied. $\delta^{13}C$ was influenced by seasonal trends, including inversion, transport, population density, and photochemical activity. Variations in $\delta^{13}C$ among particle size fractions were caused by sources that generate particles in different size modes.

An analysis of PM from urban and suburban sites in northeastern France shows how both fog and rain can cause measurable changes in the $\delta^{13}C$ of PM. The $\delta^{13}C$ of PM

was consistent over time when no weather events occurred, but particles were isotopically depleted by up to 1.1‰ in the presence of fog due to preferential scavenging of larger isotopically enriched particles. Finally, the $\delta^{13}C$ of the dissolved organic carbon in fog collected on the coast of Southern California is discussed. Here, temporal depletion of the $\delta^{13}C$ of fog by up to 1.2‰ demonstrates its use in observing the scavenging and deposition of organic PM.

ACKNOWLEDGMENTS

I would first like to thank my adviser, Pierre Herckes, for his guidance and support throughout my graduate career. He has continuously inspired me do my best work, develop my strengths, and understand and improve upon my weaknesses.

I would like to acknowledge my supervisory committee members, Matthew Fraser and Everett Shock, for their valuable comments and wisdom as I prepared my dissertation. I am also grateful to Ariel Anbar and Hilairy Hartnett for their support and advice over the years.

I would like to thank Andrea Clements and Alexandra Boris for their support and camaraderie during our field campaign in Santa Barbara, and Maurice Millet and Olivier Delhomme for their help and support during my field campaign in France.

I am forever grateful to Natasha Zolotova for all of her help and guidance in the Keck Lab, and to Steve Romaniello and Gwyn Gordon for their continued support and friendship.

I would like to acknowledge the support of all my fellow lab members, past and present: Youliang Wang, Sarah Frey, Aurelie Marcotte, Christy Rose, Jinwei Zhang. Jershon Eagar, Takayuki Nosaka, Alyssa Sherry, and Samantha Donovan.

I would like to acknowledge my funding sources, including the EPA Science to Achieve Results (STAR) Graduate Fellowship (FP-91780301-0), the Chateaubriand Fellowship of the Office for Science & Technology of the Embassy of France in the United States, the Roche/ARCS Foundation Scholar Award Program in the Life Sciences, and the Alumnae Association of Barnard College Fellowship for Graduate Study.

Finally, I would like to thank my husband, Zach, for his support and eternal patience over the past six years, and my parents, George and Carol, for helping me become a person who is always motivated, always curious, and always striving to be my best self.

TABLE OF CONTENTS

Page

CHAPTER Page

CHAPTER Page

LIST OF TABLES

Table Page

LIST OF FIGURES

Figure Page

Figure Page

Figure Page

CHAPTER 1

INTRODUCTION AND BACKGROUND

Aerosol Characterization and Sources

Atmospheric particulate matter (PM) is defined as solid particles suspended in the atmosphere. PM falls under the classification of atmospheric aerosols, which include both solids and liquid droplets. PM is found in a wide array of sizes, from submicron particles primarily formed from chemical reactivity and nucleation, to super-micron particles formed through mechanical abrasion (Seinfeld & Pandis, 2016). PM can originate from a variety of biogenic and anthropogenic sources, including vegetation, resuspension of dust and soils, vehicle emissions, sea spray, and biomass burning. Depending on the particle source and formation mechanism, particles from different sources can be found in different particle size fractions. The composition of PM is dependent on its source, but common constituents include inorganic ions (such as sulfate, nitrate, ammonium, and chloride), trace metals, and carbonaceous matter (including organic carbon, elemental carbon, and carbonate) (Seinfeld & Pandis, 2016).

Particulate matter has been shown to have negative effects on human health, causing respiratory stress and disease (Folinsbee, 1993; MacNee & Donaldson, 2003; Oberdörster, 2001; Tsai et al., 2013). The degree to which particles enter the human respiratory tract and affect health outcomes is dependent on particle size (Heyder et al., 1986). Fine particles in the $PM_{2.5}$ size mode (particles with $d_p \leq 2.5$ μm) are associated with increased mortality rates in urban populations (Happo et al., 2008), while PM_{10} (particles with $d_p \leq 10$ μm), and more specifically, coarse particulate matter (particles in the size range 2.5 μm $\leq d_p \leq$ 10 μm) is associated with asthma and cardiac stress (Happo

et al., 2008; Lipsett et al., 2006; Mar et al., 2000). It can therefore be beneficial to characterize PM in different size fractions. In addition to the negative health effects of particles, PM also has a pronounced effect on our climate. Particles cause cooling at the Earth's surface through the scattering of solar radiation as well as warming of the troposphere by absorbing radiation (Marley et al., 2009). Both organic and elemental carbon found in particulate matter have been shown to absorb solar radiation (Kirchstetter et al., 2004).

Processing of Organic Matter in the Aqueous Phase

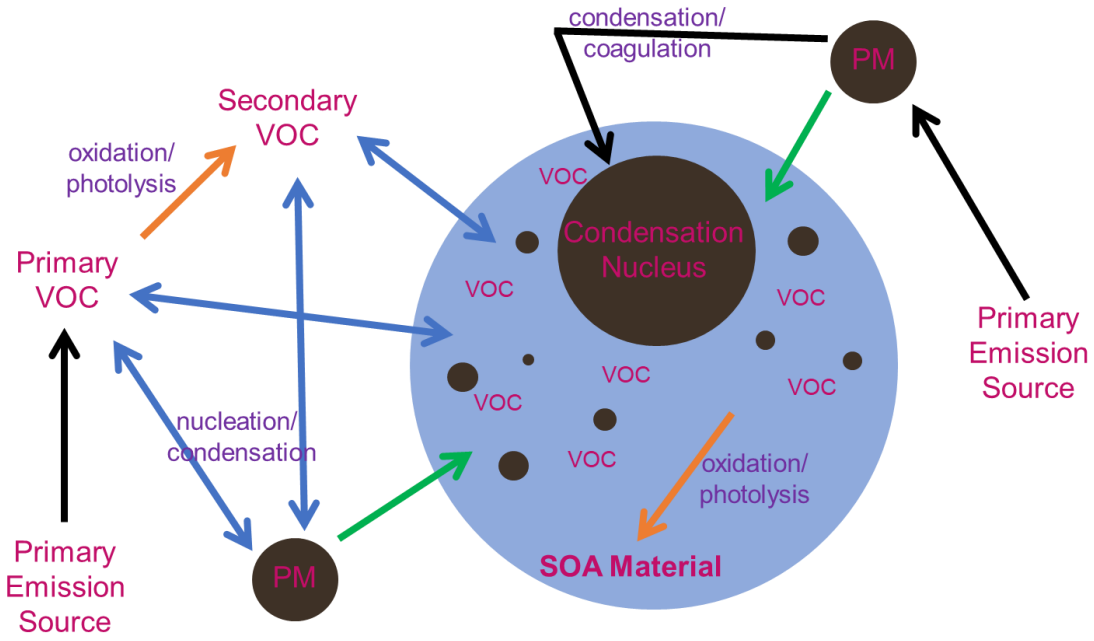

Figure 1.1. A schematic outlining the scavenging of organic particles and VOCs to form SOA material. Arrows are color-coded based upon the type of isotope process that occurs (black = no /unknown fractionation; orange = kinetic fractionation; blue = equilibrium fractionation; green = size-dependent particle scavenging).

As shown in Figure 1.1, primary sources of emissions release organic substances into the atmosphere. Gas-phase organics are referred to as primary volatile organic compounds (VOCs), and solid- and liquid-phase organics are referred to as primary

organic aerosols (POAs). In gas-phase reactions, primary VOCs can oxidize or photolyze into secondary VOCs, which are the products of atmospheric reactions. Based upon the properties of the VOCs and atmospheric conditions, primary and secondary VOCs may remain in the gas phase, nucleate to form new particles, or condense onto existing particles.

In the presence of fog or clouds, organic substances can be scavenged into the aqueous phase via multiple routes (Figure 1.1). A water droplet first forms when water condenses on the surface of a particle known as a cloud condensation nucleus (CCN). A CCN must have a minimum diameter of approximately 100-200 nm for a droplet to form around it (Seinfeld & Pandis, 2016), and it can grow to this critical diameter through condensation of VOCs onto the surface or coagulation with other particles to form larger PM (Seinfeld & Pandis, 2016). Additional particulate matter can be incorporated into droplets through collisions, and VOCs that are water soluble can dissolve into aqueous droplets. Once organic compounds are scavenged by a water droplet, aqueous phase organic reactions occur, which might form secondary organic aerosol (SOA) material (Kaul et al., 2011).

Stable Isotope Systems

An important analytical tool used to study the dynamic composition of the atmosphere is the chemistry of stable isotopes. Stable isotopes are not produced by long-lived radioactive decay, and do not decay themselves. The stable isotope composition of a substance is generally defined as R, the ratio of the abundance of the rare isotope to the abundance of the more common isotope. For stable carbon isotopes, this is defined using the abundances of ^{13}C and ^{12}C:

$$R = \frac{^{13}C}{^{12}C} \quad (1.1)$$

In order to standardize measurements, the R of a sample is compared to the R of a standard material. For carbon, the internationally accepted standard is Vienna Peedee Belemnite (VPDB), a scale based upon the R of calcium carbonate minerals found in the Peedee formation of South Carolina (Goldstein & Shaw, 2003). As differences in natural abundances of carbon isotopes are small, the differences between the R of a sample and R of a standard are expressed in units of permille (‰), using delta (δ) notation:

$$\delta^{13}C_{VPDB} = \left[\frac{\left(\frac{^{13}C}{^{12}C}\right)_{sample}}{\left(\frac{^{13}C}{^{12}C}\right)_{VPDB}} - 1 \right] \times 1000 \quad (1.2)$$

Stable isotopes undergo isotope fractionation, in which the isotopes of an element separate into pools with different $\delta^{13}C$ values in thermodynamic and kinetic processes due to differences in bond strength, where heavier isotopes form stronger and more stable bonds than lighter isotopes (Goldstein & Shaw, 2003). In atmospheric processes such as fog formation and particle/VOC scavenging, different types of fractionation might occur (Figure 1.1). In equilibrium processes, such as phase changes (blue arrows), heavy isotopes prefer the most stable binding environments. In the equilibrium of VOCs between the gas and particle phases, the particle phase will be enriched in $\delta^{13}C$ relative to the gas phase. Similarly, in the equilibrium of VOCs between the gas and aqueous phases, the aqueous phase will be enriched in $\delta^{13}C$ relative to the gas phase. In kinetically-driven reactions, such as in the formation of secondary VOCs in the gas phase or the formation of aqueous-phase SOA material (orange arrows), molecules containing lighter isotopes will react faster than those containing heavier isotopes, since lighter

isotopes form weaker bonds. In these cases, the $\delta^{13}C$ of the reaction products will be depleted relative to the reactants, and the reactant pool will become increasingly isotopically enriched. In a closed system, if the reaction goes to completion, the $\delta^{13}C$ of the reactants will equal the $\delta^{13}C$ of the products. The atmosphere, however, is an open system, and factors such as Rayleigh effects need to be accounted for when studying kinetic reactions (Goldstein & Shaw, 2003). Measurements of these isotopic fractionation processes in sum can provide useful information on temporal changes, sources, partitioning, and reactivity in the atmosphere. As will be discussed in the following section, the use of stable isotopes is a widely accepted and established practice that has an enormous potential for investigating active atmospheric processes.

Current Understanding of Stable Isotopes in the Atmosphere

Studies of the isotopic composition of PM and VOCs are widely documented in literature, as are observations of the isotope effects that can occur in these phases. As this work focuses on carbon in the particle and aqueous phases, studies involving the $\delta^{13}C$ of aerosols will be discussed here. Numerous biogenic and anthropogenic sources contribute to the composition of particles in the atmosphere, and many studies have demonstrated that different sources of aerosol particles have distinguishable carbon isotope compositions (Fisseha et al., 2009; Gleason & Kyser, 1984; Moura et al., 2008; Pichlmayer et al., 1998; Rudolph et al., 2003; Wang et al., 2005; Widory et al., 2006; Wozniak et al., 2012). For example, C_3 and C_4 plants, which undergo different photosynthetic processes, have very different carbon isotope signatures (Wozniak et al., 2012), and various types of fuel, such as diesel and gasoline, can be distinguished by carbon isotopes (Fisseha et al., 2009). Studies have shown that POAs have similar

isotopic signatures to their sources (visualized as black arrows in Figure 1.1), but SOA material tends to be depleted in $\delta^{13}C$ due to kinetic isotope effects (Fisseha et al., 2009).

Since the 1970s (Cachier et al., 1986 and references therein), $\delta^{13}C$ measurements of PM have been used primarily to determine sources of carbonaceous particulate matter. For example, the analysis of the $\delta^{13}C$ of total carbon (referred to hereafter as $\delta^{13}C_{TC}$) in $PM_{2.5}$ and PM_{10} in Paris showed that emissions from diesel fuel were the dominant source of atmospheric carbon (Widory et al., 2004). Cao and coworkers (2011) found that the $\delta^{13}C_{TC}$ of $PM_{2.5}$ collected in 14 cities across China was dominated by coal emissions and motor vehicle exhaust; the 1998 prohibition of biomass burning in urban areas was reflected in these results, as the $\delta^{13}C_{TC}$ of $PM_{2.5}$ was dissimilar to the $\delta^{13}C$ of both C_3 and C_4 plants. In Rio de Janeiro, Brazil, isotope compositions of organic and elemental carbon ($\delta^{13}C_{OC}$ and $\delta^{13}C_{EC}$, respectively) in total suspended particulates (TSP) suggested that biogenically-derived alcohol fuel contributed to the urban background, with no measurable diurnal or weekday/weekend patterns (Tanner & Miguel, 1989). In another study in Vancouver, Canada, Huang and coworkers (2006) measured the $\delta^{13}C_{OC}$ and $\delta^{13}C_{EC}$ of $PM_{2.5}$ in a provincial park (biogenic background), tunnel (motor vehicle emissions), and an urban background site; they found though comparison that the urban background site had a greater influence from motor vehicle exhaust than biogenic emissions. A study of PM_{10} in Wroclaw, Poland found seasonal differences in $\delta^{13}C_{TC}$, with coal burning emissions dominating in the winter and emissions from transported vegetation dominating in the summer; this was manifested in enriched wintertime $\delta^{13}C_{TC}$ relative to the summer (Gorka et al., 2014). In Kathmandu, Nepal, the analysis of $\delta^{13}C_{TC}$ of bulk aerosols confirmed the dominance of anthropogenic emissions in the winter

(Shakya et al., 2010). PM_2 sampled in two forested areas in Brazil showed distinct differences in the $\delta^{13}C$ of water soluble organic carbon ($\delta^{13}C_{WSOC}$) due to the dominance of C_3 versus C_4 plants in the two locations (Martinelli et al., 2002). All these studies show that $\delta^{13}C$ measurements are useful in PM source identification and apportionment.

While $\delta^{13}C$ measurements of PM are mostly used for primary emissions sourcing (as described above), they can also be used to an extent to deduce reactivity and SOA formation. For example, López-Veneroni (2009) determined through source apportionment of $\delta^{13}C_{TC}$ that $PM_{2.5}$ and PM_{10} in Mexico City, Mexico were mainly influenced by vehicle emissions and agricultural soils. However, the $\delta^{13}C_{VPDB}$ values were found to deviate from a simple mixing model, suggesting the formation of SOA material: ^{13}C-enriched molecules were thought to partition into the particle phase, while ^{13}C-depleted molecules likely partitioned into the gas phase. Nguyen and coworkers (2016) found the $\delta^{13}C_{TC}$ of $PM_{2.5}$ in Sonla, Vietnam to be influenced mainly by fossil fuel and biomass burning, but suggested that small changes in $\delta^{13}C_{TC}$ could be due to the formation of SOA through photochemical processing of individual compounds. The $\delta^{13}C_{TC}$ of PM_{10} in Mumbai was found to be consistent with urban particle sources (biofuel and biomass burning), but seasonal differences pointed to prolonged photochemical processing and SOA formation in the wintertime when aerosols had longer residence times: Winter $\delta^{13}C_{TC}$ averaged -25.9 ± 0.3‰, while summer $\delta^{13}C_{TC}$ averaged -26.5 ± 0.3‰ (Aggarwal et al., 2013). Similarly, measurements of the $\delta^{13}C_{TC}$ of TSP in Nainital, India, a remote location in the Himalayas (Hegde et al., 2016), showed wintertime $\delta^{13}C_{TC}$ measurements averaged -24.0‰, characterized mainly by biomass burning of C_4 plants and long residence times caused by boundary layer dynamics.

Summer $\delta^{13}C_{TC}$ values averaged -26.0‰, which was attributed to high winds transporting fresh biogenic (C_3) and fossil fuel combustion emissions. In the Sapporo forest in Japan, isotope measurements of water soluble organic carbon ($\delta^{13}C_{WSOC}$) in TSP reflected the expected biogenic sources year-round, but $\delta^{13}C_{WSOC}$ was depleted in the summer compared to the winter; this was indicative of higher biological activity and SOA formation in the summer (Miyazaki et al., 2012). The $\delta^{13}C_{WSOC}$ of TSP collected in the Maldives was enriched by 3 – 4‰ relative to central India, consistent with the expected aging of WSOC that occurs during long-range transport of particles over the ocean from India to the Maldives (Kirillova et al., 2013). With knowledge of the location, particle sources, and weather patterns (i.e., long-range transport versus inversion and long residence times), observations of changes in $\delta^{13}C_{TC}$ could be valuable in explaining aging and SOA formation.

Bulk $\delta^{13}C$ measurements (total, organic or elemental carbon) are mainly interpreted for source apportionment, but reactivity is mostly studied through the analysis of the $\delta^{13}C$ of individual compounds. Fisseha and coworkers (2009), for example, used the $\delta^{13}C_{TC}$ of aerosols in Zurich, Switzerland to determine the major sources of PM (wood combustion and vehicle exhaust), but also correlated changes in the $\delta^{13}C$ of gaseous formic and acetic acids with ozone to show the prominence of SOA formation in the summer through kinetic isotope effects. The $\delta^{13}C$ analysis of individual dicarboxylic acids collected in size-resolved PM fractions in urban Xi'an, China were used to show the isotope effects that occur due to kinetic reactions, as well as to demonstrate the condensation of VOCs onto coarse particles (Wang et al., 2012). Aggarwal and Kawamura (2008) measured the $\delta^{13}C$ of individual dicarboxylic acids in TSP from the

city of Sapporo, Japan, and found decreasing $\delta^{13}C$ values with increasing molecule size, attributed to the isotopic fractionation that occurs during photochemical degradation.

Objectives

As described above, the use of $\delta^{13}C$ measurements in atmospheric studies is ubiquitous; in fact, two comprehensive reviews explain in detail the current state and future potential of isotope studies of organic atmospheric constituents (Gensch et al., 2014; Goldstein & Shaw, 2003). However, one major component of the atmosphere is missing in all of these studies: $\delta^{13}C$ of fog and cloud. The $\delta^{13}C$ composition of fog and cloud, as well as interactions of other phases (VOC, PM) with fog and cloud studies through $\delta^{13}C$, have not yet been explored.

While studies of the chemical composition of fog have been conducted since the mid-20th Century (Houghton, 1955), the analysis of the organic compounds present in fog is relatively new and only began to become a field of interest in the 1990s (e.g., Herckes et al., 2013 and references therein). Most aqueous phase SOA generation processes remain poorly understood, and this lack of knowledge is thought to be a reason for substantial errors in atmospheric models used in climate and air quality studies (Ervens, 2015). It has been shown that the addition of aqueous phase SOA formation to models dramatically improves predictions of organic carbon concentrations (Carlton et al., 2008).

This work will strive to provide a better understanding of the fate of organic matter in heterogeneous atmospheric systems through the use of stable carbon isotope analysis. The focus will be on the scavenging and deposition of particles by fog, as well as the effect of scavenging on both the composition of interstitial particulate matter and the dissolved organic carbon (DOC) present in fog. Chapter 2 will begin with an

overview of what is known about the $\delta^{13}C$ of POA sources and how these sources are reflected in the $\delta^{13}C$ measurements of PM and fog. Chapter 3 will discuss a new method to quantify carbonates in PM samples, which is necessary in understanding the $\delta^{13}C$ of particles in locations affected by blown dust sources. One such location is Tempe, AZ, where the $\delta^{13}C$ of total carbon and individual *n*-alkanes in size-resolved particulate matter was measured and will be discussed in Chapter 4. Chapter 5 will focus on urban and suburban PM collected in northeastern France, and how both fog and rain can cause measurable changes in the $\delta^{13}C$ of PM. Finally, the $\delta^{13}C$ of the DOC of fog collected on the coast of Southern California will be discussed in Chapter 6. Implications of the changes in $\delta^{13}C$ of fog over time will be addressed, and other stable isotope systems ($\delta^{2}H$ and $\delta^{18}O$) will be used to evaluate the evolution of a fog event. Chapters 5 and 6 will discuss the selective scavenging of particles by fog, which results in measurable changes in the $\delta^{13}C$ of PM (visualized as green arrows in Figure 1.1). Primary aerosol sources form particles in different size fractions (Seinfeld & Pandis, 2016), and each primary source has a distinct $\delta^{13}C$; It is therefore hypothesized that changes in $\delta^{13}C$ of both PM and fog are caused by size-selective scavenging of particles.

CHAPTER 2

OVERVIEW OF CARBON ISOTOPES IN ATMOSPHERIC PARTICULATE MATTER AND FOG

This chapter will provide an overview of what is known about the $\delta^{13}C$ of POA source signatures in literature, and how both aerosol particles and fog can reflect the $\delta^{13}C$ of these sources. Insight into the mechanism of how carbonaceous material is scavenged by fog will also be introduced.

As discussed in Chapter 1, measurements of the $\delta^{13}C_{TC}$ of aerosol PM reflect the combined $\delta^{13}C$ of the sources that contribute POA to a specific location. It is expected that the $\delta^{13}C_{TC}$ of aerosol presented in this chapter will reflect the $\delta^{13}C$ signatures of major primary aerosol sources. It is additionally hypothesized that the $\delta^{13}C_{DOC}$ of fog will reflect POA sources, since POA is scavenged by fog. However, since the scavenging of particles and gases by fog is selective based upon the chemical composition of carbonaceous atmospheric constituents and the sizes of existing particles, it is hypothesized that the $\delta^{13}C_{DOC}$ of fog will differ from the $\delta^{13}C_{TC}$ of coexisting interstitial aerosol. Knowledge of the primary aerosol sources of different locations will allow a broad interpretation of how $\delta^{13}C$ of fog and PM will reflect these sources.

Materials and Methods

Sample collection.

Fog and particulate matter samples were collected in Davis, CA from January 6 – 26, 2011 (Ervens et al., 2013). Particulate matter and cloud samples from Whistler, BC were collected during the "Whistler Aerosol and Cloud Study" (WACS2010) from June 22 – July 28, 2010 (Ervens et al., 2013). Particulate matter samples were collected in

Bakersfield from January 17 – February 12, 2013, in a lot situated between a church and residential community, and approximately 100 yards from an oil field (Wang, 2014). From June 8 – 14. 2015, fog samples were collected in Casitas Pass along the Santa Barbara Channel, and particulate matter samples were collected at Serra Cross Park in Ventura, CA (Boris et al., 2018). These samples are discussed in greater detail in Chapter 6. Particulate matter samples were collected in Tempe, AZ on January 6 – 13, March 31 – April 7, June 19 – 26, and September 30 – October 7, 2014, and are discussed in greater detail in Chapter 4.

Particulate matter samples were collected in the Monterrey, MX metropolitan area in the spring and fall of 2011 and 2012 (Mancilla et al., 2015). Particulate matter and fog samples were collected in Strasbourg and Geispolsheim, France in the fall of 2016 and are discussed in detail in Chapter 5. Fog samples were also collected in Geispolsheim from October 26, 2015 through January 1, 2016, in Erstein, France (48.4213°, 7.6588°) from October 27 – December 15, 2016, and in Metz, France (49.1099°, 6.2224°) from November 13, 2015 – January 1, 2016. Fog samples from Baengnyeong Island, South Korea were collected from June 29 – July 21, 2014 (Boris et al., 2016).

The following potential local source materials of particulate matter were collected and analyzed in Tempe, AZ: Plant material, tailpipe emissions, parking structure emissions, fireplace emissions, biomass burning emissions, and resuspended soil. Details of the sampling and analysis of these materials can be found in Appendix B.

Sample analysis.

Isotopic measurements for $\delta^{13}C_{VPDB}$ of TC in aerosol PM were performed using a Costech Elemental Analyzer coupled to a Thermo Delta Plus Advantage Isotope Ratio

Mass Spectrometer (EA-IRMS). The analytical uncertainty of samples analyzed using this method is 0.2‰. NIST 2710 (Montana soil) was used as a linearity standard. Three in-house glycine standards were used to perform and verify a two-point isotopic calibration.

Fog samples were filtered through a prebaked quartz filter for isotopic analysis of dissolved organic carbon (DOC). Isotopic measurements for $\delta^{13}C_{VPDB}$ of DOC of fog samples were performed using an OI Analytical TOC Analyzer coupled to a Thermo Delta Plus Advantage Isotope Ratio Mass Spectrometer (TOC-IRMS). The analytical uncertainty of the samples analyzed using this method is 0.3‰. Potassium hydrogen phthalate (KHP, Sigma Aldrich, 99.995%) with a known isotopic composition was used as a linearity standard. Three in-house glycine standards were used to perform and verify a two-point isotopic calibration.

Results and Discussion

The $\delta^{13}C$ of primary aerosol sources.

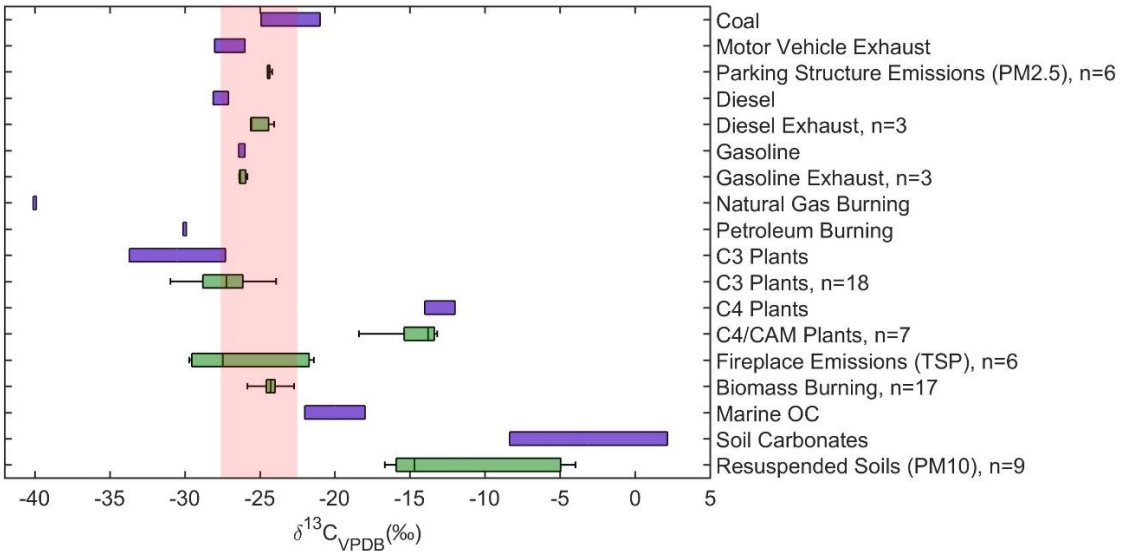

Figure 2.1. Examples of the $\delta^{13}C$ values of primary aerosol sources. Literature values are shown in purple and are reported observations of coal (Gleason & Kyser, 1984; Widory, 2006), motor vehicle exhaust (Widory, 2006), diesel and gasoline (Fisseha et al., 2009), natural gas and petroleum burning (Pichlmayer et al., 1998), C_3 plants (Moura et al., 2008), C_4 plants (Wozniak et al., 2012), marine organic carbon (Wozniak et al., 2012), and soil carbonates (Wang et al., 2005). Samples collected in Tempe, AZ are shown in green, and are discussed in detail in Chapter 4.The shaded area represents the $\delta^{13}C$ range for atmospheric samples measured in this study (Figure 2.2).

Numerous biogenic and anthropogenic sources contribute to the composition of aerosols in the atmosphere, and several studies have been conducted that measure the $\delta^{13}C$ of these primary aerosol sources. The reported $\delta^{13}C$ values of select sources are summarized in Figure 2.1. These studies demonstrate that different sources of aerosol particles have distinguishable isotopic compositions. For example, C_3 and C_4 plants have been shown to have different isotopic signatures (C_3: -33.7 – -27.3‰, (Moura et al., 2008); C_4: -14 – -12‰, (Wozniak et al., 2012) due to differences in their photosynthetic

processes (Bender, 1971; O'Leary, 1981; Park & Epstein, 1960). Even within the common source class of vehicle emissions, it is possible to distinguish between diesel and gasoline fuel types (Fisseha et al., 2009), as they are sourced from different fractions of petroleum (Silverman, 1967). Emissions of natural gas burning are isotopically depleted relative to petroleum (-40‰ versus -30‰, respectively, Pichlmayer et al., 1998); as the molecular constituents in petroleum break down, isotope effects in chemical reactions cause smaller product molecules (methane) to be depleted in $\delta^{13}C$ (Silverman, 1967). Coal has been observed to be enriched in $\delta^{13}C$ relative to liquid or gaseous fossil fuels (-24.9 – -21‰, Gleason & Kyser, 1984; Widory, 2006). Soil carbonates are isotopically enriched relative to organic carbon (-8.35 – +2.15‰, Wang et al., 2005) because of the formation of carbonate minerals from atmospheric CO_2 dissolved in water (McCrea, 1950). Marine OC falls within -22 – -18‰ (Wozniak et al., 2012) due to the role that CO_2 dissolved in the oceans plays in marine photosynthesis (Park & Epstein, 1960).

Samples of emissions from a parking structure collected in Tempe, AZ were isotopically enriched (ranging from -24.5 – -24.2‰) compared to motor vehicle exhaust reported in Paris, France (-28 – -26‰, Widory, 2006), possibly due to regional differences in fuel source and use (France versus the United States). The $\delta^{13}C$ of gasoline exhaust collected in Tempe (-26.4 – -25.8‰) are similar to literature values, but diesel emissions in Tempe were enriched in $\delta^{13}C$ (-25.6 – -24.1‰) relative to reported literature values. These samples are discussed in more detail in Chapter 4. The $\delta^{13}C$ of C_3 (-30.1 – -23.9‰) and C_4/CAM plants (-18.4 – -13.2‰) were similar to reported ranges in literature. The $\delta^{13}C$ of resuspended soils (-16.7 – -4.0‰) were isotopically enriched relative to other collected sources, due to the presence of carbonates in the soils. They

are, however, depleted compared to isolated soil carbonates, as they contain anthropogenically and biogenically emitted particulates as well.

Organic aerosol particles that are directly emitted by primary sources are known as primary organic aerosols (POAs). POAs have similar isotopic compositions to their sources (Fisseha et al., 2009; Martinelli et al., 2002; Rudolph et al., 2003; Sakugawa & Kaplan, 1995). Based on the differences in $\delta^{13}C$ among POA sources, these measurements can be used as a tool to differentiate among sources that contribute to the carbon in atmospheric particulate matter.

$\delta^{13}C$ of the total carbon of particulate matter samples.

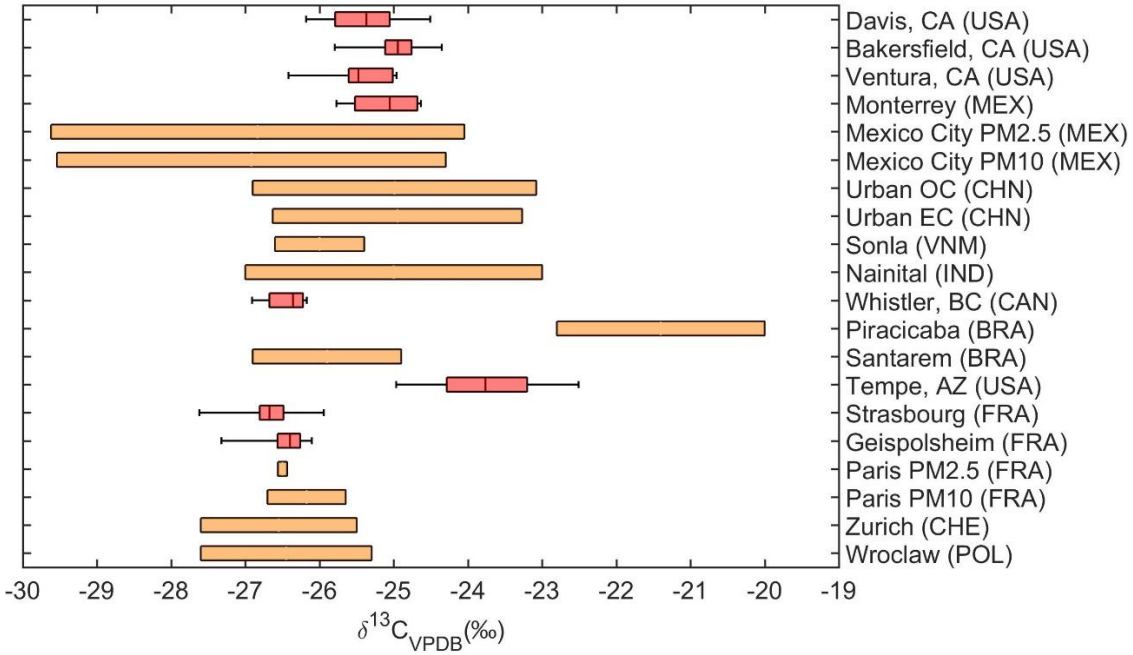

Figure 2.2. Measurements of the $\delta^{13}C$ of aerosol samples. Samples in red are measurements from this study, and samples in orange are reported in literature. All samples from this study are measurements of $\delta^{13}C_{TC}$. Literature particulate matter measurements are of $\delta^{13}C_{TC}$ of $PM_{2.5}$ and PM_{10} in Mexico City, Mexico (López-Veneroni, 2009), $\delta^{13}C_{OC}$ and $\delta^{13}C_{EC}$ of $PM_{2.5}$ in urban locations across China (Cao et al., 2011), $\delta^{13}C_{TC}$ of $PM_{2.5}$ in Sonla, Vietnam (Nguyen et al., 2016), $\delta^{13}C_{TC}$ of TSP in Nainital, India (Hegde et al., 2016), $\delta^{13}C_{TC}$ of PM_2 in Piracicaba and Santarem, Brazil (Martinelli et al., 2002), $\delta^{13}C_{TC}$ of $PM_{2.5}$ and PM_{10} in Paris, France (Widory et al., 2004), $\delta^{13}C_{TC}$ of aerosols in Zurich, Switzerland (Fisseha et al., 2009), and $\delta^{13}C_{TC}$ of PM_{10} in Wroclaw, Poland (Gorka et al., 2014).

Figure 2.2 shows the measurements of the $\delta^{13}C_{TC}$ of aerosol samples in several locations measured in this study, as well as literature values. The range of $\delta^{13}C_{TC}$ of aerosol samples measured for this work (-27.6 – -22.5‰) is much narrower than POA sources overall (-40 – +2.15‰, Figure 2.1); the x-axis of Figure 2.2 is shown as a shaded region in Figure 2.1 for perspective. The $\delta^{13}C_{TC}$ of aerosols from Davis (-26.2 – -24.5‰), Bakersfield (-25.8 – -24.4‰), and Ventura, CA (-26.4 – -25.0‰) fell in similar ranges and likely had similar sources of POA. $\delta^{13}C_{TC}$ in Monterrey (-25.8 – -24.6‰) was similar to the three sites in California. Sources of fine particles in Monterrey are mainly

attributed to burning, with vehicle exhaust, meat cooking, and biomass and vegetative waste burning dominating (Mancilla et al., 2016). Similarly, the $\delta^{13}C_{TC}$ of $PM_{2.5}$ and PM_{10} in Mexico City averaged -25.4 ± 1.2‰, but vehicular emissions and agricultural soils were determined to be the dominant particle sources (López-Veneroni, 2009). The $\delta^{13}C_{OC}$ and $\delta^{13}C_{EC}$ of $PM_{2.5}$ from cities in China fell in a wide range that encompasses the $\delta^{13}C_{TC}$ of other urban aerosols and is attributed to emissions from coal and motor vehicle exhaust (Cao et al., 2011). The $\delta^{13}C_{TC}$ values of $PM_{2.5}$ in Sonla, Vietnam were attributed to biomass burning and fossil fuel emissions (Nguyen et al., 2016). In Nainital, India, located in free troposphere in the Himalayas, TSP was found to have a high contribution of biomass burning sources in the winter, and transported fossil fuel sources in the summer, based upon the measured range of $\delta^{13}C_{TC}$ (Hegde et al., 2016).

$\delta^{13}C_{TC}$ in Whistler (-26.9 – -26.2‰) was depleted compared to aerosol in the California sites and Monterrey. The Whistler site is rural and aerosol is dominated by the contribution of C_3 biogenic emissions (Ervens et al., 2013), which overall has a lighter $\delta^{13}C$ than vehicle exhaust (Figure 2.1). In Brazil, a study of the $\delta^{13}C_{TC}$ of fine aerosols (PM_2) collected in two forested sites showed a clear differentiation between emissions from a C_3 forest (Santarem) and land covered with C_4 plants, sugarcane and pastures (Piracicaba) (Martinelli et al., 2002).

Tempe particulate matter was enriched in $\delta^{13}C_{TC}$ relative to other urban sites (-25.0 – -22.5‰) due to the elevated presence of carbonate in desert aerosol; the measured isotopic composition of the carbonate fraction of aerosol in Tempe ($\delta^{13}C_{CC}$) was in the range of -8 – -5‰. The measurement of carbonates in Tempe aerosol samples is further discussed in Chapter 4.

Particles in both Strasbourg (-27.6 – -25.9‰) and Geispolsheim (-27.3 – -26.1‰) were depleted in $\delta^{13}C_{TC}$ relative to urban sites in North America, likely due to the greater use of diesel fuel than gasoline in France (Delhomme & Millet, 2012). The $\delta^{13}C_{TC}$ of particles collected in these two locations in France are further discussed in Chapter 5. Similarly, $PM_{2.5}$ and PM_{10} in Paris, France were both found to be dominated by diesel emissions, based upon $\delta^{13}C_{TC}$ measurements (Widory et al., 2004). $\delta^{13}C_{TC}$ of aerosols in Zurich, Switzerland were found be influenced by wood combustion as well as vehicle exhaust (Fisseha et al., 2009), and the $\delta^{13}C_{TC}$ of PM_{10} in Wroclaw, Poland was found to have seasonal variations, with coal burning dominating in the winter and transported vegetative emissions dominating in the summer (Gorka et al., 2014).

As seen in Figure 2.1, while many POA sources are isotopically distinguishable, some have similar or overlapping $\delta^{13}C$ ranges. Notably, $\delta^{13}C$ for C_3 plants (-33.7 – -27.3‰, Moura et al., 2008) and motor vehicle exhaust (-28 – -26‰, Widory, 2006), which typically make up a bulk of directly emitted particles in urbanized environments, could be found in similar ranges. Additionally, the $\delta^{13}C$ of a POA source can vary based upon the sampling site, as the types of plants, cars, and other emission sources can be different among sampling locations. As discussed above, atmospheric particulate matter represents a mixture of primary carbonaceous aerosol sources, and the significance of secondary aerosols can vary seasonally, diurnally, and geographically. Still, some assumptions about the major emission sources comprising a particulate matter sample can be made based on knowledge of the sampling location.

$\delta^{13}C$ of the dissolved organic carbon of fog samples.

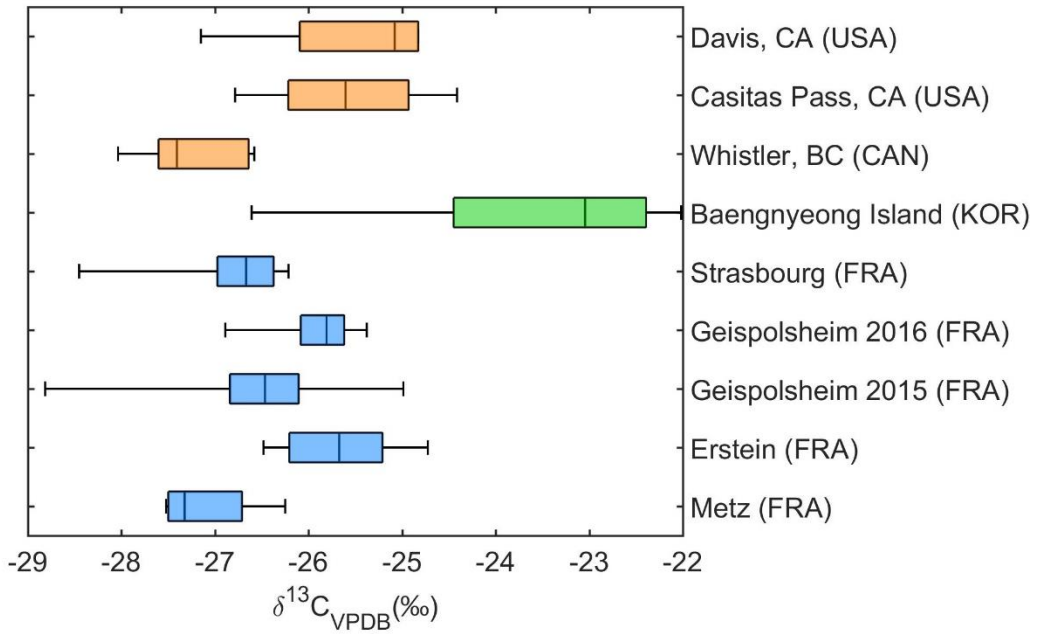

Figure 2.3. Measurements of the $\delta^{13}C_{DOC}$ of fog and cloud samples. Samples are color-coded based upon the region (orange = North American west coast; green = South Korea; blue = France).

Currently, there are no published studies available that analyzed the $\delta^{13}C$ of fog or cloud samples. Figure 2.3 shows the measurements of the $\delta^{13}C_{DOC}$ of fog and cloud samples collected in several locations for this work. Fog collected in Davis (-27.2 – -24.8‰) and Casitas Pass, CA (-26.8 – -24.4‰) fell within a similar range of $\delta^{13}C_{DOC}$, and cloud in Whistler was depleted in $\delta^{13}C_{DOC}$ relative to these sites (-28.0 – -26.6‰) due to the dominant influence of biogenic aerosol relative to the urbanized sites in California (Ervens et al., 2013). Fog collected on Baengnyeong Island, South Korea was enriched in $\delta^{13}C_{DOC}$ relative to other sampling locations (-26.6 – -22.0‰) because of the enrichment of marine OC relative to anthropogenic emissions. Fog in this location was shown to have significant marine influence, and upwind trajectories of the air masses showed passage over either the Yellow Sea or the Sea of Japan (Boris et al., 2016).

Fog samples from four urban (Strasbourg, Metz) and suburban (Geispolsheim, Erstein) sites in Northeastern France were analyzed. Overall, fog collected in the cities of Strasbourg and Metz in 2016 was depleted in $\delta^{13}C_{DOC}$ relative to Davis and Casitas Pass (-28.5 – -26.2‰ and -27.5 – -26.2‰, respectively), as was observed in aerosol $\delta^{13}C_{TC}$ (Figure 2.2). However, fog samples collected in Erstein in 2016 were similar in $\delta^{13}C_{DOC}$ to those collected in California (-26.5 – -24.7‰), and fog collected in Geispolsheim had different ranges of $\delta^{13}C_{DOC}$ in 2016 (-26.9 – -25.4‰) and 2015 (-28.8 – -25.0‰). Geispolsheim and Erstein are both suburban towns south of Strasbourg, and are likely influenced by both urban and agricultural sources. Additionally, as is evident in Geispolsheim, atmospheric sources may be variable and are dependent on the weather conditions at the time of sampling.

In a similar fashion of the $\delta^{13}C_{TC}$ of aerosol, the $\delta^{13}C_{DOC}$ of fog and cloud appears to reflect the local sources of carbonaceous material. The carbon contained in a fog droplet, however, is inherently different from the total carbon of aerosol: Fog droplets are more likely to contain water soluble organics than water insoluble organics from both the aerosol and gas phases. Fog and clouds may also size-selectively scavenge particles, which would result in an isotope fractionation between the particle phase and aqueous phase; this topic will be discussed further in Chapters 5 and 6.

Comparison of fog and interstitial aerosol $\delta^{13}C$.

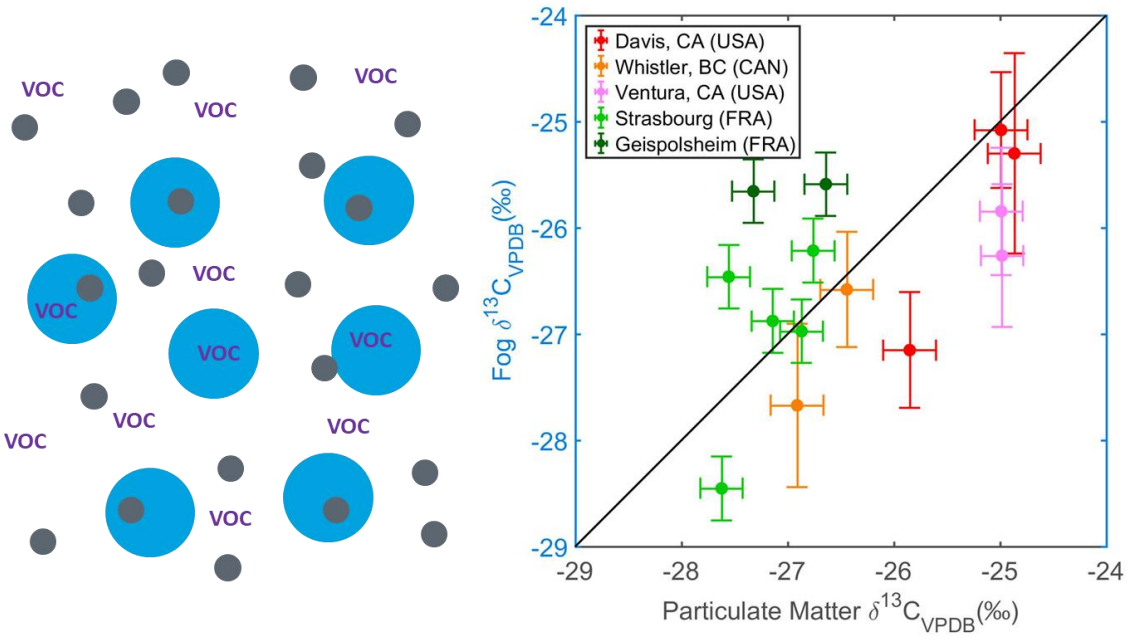

Figure 2.4. A comparison of the $\delta^{13}C$ of the dissolved organic carbon of fog samples and the total carbon of interstitial PM samples. Left: An illustration of the collected samples, where the grey dots represent PM and blue dots represent fog water; note that the fog water can incorporate both VOCs and particles. Fog water and interstitial PM (particles not scavenged by fog droplets) were collected simultaneously. Right: A comparison of the results of isotopic analysis, with a 1:1 line drawn as a visual aid.

During five of the field sampling campaigns discussed in this chapter, fog and PM were able to be collected simultaneously, and samples of fog and interstitial PM (i.e., PM that has not been scavenged by fog droplets) were analyzed for $\delta^{13}C_{DOC}$ and $\delta^{13}C_{TC}$, respectively. Results are shown in Figure 2.4. During the campaigns in Davis, CA, Whistler, BC, and Ventura, CA, the $\delta^{13}C_{TC}$ of interstitial PM was enriched relative to the $\delta^{13}C_{DOC}$ of the fog. In Geispolsheim, both fog samples were enriched in $\delta^{13}C_{DOC}$ relative to the $\delta^{13}C_{TC}$ of interstitial PM. In Strasbourg, fog $\delta^{13}C_{DOC}$ was enriched relative to the $\delta^{13}C_{TC}$ of interstitial PM during three of the five fog events.

Overall, the relationships between fog $\delta^{13}C_{DOC}$ and interstitial PM $\delta^{13}C_{TC}$ in France and in California/British Columbia are different, but the reasons for these

differences are not known. These observations do provide information that can aid in interpreting isotope results, but also point out the limitations in applying these observations. Figure 2.4 illustrates some of the complexities that must be accounted for when interpreting isotopic results. Fog droplets will form on cloud condensation nuclei, and over time the droplets will grow and scavenge both gas-phase organics (known as volatile organic compounds, or VOC) and particle-phase organics. Scavenging will depend on the composition of particles and VOCs at the location and time of the fog event. Higher concentrations of VOCs will cause more diffusion into droplets based on Henry's Law constants; as the $\delta^{13}C$ of bulk or individual VOCs was not measured, the relationship between fog $\delta^{13}C_{DOC}$ and aerosol $\delta^{13}C_{TC}$ cannot be directly quantified. Particles that are aged and/or are more hygroscopic will also be more readily scavenged by fog. Weather conditions will play a part as well, as the relative humidity and temperature will affect the liquid water content and the size of the droplets.

Conclusions

The $\delta^{13}C$ of several primary aerosol sources have been extensively reported in literature. Based upon the $\delta^{13}C$ of these sources, the $\delta^{13}C_{TC}$ of particles and $\delta^{13}C_{DOC}$ of fog were evaluated to determine the sources that would contribute to the carbonaceous particulates in each location. The PM in Tempe, AZ is enriched in $\delta^{13}C_{TC}$ compared to other sampling locations due to the presence of carbonate minerals; the composition of PM in Tempe will be further addressed in Chapter 4. Particles and fog in Whistler is depleted in $\delta^{13}C_{TC}$ compared to urban sampling sites in California due to the greater influence of C_3 biogenic material to POA. Particles in Strasbourg and Geispolsheim, France were found to be depleted in $\delta^{13}C_{TC}$ relative to cities in North America because of

the greater use of diesel fuel versus gasoline. However, the $\delta^{13}C_{DOC}$ of fog in suburban sampling locations in France were variable, likely because of the influence of agricultural POA sources. Fog on Baengnyeong Island was found to be enriched in $\delta^{13}C_{DOC}$ relative to other locations due to the influence of marine OC.

A comparison of the $\delta^{13}C_{DOC}$ of fog and in $\delta^{13}C_{TC}$ of interstitial PM showed that the two coexisting phases are isotopically distinct. The scavenging of organics by fog is a complex process, and a multitude of physical and chemical processes, including the selective uptake of particles, the scavenging of VOCs, and the formation of SOA material in the aqueous phase, can impact the $\delta^{13}C_{DOC}$ of fog. Overall, the results of these analyses show that $\delta^{13}C$ measurements have the potential to provide interesting insight into fog formation and the processing of organic material in the aqueous phase. Tandem measurements of gas-phase species along with the particle and aqueous phases could be useful in elucidating the $\delta^{13}C_{DOC}$ of fog. As will be discussed in Chapter 6, sample collection with higher temporal resolution can provide insight into the process that affect the composition of DOC over the lifetime of a fog.

CHAPTER 3

A NEW TECHNIQUE FOR THE QUANTIFICATION OF CARBONATE IN AEROSOL PARTICULATE MATTER

Carbonate is an important component of atmospheric particulate matter. Blown dust from sources such as soils, road dust, and construction materials is known to be a major source of particulate matter in the Phoenix area (Brown et al., 2007; Cahill, 2013; Lewis et al., 2003; Ramadan et al., 2000; Upadhyay et al., 2011) and elsewhere (Manoli et al., 2002), and is a contributor to mineral dust, including carbonates, to coarse atmospheric particulate matter (Garbaras et al., 2009; López-Veneroni, 2009; Masalaite et al., 2015). However, the measurement of carbonate carbon (CC) in atmospheric aerosol samples has been an ongoing challenge in the characterization of the carbonaceous components of particulate matter. Several methods of determining CC concentrations have been proposed and utilized, each with their own advantages and drawbacks.

Carbonate carbon in atmospheric particulate matter is most commonly quantified using a thermal/optical carbon analyzer. The three most common quantification methods include the analysis of evolved CO_2 from the acidification of carbonate in the instrument, the removal of CO_2 before analysis by acidification, or the integration of a CC peak in the thermogram. The DRI Thermal/Optical Carbon Analyzer is fitted with an injection port to allow the addition of HCl directly to the filter under an inert atmosphere to evolve CO_2 (Chow & Watson, 2002; Chow et al., 2001). Similarly, Cao and coworkers (2005) have directly acidified $PM_{2.5}$ sample filters with 25% v/v H_3PO_4 under helium inside of a DRI Model 2001 Thermal/Optical Carbon Analyzer, quantifying CC collected in Xi'an to determine the importance of various dust sources. Differences in CC concentrations using

this method were reported to be less than 5% between replicate 0.526 cm^2 quartz filter punches.

The Sunset Lab OCEC Aerosol Analyzer is not equipped with an injection port for *in situ* acidification of a sample for CC removal. A recommended method for CC quantification with this instrument is to analyze two aliquots of a filter separately, one after exposure to HCl fumes and another untreated with acid (Birch & Cary, 1996). In a similar approach used by other investigators, CC can be removed from aerosol samples before analysis through exposure to HCl vapor to quantify only organic or elemental carbon fractions (Cachier et al., 1989).

The technique of comparing acid-treated and untreated filters, however, assumes that aerosol collection on a filter is homogenous and all analyzed filter samples (with a maximum area of 1.5 cm^2) are uniform and comparable. This is not necessarily the case for all types of aerosol samples. For example, slotted filters used in cascade impactors (such as those used in Chapter 4) collect sample in narrow bands (1-2 mm wide) that make up only approximately 10% of the analyzed filter area, greatly decreasing the amount of sample that can be analyzed at once in a thermal/optical instrument. This, in addition to the coarse particle size modes collected in cascade impaction, decreases the likelihood of uniformly distributed aerosol over the filter area.

The integration of the CC peak in a thermogram is another possibility for CC quantification ("Sunset Laboratory Inc.," 2018). However, when CC is analyzed using a thermal-optical method without acidification, the evolution temperature of CC varies considerably, due to several factors including the mineral form of the carbonate (for example, calcite versus dolomite) and the presence of other materials in the sample

matrix (Webb & Kruger, 1970), as well as the particle size (Criado & Ortega, 1992). The analysis protocol also affects the evolution of CC: for example, dolomite would be expected to evolve in the OC4 fraction of the NIOSH protocol and in the OC3 fraction of the IMPROVE protocol (Chow et al., 2001). Additionally, the possibility of organic carbon coevolving with CC cannot be ruled out, since ambient particulate matter samples are unique to their sampling locations and PM composition cannot be generalized. Integration software for the Sunset Lab OCEC Aerosol Analyzer allows for the opportunity to integrate a specific peak known to be CC to either the thermogram baseline or to the base of the peak, but previous knowledge of the characteristics of CC and organic carbon of the sample is necessary to determine which integration method is most suitable (Cary, 2017). For these reasons, CC peak integration may not be an effective method of CC quantification for all aerosol samples.

Alternative methods for CC measurements have been proposed. Carbonates in geological samples have traditionally been analyzed by acidification with concentrated phosphoric acid (McCrea, 1950), and has since been adapted to measure the amount and isotopic composition of carbonates in aerosol samples (Chen et al., 2015; Chen et al., 2016). However, this method involves the reaction of samples *in vacuo*, followed by the cryogenic purification of CO_2, which may not be available to laboratories that do not perform routine isotopic analysis. Another method using the IR absorption of CO_2 formed from acidification has been used for samples containing CC concentrations as low as 10 µg CO_3^{2-} per filter (Clarke & Karani, 1992). In this setup, one half of a 37 mm filter was placed into an FTIR cell (100 cm^3), which was evacuated, filled with vapor

containing HCl, and analyzed directly after 10 minutes (after which the IR absorbance was stable).

This chapter presents an alternate method for quantifying CC in atmospheric particulate matter, through the acidification of aerosol filters at ambient pressure and temperature and the subsequent measurement of the CO_2 released upon acidification. This method allows the customization of the filter area used for analysis (up to 24 cm^2) so that enough CO_2 can be detected when released, while also making the sample analyzed more representative of the whole filter. This method can provide a precise estimate of carbonate in PM regardless of sampling method, particle size, sample concentration per unit area of filter, or sample homogeneity. Additionally, since no heat is involved in this analysis, this method allows for the analysis of samples collected on filter media other than quartz, such as Teflon, cellulose, or glass fiber.

Materials and Methods

Experimental setup.

The goal of these experiments was to measure the amount of gaseous CO_2 produced when an aerosol filter sample was acidified. The CO_2 formed by acidification would be used to calculate the concentration of carbonate carbon in the sample. Experiments were conducted using Nalgene jars (approximately 125mL) with a rubber septum attached to the side (Figure 3.1). This setup has been used to incubate soil crusts in determining nitrogen fixation activity (Noonan, 2012). Before performing any experiments, a glass petri dish was placed in each jar, and the volumes of the incubation jars with petri dishes were measured by massing each jar, filling them to capacity with ultrapure water (18.2 MΩ·cm), and massing again, assuming a water density of 1 g/mL.

All measurements of CO_2 concentration were made using an EGM-4 CO_2 monitor (PP Systems, Amesbury, MA), which determines CO_2 concentration (ppmv) by infrared absorbance. The instrument was zeroed to ambient CO_2 pressure before each measurement.

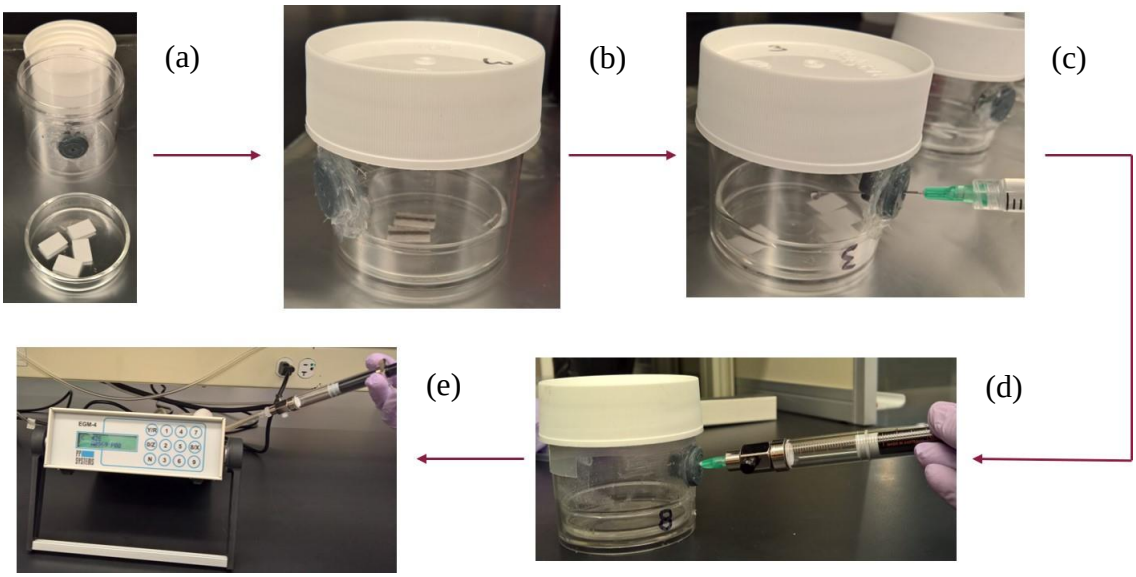

Figure 3.1. Flow diagram depicting the acidification of atmospheric particulate matter samples and subsequent measurement of CO_2. (a) A Nalgene jar with a septum attached to the side is used for the experiment. Filter punches, each with an area of 1.5 cm^2, are placed in a glass petri dish. (b) The petri dish is placed in the jar, and the jar is sealed. (c) Acid is added to the jar via syringe. (d) A gas-tight syringe is used to sample the air inside of the jar. (e) The concentration of CO_2 is measured with a PP Systems EGM-4 CO_2 monitor.

To perform this CC quantification method, a bicarbonate standard or aerosol sample was placed onto the petri dish inside of an incubation jar, and the jar was closed firmly (Figure 3.1a, 3.1b). The concentration of CO_2 inside of the jar was measured by removing 5 mL of air using a gas-tight syringe and injecting the air into the CO_2 monitor. The maximum stable CO_2 concentration after injection was recorded. 1M hydrochloric acid was then added dropwise to the samples via syringe (Figure 3.1c), and when the reaction was complete, the air inside of the jar was sampled again for CO_2 concentration

(Figure 3.1d). The difference in concentration before and after the reaction was used to calculate the concentration of carbonate carbon associated with the sample, taking into account the changes in volume and pressure that occur inside of the jar throughout the experiment. Ambient temperature and pressure were recorded at the start of each experiment. At the conclusion of each experiment, the pH of the liquid inside of the container was measured to ensure that an excess of acid was used.

Overview of calculations.

In calculating the amount of carbonate present in a sample, the concentration of CO_2 released during acidification of a sample must be determined, taking into account changes in the volume and pressure inside of the jar throughout the experiment. At the start of each experiment, the ambient pressure and temperature were measured and monitored throughout the course of the experiment to ensure that no large fluctuations occurred. The ambient pressure and temperature were assumed to be the same as the initial pressure and temperature inside of the incubation jar.

The ideal gas law was first used to determine the moles of gas initially present in the container:

$$n = \frac{p \times V}{R \times T} \tag{3.1a}$$

where n = moles of gas, p = pressure, V = volume of the container, R = 0.082058 L atm mol^{-1} K^{-1} (ideal gas constant), and T = temperature. To provide an example, the calculations for jar C in the experiments performed in Table 3.1 are detailed below. The jar has a volume of 177.05 mL and contained 0.07622 mg (9.073×10^{-7} mol) of solid $NaHCO_3$ at an ambient pressure of 0.9891 atm and temperature of 294.4 K. The moles of gas initially present in the container are:

$$n = \frac{0.9891\ atm \times 0.17705\ L}{0.082058\ L\ atm\ mol^{-1}K^{-1} \times 294.4\ K} = 0.007249\ mol \quad (3.1b)$$

5 mL of air were then removed from the container using a gas-tight syringe to measure the background CO_2 concentration, resulting in a change in volume of the system:

$$V_1 = V + 0.005\ L \quad (3.2a)$$

where V_1 is the sum of the volume of the container and the volume of the syringe. For this particular jar,

$$V_1 = 0.17705\ L + 0.005\ L = 0.18205\ L \quad (3.2b)$$

A new pressure of the system was calculated based on the change in volume:

$$p_1 = \frac{n \times R \times T}{V_1} \quad (3.3a)$$

Where p_1 is the new system pressure. For the above example,

$$p_1 = \frac{0.007249\ mol \times 0.082058\ L\ atm\ mol^{-1}K^{-1} \times 294.4\ K}{0.18205\ L} = 0.9619\ atm \quad (3.3b)$$

This pressure was then used to calculate the moles of air removed from the container via the 5mL syringe:

$$n_1 = \frac{p_1 \times 0.005\ L}{R \times T} \quad (3.4a)$$

where n_1 = the moles of air in the 5mL syringe. For this example,

$$n_1 = \frac{0.9619\ atm \times 0.005\ L}{0.082058\ L\ atm\ mol^{-1}K^{-1} \times 294.4\ K} = 1.991 \times 10^{-4}\ mol \quad (3.4b)$$

The new moles of air in the incubation jar, n_2, was calculated via subtraction:

$$n_2 = n - n_1 \quad (3.5a)$$

In this system:

$$n_2 = 0.007249\ mol - 1.991 \times 10^{-4}\ mol = 0.007050\ mol \quad (3.5b)$$

A new pressure inside of the jar, p_2, was then calculated:

$$p_2 = \frac{n_2 \times R \times T}{V} \quad (3.6a)$$

$$p_2 = \frac{0.007050\ mol \times 0.082058\ L\ atm\ mol^{-1}K^{-1} \times 294.4\ K}{0.17705\ L} = 0.9619\ atm \quad (3.6b)$$

The background CO_2 concentration, $[CO_2]_b$, was measured in this jar to be 500 ppmv. 2.2 mL of 1M HCl was then added to the jar, resulting in a new container volume, V_3:

$$V_3 = V - V_{HCl} \quad (3.7a)$$

$$V_3 = 0.17705\ L - 0.0022\ L = 0.17485\ L \quad (3.7b)$$

After sufficient time was provided for the acid to react with the carbonate sample, 5 mL of air were again removed for CO_2 measurements, resulting in V_4, the volume of the container containing acid and with the 5 mL syringe in place:

$$V_4 = V_3 + 0.005\ L \quad (3.8a)$$

$$V_4 = 0.17485\ L + 0.005\ L = 0.17985\ L \quad (3.8b)$$

A new pressure inside of the jar, p_3, was calculated:

$$p_3 = \frac{n_2 \times R \times T}{V_4} \quad (3.9a)$$

$$p_3 = \frac{0.007050\ mol \times 0.082058\ L\ atm\ mol^{-1}K^{-1} \times 294.4\ K}{0.17985\ L} = 0.9470\ atm \quad (3.9b)$$

The moles of air removed by the 5 mL syringe during sampling, n_3, were calculated,

$$n_3 = \frac{p_3 \times 0.005\ L}{R \times T} \quad (3.10a)$$

$$n_3 = \frac{0.9470\ atm \times 0.005\ L}{0.082058\ L\ atm\ mol^{-1}K^{-1} \times 294.4\ K} = 1.960 \times 10^{-4}\ mol \quad (3.10b)$$

followed by the moles of air remining in the jar, n_4,

$$n_4 = n_2 - n_3 \tag{3.11a}$$

$$n_4 = 0.007050\ mol - 1.960 \times 10^{-4}\ mol = 0.006854\ mol \tag{3.11b}$$

assuming that the moles of CO_2 gas formed would have a minimal contribution to the total moles n_2 or n_4. The new pressure in the container, p_4, was then determined:

$$p_4 = \frac{n_4 \times R \times T}{V_3} \tag{3.12a}$$

$$p_4 = \frac{0.006854\ mol \times 0.082058\ L\ atm\ mol^{-1}K^{-1} \times 294.4\ K}{0.17485\ L} = 0.9470\ atm \tag{3.12b}$$

The concentration of CO_2 gas in the system, $[CO_2]_1$, was measured as 596 ppmv. The concentration of CO_2 that formed in the reaction $[CO_2]_f$, was calculated,

$$[CO_2]_f = [CO_2]_1 - [CO_2]_b \tag{3.13a}$$

$$[CO_2]_f = 596\ ppmv - 500\ ppmv = 96\ ppmv \tag{3.13b}$$

and the moles of CO_2 formed were determined:

$$n_{CO_2} = \frac{[CO_2]_f \times 10^{-6} \times p_3 \times V_4}{R \times T} \tag{3.14a}$$

$$n_{CO_2} = \frac{96\ ppmv \times 10^{-6} \times 0.9470\ atm \times 0.17985\ L}{0.082058\ L\ atm\ mol^{-1}K^{-1} \times 294.4\ K} = 6.769 \times 10^{-7}\ mol \tag{3.14b}$$

If subsequent measurements of $[CO_2]_f$ were made, the moles of formed CO_2 that were removed by the syringe were calculated, and this value was added to the next calculation of n_{CO2} to account for sampling loss:

$$n_{CO_2}sampled = \frac{0.005\ L}{V_4} \times n_{CO_2} \tag{3.15a}$$

$$n_{CO_2}sampled = \frac{0.005\ L}{0.17985\ L} \times 6.768 \times 10^{-7}\ mol = 1.882 \times 10^{-8}\ mol \tag{3.15b}$$

Optimization of experimental parameters.

Before performing measurements of the carbonate concentration on atmospheric particulate matter samples, several components of the setup needed to be tested to ensure the integrity of the method. First, each jar was tested to ensure that the seals around the lid and septa were adequate. Then, the optimal time for the carbonate to react with 1M hydrochloric acid (referred to hereafter as the incubation time) was developed. The volume of acid to be used in each experiment was then determined.

For all method development tests, a mixture of sodium chloride (crystal, 99%, Mallinckrodt Chemicals) and sodium bicarbonate (ACS Reagent, 99.7-100.3%, Sigma Aldrich) was prepared by homogenizing 5.2655g of NaCl and 0.0391g of $NaHCO_3$ using a mortar and pestle, resulting in a powder of 0.51 mol %/0.74 mass % of $NaHCO_3$. This sodium bicarbonate mixture was used in all tests to optimize the experimental conditions.

Incubation jar seal tests.

It was critical to select incubation jars that were adequately sealed from ambient conditions. Among the most likely causes of a poor seal would be an ill-fitting lid; since lids were not specifically assigned to incubation jars, eleven jars and lids were randomly selected and paired. Once the volumes of the jars were determined, approximately 4-15 mg of the 0.74 mass % $NaHCO_3$ standard mixture was added to the petri dish placed inside of each jar. The background CO_2 concentration was measured, and 1M HCl was added to each jar. The jars were gently swirled to ensure that all of the solid came into contact with the acid and that any bubbles of CO_2 gas were released from within the aqueous phase. Three measurements of CO_2 were made in 5-minute increments, and a fourth was made after 2 hours (Table 3.1).

Table 3.1

Experiments performed on eleven containers to determine those that were most suitable for CO_2 pressure measurements.

Incubation Jar Number	Ambient Pressure (atm)	Ambient Temperature (K)	Amount of $NaHCO_3$ ($\times 10^{-7}$ mol)	Volume of Container (L)	Background CO_2 Concentration (ppmv)	Volume 1M HCl added (L)	5 Minute Incubation		
							CO_2 Pressure (ppmv)	Moles CO_2 Formed ($\times 10^{-7}$ mol)	Relative Error (%)
A	0.9891	294.4	12.51	0.1798	524	0.0028	645	8.666	-30.72
B	0.9891	294.4	3.700	0.1754	474	0.0026	515	2.864	-22.59
C	0.9891	294.4	9.073	0.1771	500	0.0022	596	6.769	-25.39
D	0.9891	294.4	6.342	0.1783	471	0.0026	528	4.049	-36.16
E	0.9891	294.4	6.518	0.1759	505	0.0028	566	4.272	-34.46
F	0.9891	294.4	3.435	0.1795	480	0.0028	514	2.431	-29.23
G	0.9891	294.4	9.689	0.1787	500	0.0028	591	6.479	-33.13
H	0.9891	294.4	5.990	0.1790	485	0.0028	534	3.493	-41.68
I	0.9891	294.4	8.632	0.1778	483	0.0028	567	5.948	-31.10
J	0.9891	294.4	5.109	0.1776	475	0.0028	532	4.033	-21.07
K	0.9891	294.4	8.985	0.1773	474	0.0028	568	6.639	-26.11

Table 3.1 (continued)

Experiments performed on eleven containers to determine those that were most suitable for CO_2 pressure measurements.

Incubation Jar Number	10 Minute Incubation			15 Minute Incubation			2 Hour Incubation		
	CO_2 Pressure (ppmv)	Moles CO_2 Formed ($\times 10^{-7}$ mol)	Relative Error (%)	CO_2 Pressure (ppmv)	Moles CO_2 Formed ($\times 10^{-7}$ mol)	Relative Error (%)	CO_2 Pressure (ppmv)	Moles CO_2 Formed ($\times 10^{-7}$ mol)	Relative Error (%)
A	643	8.527	-31.83	644	8.594	-31.29	652	9.121	-27.08
B	515	2.864	-22.59	514	2.798	-24.37	514	2.798	-24.37
C	596	6.769	-25.39	596	6.769	-25.39	584	5.991	-33.96
D	529	4.118	-35.07	530	4.185	-34.01	540	4.838	-23.72
E	564	4.136	-36.55	563	4.070	-37.56	563	4.070	-37.56
F	515	2.501	-27.21	514	2.433	-29.18	515	2.499	-27.26
G	586	6.133	-36.71	584	5.998	-38.10	504	0.762	-92.14
H	534	3.493	-41.68	534	3.493	-41.68	543	4.083	-31.83
I	567	5.948	-31.10	565	5.814	-32.65	567	5.944	-31.14
J	532	4.033	-21.07	531	3.966	-22.38	540	4.551	-10.92
K	568	6.639	-26.11	568	6.639	-26.11	572	6.899	-23.22

Determination of incubation time.

Three separate trials using three incubation jars selected for best performance were done to determine a suitable incubation time. Enough time should be allowed for the carbonate to fully react with the acid, but the jars should be sampled soon enough to limit any possibility of equilibration of CO_2 with ambient conditions. For each trial, approximately 4-5 mg of the 0.74 mass % $NaHCO_3$ mixture was spread onto each of three prebaked (600°C overnight) 25 mm round quartz fiber filters. Each filter was placed onto a petri dish and sealed in an incubation jar. The background CO_2 concentration was measured, and 3 mL of 1M HCl was added to each jar, making sure to saturate the filter. The jar was gently swirled every few minutes to ensure complete release of CO_2 bubbles from the aqueous phase. Measurements of CO_2 were made at different time intervals, detailed in Figure 3.2 and Tables A1-A3 in the Appendix.

Volume of hydrochloric acid.

Hydrochloric acid was chosen to acidify the samples, since this acid is commonly used to fume atmospheric particulate matter samples to remove CC for thermal/optical analysis, as well as to measure the carbonate present in soils and sediments (Chow & Watson, 2002; Clarke & Karani, 1992; Salomons, 1975). 1M HCl was chosen over concentrated HCl to ensure safer solvent transfer. Enough acid to saturate the filters was needed, while still keeping the volume low enough to minimize the equilibration of CO_2 with the aqueous phase. It was observed that 0.5 mL of 1M HCl was enough to saturate one round 25 mm quartz filter (with an area of 4.9 cm^2). However, since it was anticipated that aerosol samples may require a sample with a larger area to be used for analysis, 3 mL of 1M HCl was used.

The Henry's law constant for CO_2 with water as a solvent has been reported to be between 3.1 – 4.5 x 10^{-4} mol m^{-3} Pa^{-1} at 298.15 K (Sander, 2015). Using these values and the established experimental parameters, it was calculated that less than 2% of the CO_2 formed would partition into the aqueous phase in all trials; since HCl is used as the solvent here (confirmed to be in excess by a litmus paper test at the end of each experiment), the actual solubility of CO_2 would be expected to be even smaller. Therefore, the partitioning of CO_2 into the aqueous phase was not accounted for in these experiments.

Atmospheric particulate matter sample collection.

A particulate matter sample collected on the Tempe campus of Arizona State University was analyzed. The sample was collected over four days (March 27-30, 2014) using a Tisch high-volume aerosol sampler (1.13 m^3/min) equipped with a size-fractionating stage to collect $PM_{2.5}$ (particulate matter with an aerodynamic diameter of 2.5 μm and below) and $PM_{>2.5}$ (particulate matter with an aerodynamic diameter greater than 2.5 μm) onto quartz fiber filters.

Atmospheric particulate matter sample analysis.

Large atmospheric particles are expected to contain a higher concentration of carbonate than small particles, since carbonate mineral dust is mechanically generated and is found in the coarse size mode (Garbaras et al., 2009; López-Veneroni, 2009; Masalaite et al., 2015). Therefore, the $PM_{>2.5}$ filters were used to test the reproducibility of this method. For the first trial, three 1.5 cm^2 punches were taken from three different locations on the filter and were placed into a petri dish. The petri dish was placed into a jar, the jar was closed, the background CO_2 concentration was measured, and 3 mL of 1M

HCl was added. The jar was gently swirled every few minutes to ensure complete release of CO_2 gas from the aqueous phase. The CO_2 concentration was measured after 20 minutes. This procedure was repeated with two other jars, using two 1.5 cm^2 filter punches instead of three since the amount of CO_2 formed in the first jar was high (235 ppmv). This procedure was repeated in additional trials using two 1.5 cm^2 punches in each of the three incubation jars.

Atmospheric particulate matter samples collected in six size fractions were also analyzed using this method. Sampling details for these filters are discussed in Chapter 4. The area of filter used to analyze these samples varied from 3 – 6 cm^2, which was estimated based upon the known concentration of total carbon on the filters (Table 3.3). The amount of CO_2 formed from acidification of these filters was measured using the same technique used for the $PM_{>2.5}$ filter.

Results and Discussion

Incubation jar seal tests.

Before any tests for accuracy could be performed, a set of incubation jars needed to be chosen. The major concern in using these containers for gas measurements would be a leak resulting from a poor-fitting lid, a septum that is not properly sealed into the side of a jar, or an over-pierced septum. Eleven containers were initially tested using a known mass of sodium bicarbonate to react with acid. Each jar was sampled four times over 2 hours to determine which jars would result in the lowest percent relative error from the expected amount of CO_2 to be formed, which jars would maintain the internal CO_2 pressure after multiple samplings, and which jars would result in the most consistent results. As seen in Table 3.1, the results varied widely among the jars: The relative error

after 5 minutes of incubation ranged from 21 – 42% below the actual amount of bicarbonate present in the jar. Two jars did not maintain internal pressure over 2 hours, while five jars showed an increase of 4 – 10 ppmv of CO_2. The [CO_2] in the remaining four jars remained consistent within 2 ppmv over 2 hours. Because of these irregularities, it was decided that two hours of incubation is likely too long for this type of experiment. In all jars aside from jar G, the measured amount of CO_2 formed was consistent over 15 minutes of incubation. The three jars to be used in subsequent trials (jars C, J, and K) were chosen among those that exhibited lower relative errors and the most consistent results for the first three measurements.

Determination of incubation time.

After choosing the jars to perform acidification experiments, an incubation time was determined. Enough time for the acid to react with carbonate was necessary to ensure that the method would be both accurate and reproducible. Additionally, since the bicarbonate standard was spread onto quartz sampling filters instead of being added directly to the petri dish, enough time was needed to ensure that the carbonate embedded in the filter could still react efficiently with the acid.

Three separate trials were performed using all three jars so that a variety of incubation times could be explored (Figure 3.2). In the first trial, three sample measurements were taken from each jar 5, 15, and 25 minutes after acid addition, and the fourth after four hours (Figure 3.2a). Between the first and third measurements, the concentration of CO_2 decreased by up to 10 ppmv. It is apparent in these trials that jars C and J performed poorly, with respective errors of -41% and -38% after 5 minutes of incubation, which became worse over time. Jar K had a low relative error in comparison

to the other jars (-5%), but it still lost CO_2 over time. These issues may be attributed to a high CO_2 concentration inside the jar (Table A1) before addition of acid relative to the ambient concentration, which ranged from approximately 420-480 ppmv depending on the activity in the room. The elevated CO_2 pressures in the jars were likely caused by the experimenter's breath entering the jars just before they were closed, causing a gradient in CO_2 partial pressures between the jar and atmosphere and accelerating the equilibration of CO_2 with the ambient pressure. It was therefore important to ensure that the background CO_2 pressure inside of the jars was not elevated relative to the ambient CO_2 pressure.

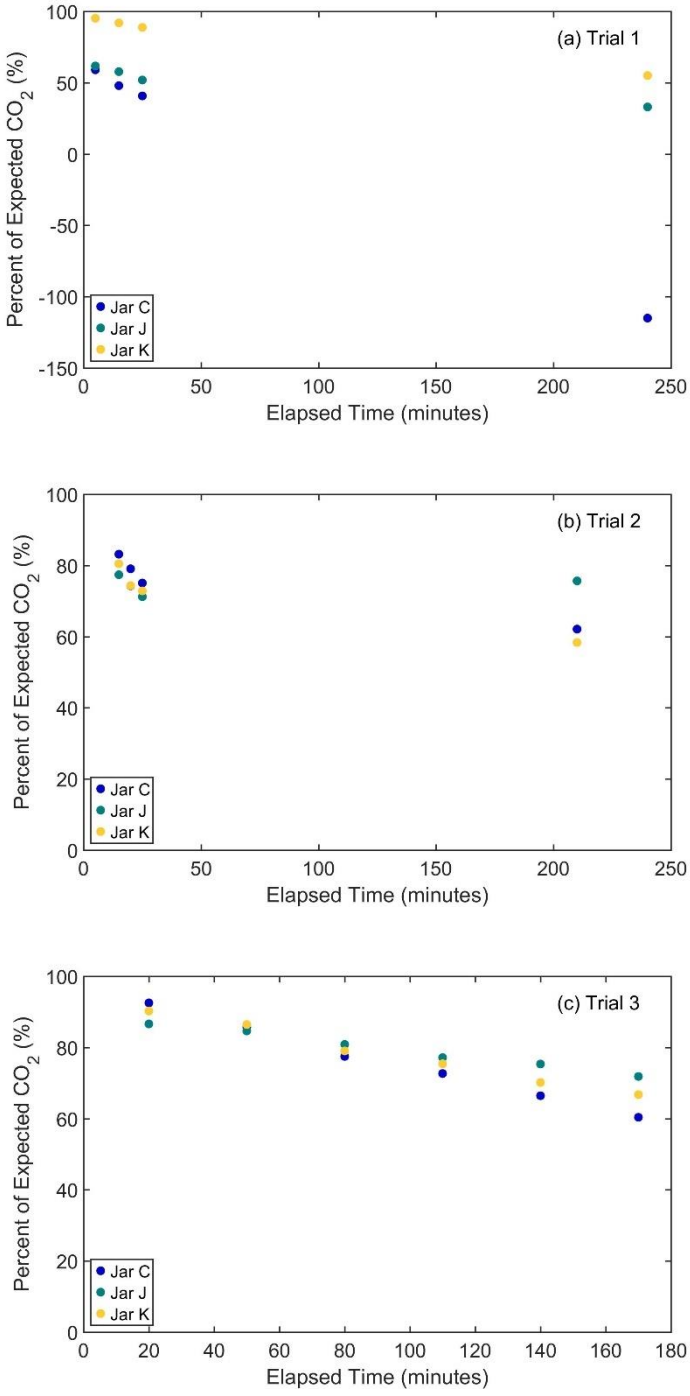

Figure 3.2. Plots of the three trials performed to determine the incubation time needed for the carbonate present on the quartz filters to react with 1M HCl and form CO_2. In all three trials, the first measurement taken had the highest concentration of measured CO_2.

It was also noted during this trial that gas bubbles were still evolving from the filters about 10 minutes after acidification. It is possible that the bicarbonate standard becomes engrained in the filter and is slower to react with the acid than when it is loose in the petri dish. Therefore, an incubation time greater than 10 minutes should be used to ensure complete reaction of bicarbonate with acid and release of CO_2 from the filter.

The second trial was used to test changes in CO_2 measurements over short increments and to again see how the jars faired when sitting for several hours after bicarbonate acidification. Sodium bicarbonate standard was again spread onto a quartz filter and acidified in the jars, ensuring that the initial CO_2 pressures inside of the jars were not excessively elevated relative to the ambient pressure. CO_2 measurements were made 15, 20, and 25 minutes after acid addition, and again after 3.5 hours. Results are shown in Figure 3.2b. Between the first and third measurements of CO_2 (at 15 and 25 minutes after HCl addition), the concentration of CO_2 decreased by up to 6 ppmv. However, the relative error in the measurement of CO_2 formed remained under 30% for all trials. Since the highest CO_2 pressure was recorded at 15 minutes, it can be assumed that the reaction is complete at this time point. After 3.5 hours, an additional 10 ppmv of CO_2 was lost from jars C and K, further emphasizing that incubation over several hours is not ideal for this system.

In the final trial, incubation times from 20-170 minutes in 30-minute increments were tested to determine if there were notable changes in measured CO_2 within the first hour of acid addition, and to again assess if the jars could stay pressurized over several hours. As shown in Figure 3.2c, the highest CO_2 pressure in each jar was measured 20 minutes after acid addition, with all relative errors of CO_2 concentration within 15% of

the expected concentration of CO_2. Between each subsequent measurement, 1 – 5 ppmv of CO_2 was lost, and relative errors for jars C, J, and K increased by the end of the trial to 39.6%, 28.1%, and 33.2%, respectively, below the expected concentration of CO_2. These results indicate that it would be reasonable to sample CO_2 from the reaction of sodium bicarbonate and HCl 20 minutes after the addition of HCl, since the reaction should be complete at this point and later sampling times indicate that CO_2 is escaping the jars over time.

Based upon these optimization tests, jars C, J, and K were deemed adequate for use with atmospheric particulate matter samples. 3 mL of 1M HCl will be added to each jar, and the sample will react with the acid for 20 minutes, at which point the measured concentration of CO_2 is expected to be within 15% of the actual value.

Application to atmospheric particulate matter samples.

A sample of atmospheric particulate matter collected on the Arizona State University Tempe Campus from March 27-30, 2014 was analyzed. The high-volume sampler was equipped with a size-fractionating stage to collect $PM_{2.5}$ and $PM_{>2.5}$; the coarse PM sample ($PM_{>2.5}$) was analyzed, since common sources of carbonate are expected to be found in the coarse mode (Garbaras et al., 2009; López-Veneroni, 2009; Masalaite et al., 2015). In the first trial, 4.5 cm^2 of the filter was used, and the CO_2 concentration measured 20 minutes after acid addition was 687 ppmv. Since the reproducibility tests using sodium bicarbonate results in measured CO_2 concentrations near 500 ppmv, the amount of filter was reduced in successive trials to 3 cm^2. Results are shown in Table 3.2.

Table 3.2

Experiments performed on aerosol particulate matter samples ($PM_{>2.5}$) to assess reproducibility on real samples.

Incubation Jar Number	Ambient Pressure (atm)	Ambient Temperature (K)	Amount of Sample Used (cm^2)	Volume of Container (L)	Background CO_2 Concentration (ppmv)	Volume 1M HCl added (L)	20 Minute Incubation		
							CO_2 Pressure (ppmv)	Moles CO_2 Formed ($\times 10^{-7}$ mol)	Carbonate Carbon Concentration (µgC/cm^2)
C	0.9905	294.5	4.5	0.1771	452	0.003	687	16.59	3.9
J	0.9905	294.4	3.0	0.1776	449	0.003	612	11.55	4.0
K	0.9905	294.4	3.0	0.1773	448	0.003	612	11.60	4.7
C	0.9946	294.4	3.0	0.1771	520	0.003	658	9.785	4.4
J	0.9946	294.4	3.0	0.1776	435	0.003	577	10.10	4.6
K	0.9946	294.4	3.0	0.1773	434	0.003	599	11.72	4.6

The average concentration of CC on this aerosol sample was found to be 4.4 μgC/cm^2, with a standard deviation of 0.3 μgC/cm^2 and a range of 3.9 – 4.7 μgC/cm^2 (Table 3.2). This is equivalent to 86 ± 6 ngC/m^3 in $PM_{>2.5}$ collected over the four-day sampling period. Other studies have found ranges of carbonate carbon in $PM_{2.5}$ from less than 100 ngC/m^3 to 420 ngC/m^3 among 58 sites in the IMPROVE network (Chow & Watson, 2002). $PM_{1.5}$ was found to contain 100 – 300 ngC/m^3 in a remote background location in central Sweden and 300 – 3000 ngC/m^3 in the Po Valley; CC was not detected in $PM_{1.5}$ collected in a third rural site on the Great Hungarian Plateau (Zappoli et al., 1999). Overall, there is good precision and reproducibility among the replicate $PM_{>2.5}$ samples, showing that this method could be promising as a way to measure CC on aerosol filters with low or inhomogeneous sample loads.

Once this method was successfully tested on an atmospheric particulate matter sample, twelve size-segregated filters collected at the same site were also analyzed for [CC]. These samples were collected during the size-segregated particle study described in detail in Chapter 4. Table 3.3 summarizes the results of these analyses. The amount of carbonate collected on each filter varied from 0.65 ± 0.02 μg/cm^2 to 3.8 ± 0.3 μg/cm^2, and the percent of total carbon that was carbonate ranged from 1.1 ± 0.2% to 10 ± 1%. The amount of carbonate mainly varied based upon the size fraction, with particles in the size range 3 μm < d_p < 7.2 μm containing the highest percent of carbonate relative to total carbon. These values are similar to a previous study which determined that coarse PM ($PM_{10-2.5}$) in Phoenix contains an average of 9% CC by thermal optical analysis of acidified filters (Turner et al., 2014). The standard deviation of replicate measurements ranged from 2 – 22% of the average carbonate concentration, with a median of 8%,

showing again that this method of quantifying CC is reproducible and results in good measurement precision.

Table 3.3

*Experiments performed on aerosol particulate matter samples to assess reproducibility on real samples. * = 4.5 cm^2 were used in one replicate, and 3 cm^2 were used in five replicates. ** = Total carbon was not measured.*

Sample Description	Amount of Sample Used (cm^2)	Carbonate Carbon Concentration ($\mu gC/cm^2$)	Standard Deviation ($\mu gC/cm^2$)	Number of Replicates	Carbonate : Total Carbon (%)	Uncertainty (%)
$PM_{>2.5}$	*	4.4	0.3	6	**	**
January $PM_{>7.2}$	3	3.8	0.3	3	4.4	0.4
January $PM_{3\text{-}7.2}$	3	3.4	0.2	3	7.4	0.7
January $PM_{1.5\text{-}3}$	3	1.7	0.3	4	5.2	0.9
January $PM_{0.95\text{-}1.5}$	3	1.0	0.2	4	2.2	0.4
January $PM_{0.49\text{-}0.95}$	4.5	0.65	0.02	3	2.3	0.1
January $PM_{<0.49}$	6	1.2	0.3	3	1.1	0.2
April $PM_{3\text{-}7.2}$	4.5	2.9	0.3	3	10	1
April $PM_{<0.49}$	6	3.7	0.2	3	5.5	0.4
June $PM_{<0.49}$	6	3.6	0.5	3	5.1	0.8
October $PM_{>7.2}$	4.5	3.01	0.06	3	5.7	0.3
October $PM_{3\text{-}7.2}$	4.5	3.0	0.1	3	7.1	0.5
October $PM_{<0.49}$	6	1.90	0.09	3	2.6	0.2

Considerations for application to particulate matter sample collection.

In order to apply this carbonate quantification method to other particulate matter samples, several considerations must be made in terms of sample collection, including the filter size, sampler type, and sampling time. The smallest amount of CO_2 liberated from a

particulate matter sample will be used as a lower limit of detection: the particle size fraction 0.49 µm < d_p < 0.95 µm collected in January yielded an average of 34 ppmv of CO_2 upon acidification. A petri dish placed into an incubation jar has an area of 24 cm^2; this is the maximum area of filter that can be tested at a time. Using equations 1 – 14 and the experimental parameters for this sample, a filter of size 24 cm^2 that liberates 34 ppmv of CO_2 upon acidification would contain 0.12 µgC/cm^2 of carbonate. Assuming that sample collection is taking place in Tempe, it is reasonable to presume that TC in Tempe will contain somewhere between 1 – 10% CC; therefore, the TC collected on this filter would range from 1.2 – 12 µgC/cm^2. The average concentration of TC in $PM_{2.5}$ in Tempe is 4.313 µgC/m^3 (Upadhyay et al., 2011). Using this information, if a high-volume sampler with sampling velocity of 1.13 m^3/min is used for collection, then enough particulate matter will be collected for carbonate analysis between 6 minutes (if CC is 10% of TC) and 60 minutes (if CC is 1% of TC) of sampling time. Carbonate can therefore be measured even when the sampling time is relatively short, provided that enough filter area is available for triplicate measurements.

The sampling time needed to measure CC concentration does, however, increase if a low-volume particulate matter sampler is used. As an example, in Chapter 5, $PM_{2.5}$ is collected using a low-volume sampler with a sampling velocity of 2.3 m^3/h and a filter deposition area of 12.6 cm^2. If the entire filter is used to quantify CC, and 34 ppmv of CO_2 is again liberated from the filter upon acidification, the filter will need to contain 0.23 µgC/cm^2 of carbonate. Again assuming that 1 – 10% of TC in Tempe is carbonate, the TC loaded onto the filter would range from 2.3 – 23 µgC/cm^2. Using this low-volume sampler, enough particulate matter will be collected for carbonate analysis between 3

hours (if CC is 10% of TC) and 30 hours (if CC is 1% of TC) of sampling time. This, again, assumes that the entire sample will be used in analysis. Ideally, triplicate measurements will be made, increasing the required sampling time threefold.

Implications of carbonates on the $\delta^{13}C$ of aerosol particulate matter.

As seen in the aerosol particulate matter data presented in this chapter, the TC mass in Tempe could be comprised of up to 10% carbonate. In non-desert environments, the concentration of carbonate would be less than 10%; low concentrations of carbonate would deem its presence negligible in most studies (Chow & Watson, 2002). However, when measuring carbon isotopes, even a small percent of carbonate could make a significant difference in the isotopic composition of total carbon ($\delta^{13}C_{TC}$). As discussed in Chapter 2, carbonate is enriched in $\delta^{13}C$ relative to other biogenic and anthropogenic primary emission sources. As an example, the TC of the $PM_{3\text{-}7.2}$ sample collected in January in Tempe is 7.4% carbonate, and the presence of carbonate causes this sample to be enriched in $\delta^{13}C_{TC}$ by 1.4‰. This is not unique to Tempe: The contribution of Saharan dust to PM_{10} in Granada, Spain has been attributed to higher $\delta^{13}C_{TC}$ values due to its carbonate content (Mladenov et al., 2011).The ability to quantify carbonate in all types of aerosol samples is therefore necessary for isotopic analyses.

A mass-balance approach may be used to determine whether carbonate could affect the $\delta^{13}C_{TC}$ of a particulate matter sample. The $\delta^{13}C_{TC}$ may be expressed as

$$\delta^{13}C_{TC} = \delta^{13}C_{CC} \times f_{CC} + \delta^{13}C_{OCEC} \times f_{OCEC}, \quad (3.16)$$

where $\delta^{13}C_{CC}$ is the isotopic composition of carbonate, f_{CC} is the fraction of TC that is carbonate, $\delta^{13}C_{OCEC}$ is the combined isotopic composition of organic and elemental

carbon, and f_{OCEC} is the fraction of TC that is organic and elemental carbon. Solving for f_{CC}, this can be rearranged as

$$f_{CC} = (\delta^{13}C_{TC} - \delta^{13}C_{OCEC}) \div (\delta^{13}C_{CC} - \delta^{13}C_{OCEC}), \quad (3.17)$$

where $f_{OCEC} = 1 - f_{CC}$. The difference in $\delta^{13}C_{TC} - \delta^{13}C_{OCEC}$ is dependent on the uncertainty in the measurement of each sample, which is at best 0.2‰; a difference between these measurement would only be significant if the difference is greater than 0.4‰. The difference between $\delta^{13}C_{CC}$ and $\delta^{13}C_{OCEC}$, or $\Delta^{13}C_{CC\text{-}OCEC}$, is dependent on the carbon sources, which will vary by location. A curve can therefore be drawn to determine the critical fraction of carbonate that would need to be present in the sample for it to have a significant effect on $\delta^{13}C_{TC}$ (Figure 3.3), using the equation

$$f_{CC} = (0.4‰) \div (\Delta^{13}C_{CC\text{-}OCEC}). \quad (3.18)$$

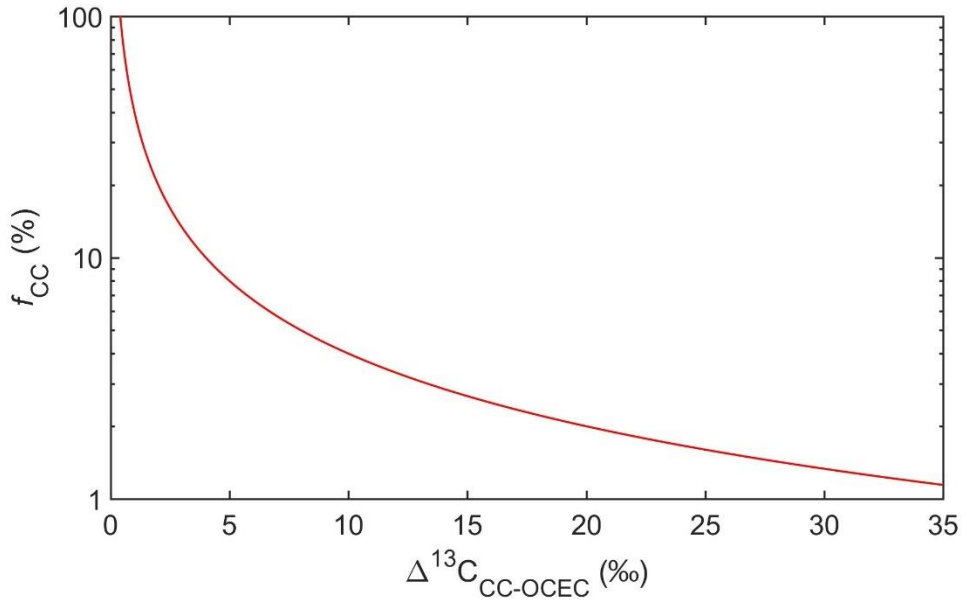

Figure 3.3. A model predicting the percent of carbonate carbon that must make up total carbon for the carbonate to affect the $\delta^{13}C_{TC}$ of a particulate matter sample.

Based on this model, as little as 1.1% of carbonate in TC can have a significant effect on the $\delta^{13}C_{TC}$ of a particulate matter sample, if the $\Delta^{13}C_{CC\text{-}OCEC}$ is very large (i.e., if the $\delta^{13}C_{CC}$ is 0‰ and the $\delta^{13}C_{OCEC}$ is -35‰). In most instances, the $\delta^{13}C_{CC}$ will be in the range of 0 – -10‰, and the $\delta^{13}C_{OCEC}$ will be in the range of -20 – -30‰; within these ranges, it is possible that 1.3 – 4% of carbonate could have an effect on $\delta^{13}C_{TC}$. The ability to measure small fractions of carbonate on all types of particulate matter samples is therefore crucial to fully understand and apportion the sources that contribute to aerosol particulate matter.

Conclusions

A new technique to quantify the carbonate carbon (CC) in atmospheric particulate matter samples has been investigated. In this technique, the amount of CO_2 formed when a sample in a sealed jar is acidified is measured via infrared absorbance, and the moles of CO_2 formed are equated to the moles of carbonate present in the sample. The analysis of a known amount of sodium bicarbonate applied to a filter resulted in a relative error within 15% of the known mass of bicarbonate when measured 20 minutes after acidification. A $PM_{>2.5}$ aerosol filter collected via cascade impaction on a high-volume aerosol sampler yielded good precision, with a CC concentration of 4.4 ± 0.3 μgC/cm^2 for six replicates. Twelve filters containing PM in various size fractions collected in Tempe, AZ were also analyzed in triplicate, with standard deviations ranging from 2 – 22% of the average carbonate concentration. The high precision, accuracy, and reproducibility of this method of CC measurement makes it a good alternative to existing quantification methods.

The concentration of CC loaded onto a filter has been measured as low as 0.65 ± 0.02 μgC/cm^2. By extrapolating this measurement to different particulate matter samplers and filter sizes, it was shown that enough sample to perform carbonate measurements could be collected on a high-volume sampler in 6 – 60 minutes, and on a low-volume sampler in 3 – 30 hours. The short sampling times that could yield results on a high-volume sampler make this method ideal for measuring carbonates during short weather events, such as fogs or dust storms.

This technique allows for the customization of the amount of sample to be analyzed based upon the expected sample load, which is not possible when using a thermal/optical aerosol carbon analyzer (fixed at 1.5 cm^2 or less). It is also possible to obtain better CC measurements on filters that have an irregular or inhomogeneous sample load, and to use filter media other than quartz, such as Teflon, cellulose, or glass, to make CC measurements, addressing limitations of traditional thermal techniques of CC quantification.

While the carbonate in a particulate matter sample is generally found at negligible concentrations and does not interfere with other measurements, low concentrations of carbonate (less than 5% of TC) can affect the $\delta^{13}C_{TC}$ of a particulate matter sample. By using the measured $\delta^{13}C_{TC}$ of a sample and the concentration of CC determined by this method, it can be estimated whether the carbonate causes significant enrichment of $\delta^{13}C_{TC}$ and whether $\delta^{13}C_{CC}$ should be measured and subtracted out of the $\delta^{13}C_{TC}$ through mass balance. Isotopic determinations of both $\delta^{13}C_{CC}$ and $\delta^{13}C_{OCEC}$ will be further discussed in Chapter 4.

CHAPTER 4

SEASONAL VARIATIONS IN THE CARBONACEOUS COMPOSITION OF SIZE-RESOLVED PARTICLES COLLECTED IN TEMPE, ARIZONA

A number of factors can cause variations in the composition of atmospheric particulate matter among size fractions. Coarser particles are formed through mechanical processes, fine particles are formed by nucleation, and aging results in particles in the accumulation range (Seinfeld & Pandis, 2016; Willeke & Whitby, 1975). Since different sources of aerosol particles have distinguishable stable carbon isotopic compositions ($\delta^{13}C$) (Fisseha et al., 2009; Gleason & Kyser, 1984; Moura et al., 2008; Pichlmayer et al., 1998; Rudolph et al., 2003; Widory, 2006; Wozniak et al., 2012, and Chapter 2 of this work), size-segregated PM samples can exhibit different $\delta^{13}C$ values among the size fractions. A source's individual organic components could also have different $\delta^{13}C$ from the bulk source material; for example, the $\delta^{13}C$ of *n*-alkanes from plant leaf waxes are depleted in ^{13}C relative to the bulk sample (Collister et al., 1994). Physical and chemical atmospheric processing can affect a sample's carbon isotopic composition as well, either through equilibrium partitioning among phases or through kinetic processes, both causing isotopic fractionation (Gensch et al., 2014; Goldstein & Shaw, 2003).

Phoenix is an urban desert city that is affected by a multitude of particle sources. The population of Phoenix is estimated to exceed 4.6 million as of 2016, an 11% increase from the 2010 Census ("Annual Estimates of the Resident Population: April 1, 2010 to July 1, 2016," 2018). Anthropogenic particle sources, including vehicle exhaust and residential wood-burning, are elevated in the winter, when the population rises due to part-time residents, and cold overnight temperatures and stagnant wind conditions cause

intense inversion, trapping emissions in the valley (Brown et al., 2007; Ramadan et al., 2000; Solomon & Moyers, 1986). The occurrence of "no-burn days" is common ("Maricopa County Air Quality Department," 2018), especially around holidays in which residential burning and the use of fireworks are prevalent (Upadhyay et al., 2011).

Blown dust is known to be a major source of coarse PM (particles larger than 2.5 μm) in Phoenix, originating from agricultural soil, native desert soil, paved and unpaved road dust, and construction materials (Brown et al., 2007; Cahill, 2013; Lewis et al., 2003; Ramadan et al., 2000; Upadhyay et al., 2011). In addition to resuspended biogenic and anthropogenic emissions, blown dust contributes carbonates to coarse PM (Garbaras et al., 2009; López-Veneroni, 2009; Masalaite et al., 2015). Coarse PM loads can increase in the summer, when dust storms are common occurrences (Raman et al., 2014; Raman et al., 2016).

Considering the variety of sources that can contribute to PM in Phoenix, differences are expected in concentrations of carbonaceous material as well as $\delta^{13}C$ among both seasons and size fractions. However, few studies exist that characterize size-resolved samples using isotopic analysis (Cachier et al., 1989; Masalaite et al., 2015; Sang et al., 2012; Wang et al., 2012). There are some challenges of size-resolved sampling, including the need for long sampling durations which prohibit temporal resolution and the multiplicity of samples to be analyzed with each added size fraction (Cahill, 2013). The characterization of size-resolved particles can be beneficial in understanding the sources and effects of local pollutants, since the degree to which particles enter the human respiratory tract and affect health outcomes is dependent on particle size (Heyder et al., 1986).

In this study, size-resolved PM samples were collected in January, April, June, and October of 2014 in Tempe, Arizona, a city in the East Valley of metropolitan Phoenix. The objective of this study is to determine the seasonal differences in particle composition among six particle size fractions through measurements of the concentration and $\delta^{13}C$ of total carbon (TC), carbonate carbon (CC), and *n*-alkanes. These measurements will be used to evaluate changes in the composition and sources of carbonaceous PM.

Materials and Methods

Sample collection.

Aerosol sampling.

Samples of aerosol PM were collected on the Tempe campus of Arizona State University in January, April, June, and October of 2014. (Table 4.1). The sampling site (hereafter referred to as LSA) is located on the roof of the Life Sciences complex on the main campus of Arizona State University (33.4196, -111.9329, 357 m a.s.l.). This location is surrounded by four major highways (Interstate 10, 3.7 km southwest; U.S. Route 60, 3.8 km to the south; Arizona State Route 101, 3.9 km to the east; and Arizona State Route 202, 1.8 km to the north) (Figure 4.1). LSA is also approximately 6 km southeast of Phoenix Sky Harbor International Airport and 1.3 km south of Tempe Town Lake, a reservoir in the riverbed of the Salt River. Along with the ASU campus, Tempe consists of residential and industrial areas. It is bordered by the cities of Phoenix to the west and Scottsdale to the north, and suburban areas to the east and south. As part of the Sonoran Desert, a significant contribution of mineral dust, including carbonate minerals, is expected in the local aerosol. Collection was performed for one week using a Tisch

high-volume aerosol sampler (1.13 m^3/min), which was equipped with five cascade impactor stages to collect particle size fractions with cutoff diameters of 7.2, 3, 1.5, 0.95, and 0.49 μm, and a backup filter to collect particles of $d_p \leq 0.49$ μm (Herckes et al., 2006). Samples were collected onto prebaked (600°C for a minimum 12 h) quartz fiber filters and were stored in aluminum foil at -20°C. Two field blank filters were collected at the start of each sampling period, using the stage of the backup filter and the filter stage collecting particles in the size range of 0.49 – 0.95 μm, and running the collector for one minute. Field blank filters were analyzed alongside all sample filters. The weather was fair, clear, and consistent over each week-long sampling period, and no significant meteorological events occurred.

Table 4.1

Aerosol sampling details and total carbon analysis results. The uncertainty in the last digit of the TC concentration is shown in parentheses. The uncertainty in all $\delta^{13}C_{TC}$ results is 0.2‰.

Sampling Period	Start Date	End Date	Start Time	End Time	Total Carbon (µg/m^3)				
					<0.49 µm	0.49µm - 0.95µm	0.95µm - 1.5µm	1.5µm - 3µm	3µm - 7.2µm	>7.2µm
January	1/6/2014	1/13/2014	4:34 PM	4:41 PM	3.8(2)	0.30(2)	0.48(3)	0.35(2)	0.50(3)	0.83(4)
April	3/31/2014	4/7/2014	12:34 PM	11:55 AM	2.4(1)	0.17(1)	0.19(1)	0.18(1)	0.30(2)	0.26(2)
June	6/19/2014	6/26/2014	10:23 AM	11:03 AM	2.5(1)	0.19(1)	0.22(1)	0.21(2)	0.24(1)	0.27(1)
October	9/30/2014	10/7/2014	1:49 PM	2:02 PM	2.6(1)	0.20(1)	0.21(1)	0.22(2)	0.45(2)	0.50(3)

Sampling Period	$\delta^{13}C_{TC}$ (‰)					
	<0.49 µm	0.49µm - 0.95µm	0.95µm - 1.5µm	1.5µm - 3µm	3µm - 7.2µm	>7.2µm
January	-24.8	-25.0	-24.9	-24.5	-24.2	-24.8
April	-23.8	-23.5	-23.5	-23.0	-22.5	-23.2
June	-24.0	-23.9	-23.6	-23.2	-22.5	-23.1
October	-24.3	-24.1	-23.8	-23.3	-23.2	-23.8

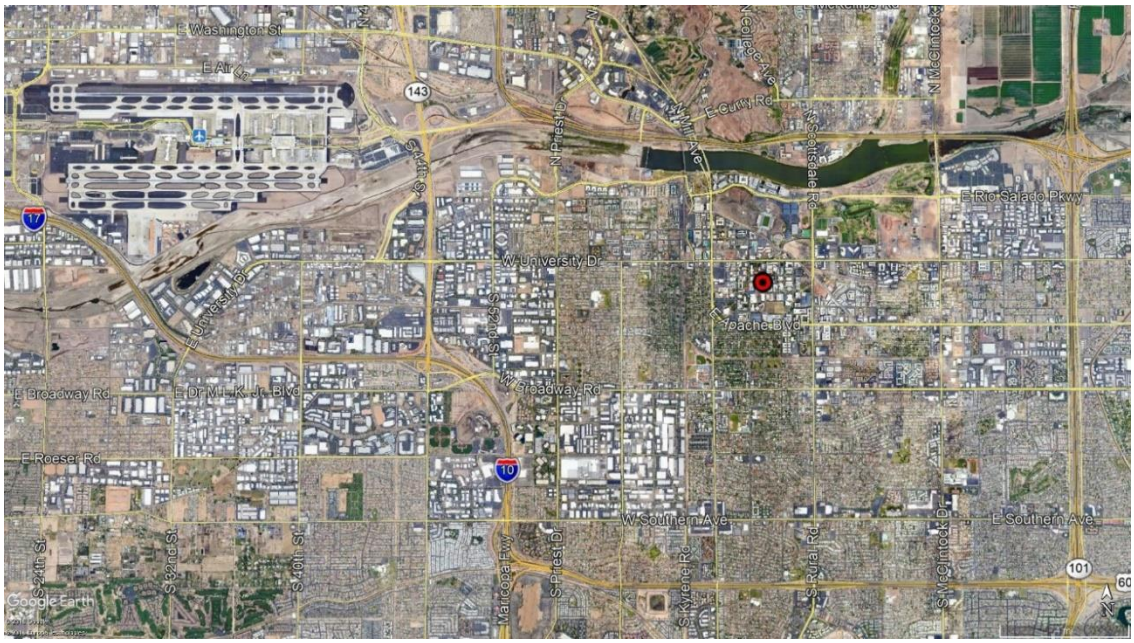

Figure 4.1. Map of sampling site (denoted by red circle with a black dot in the center).

Local source material sampling.

The following potential local source materials of particulate matter were collected and analyzed: Plant material, tailpipe emissions, parking structure emissions, fireplace emissions, biomass burning emissions, and resuspended soil. Details of the sampling and analysis of these materials can be found in Appendix B.

Sample analysis.

Total carbon quantification.

All aerosol samples and field blanks were analyzed by thermal optical transmittance (TOT) for TC concentration using a Sunset Lab OC-EC Aerosol Analyzer (Birch & Cary, 1996). Because slotted filters were used to collect samples on the cascade impactor, the width of the collected sample area on each slot was less than 1 cm. Therefore, due to the absence of samples with uniform particle distribution over 1 cm by

1.5 cm areas, the optics were not used to determine the split between organic/carbonate and elemental carbon.

Aerosol samples and field blanks were analyzed using Sunset's "Quartz" TOT method, with temperature plateaus during OC evolution at 310°C (80 seconds), 475°C (60 seconds), 615°C (60 seconds), and 870°C (90 seconds). During EC evolution, the temperature was held at 550°C, 625°C, 700°C, 775°C, and 850°C for 45 seconds each, with a final hold at 870°C for 120 seconds. Quality control included the analysis of lab blanks, field blanks, replicate samples, and a sucrose standard, which was routinely within 10% of the known concentration.

Alkane quantification.

A portion of each aerosol sample and field blank was cut into pieces of less than 1 cm^2 in size, spiked with equal volumes of deuterated *n*-alkane standards (*n*-$C_{16}D_{34}$, *n*-$C_{20}D_{42}$, *n*-$C_{24}D_{50}$, *n*-$C_{30}D_{62}$, *n*-$C_{36}D_{74}$), extracted thrice in dichloromethane (Optima, Fisher Chemical) using ultrasonic agitation, and concentrated to 250 µl under a stream of UHP nitrogen gas (Brown et al., 2002). Samples were analyzed by gas chromatography/mass spectrometry (GC/MS) using an Agilent Technologies 6890 GC System coupled to an Agilent Technologies 5973 inert Mass Selective Detector in EI mode. *n*-Alkanes were identified and quantified using an *n*-alkane standard mixture consisting of a series of authentic *n*-alkane standards ranging from *n*-$C_{12}H_{26}$ to *n*-$C_{40}H_{82}$ and the five aforementioned deuterated *n*-alkanes. Quantification was performed by manual peak integration on three characteristic *n*-alkane mass peaks of m/z 71, 85, and 99, and m/z 66, 82, and 98 for the deuterated standards.

Carbonate quantification.

Carbonate carbon (CC) concentration was measured via acidification and subsequent measurement of CO_2 released (detailed in Chapter 3 of this work). Quartz filter punches (3-6 cm^2) were first placed into a petri dish that was then placed inside of a polycarbonate Nalgene jar (125 mL) with a rubber septa. The jar was closed, and the background CO_2 pressure in ppm was measured by removing 5 mL of headspace from the jar with a gas-tight syringe and injecting it into a PP Systems EGM-4 CO_2 Monitor. 3 mL of 1M hydrochloric acid (EMD) were added to the jar, and the resulting CO_2 pressure inside of the jar was measured after 20 minutes of incubation. The amount of CO_2 formed via acidification, and hence the concentration of CC on the filters, was calculated, taking into account the changes in pressure and volume inside of the chamber during the experiment, as well as ambient pressure and temperature. Litmus paper was used to estimate the pH of the aqueous solution in the petri dish after the experiment, to ensure that the acid was added in excess. Reported results and uncertainties are the average and standard deviation of triplicate measurements. Due to sample availability, measurements of [CC] were not made for all particle size fractions in April, June, and October; only results for samples collected in January are discussed below.

Total carbon isotope measurements.

The stable carbon isotopic composition of a material is determined by its $^{13}C/^{12}C$ ratio and is expressed in $\delta^{13}C$ (‰) relative to the international standard Vienna Pee Dee Belemnite:

$$\delta^{13}C_{VPDB} = \left(\frac{(^{13}C/^{12}C)_{sample}}{(^{13}C/^{12}C)_{VPDB}} - 1 \right) \times 1000 \quad (4.1)$$

Isotopic measurements for $\delta^{13}C_{VPDB}$ of TC in aerosol PM were performed using a Costech Elemental Analyzer coupled to a Thermo Delta Plus Advantage Isotope Ratio Mass Spectrometer (EA-IRMS). The analytical uncertainty of sample analyzed on this method is reported at 0.2‰, unless the standard deviation of replicate standards is greater than 0.2‰. NIST 2710 (Montana soil) was used as a linearity standard. Three in-house glycine standards were used to perform and verify a two-point calibration from -39.6‰ to 15.7‰.

Compound specific isotope analysis.

Before isotopic analysis of *n*-alkanes, the dichloromethane extracts of the samples were purified by two-dimensional thin layer chromatography (9:1 hexanes (Optima, Fisher Chemical): diethyl ether (ChromaSolv, Sigma-Aldrich), followed by dichloromethane (Optima, Fisher Chemical) using 20 cm x 20 cm x 500 µm silica gel plates (Uniplate, silica gel GF, preparative layer with UV 254, Analtech, Inc.)). The alkanes were visualized using iodine and were scraped from the plate, extracted thrice in hexanes (Optima, Fisher Chemical) using ultrasonic agitation, concentrated to 250 µl under a stream of UHP nitrogen gas, and analyzed by gas chromatography/mass spectrometry (GC/MS) to ensure that *n*-alkanes were present. Compound-specific isotopic analysis of *n*-alkanes was performed on a Thermo GC-C-IRMS system composed of a Trace GC Ultra coupled to a MAT 253 Isotope Ratio Mass Spectrometer through a GC/C III interface. The TLC plates were not precleaned, and contamination was observed that caused coelution with *n*-alkanes smaller than *n*-$C_{24}H_{50}$; isotopic data was therefore only used for *n*-alkanes $C_{24}H_{50}$ and larger. The *n*-alkane standard mixture used in identification and quantitation on GC/MS was also analyzed. The uncertainty in

$\delta^{13}C$ for each *n*-alkane was calculated as the root sum square of the standard deviation of the *n*-alkane in the GC/MS standard calibration series and the *n*-alkane in replicates of an *n*-alkane isotope standard mix supplied by Arndt Schimmelmann of Indiana University. A two-point isotopic calibration was performed and verified using three *n*-hexadecane standards with isotopic compositions of -34.55 ± 0.02‰, -0.60 ± 0.02‰, -10.55 ± 0.03‰, also purchased from Indiana University; the same two-point calibration was used for all *n*-alkane chain lengths.

Carbonate isotope analysis.

Measurements of $\delta^{13}C_{VPDB}$ of CC were performed on a Thermo GasBench coupled to a MAT 253 Isotope Ratio Mass Spectrometer (GasBench-IRMS). Samples and standards (sodium carbonate and sodium bicarbonate) were acidified with of 85% H_3PO_4 (Aldrich) (100 µl for standards, 400 µl for samples to ensure filters were saturated) to release CO_2 from carbonate species for analysis. The analytical uncertainty is reported as the standard deviation of the triplicate analysis of one aerosol sample during this sample sequence. Analysis was performed on available samples whose concentration of CC was such that 10µg of CC was present on less than 4.5cm^2 of filter, so that the samples could fit into the analysis vials and CC could be detected.

HYSPLIT.

Back trajectories were generated using the NOAA HYSPLIT model (online version) (Rolph, Stein, & Stunder, 2017; Stein et al., 2015). The model was initiated at the LSA sampling site at a height of 500m a.g.l., generating 24h trajectories every 24h for each day of sample collection and using NARR (32km) archived meteorological data. Model vertical velocity was used to track vertical motion.

Results and Discussion

Total carbon.

Total carbon concentrations.

The total TC concentration among all size fractions was measured to be 6.3 µg/m^3 in January; 3.5 µg/m^3 in April; 3.7 µg/m^3 in June; and 4.2 µg/m^3 in October. These values are similar to previous TC measurements in Tempe in the winter (4.3 µg/m^3 in $PM_{2.5}$, 5.6 µg/m^3 in PM_{10}, Upadhyay et al., 2011) and at the Phoenix IMPROVE Supersite from April 2001 – October 2003 (average 4.06 µg/m^3 in $PM_{2.5}$, Brown et al., 2007).

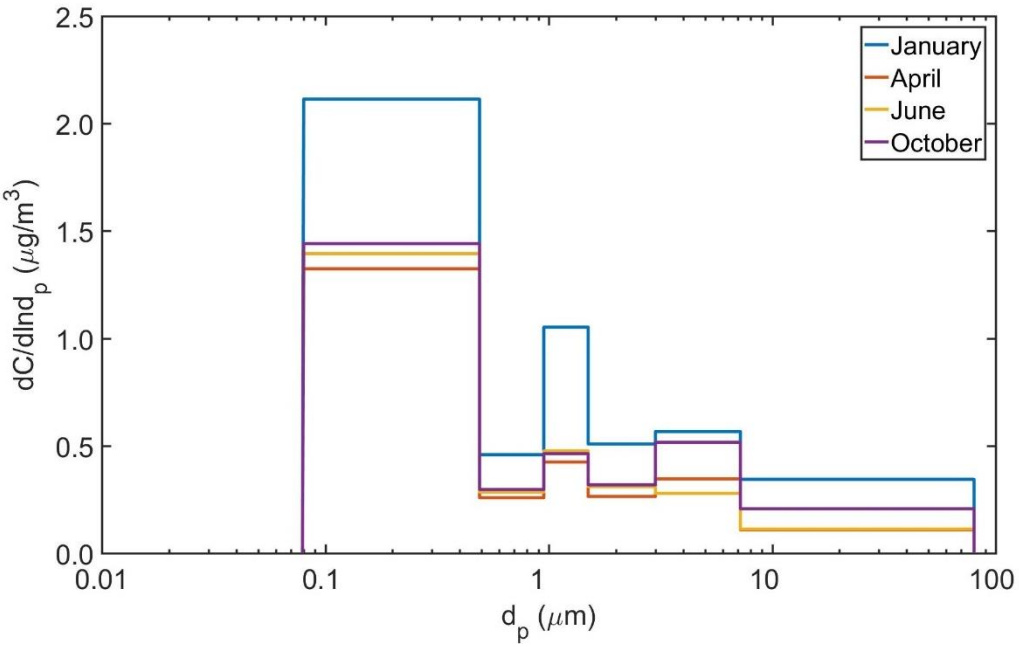

Figure 4.2. Size distributions of total carbon during the four sampling periods. TC concentrations were measured in units of µg/m^3.

Figure 4.2 shows the concentration of TC during all four sampling periods in the six size modes collected. In all sampling periods, at least 60% of the TC mass was found in particles less than 0.49 µm in diameter. A similar study in Tempe (Upadhyay et al., 2011) found 77% of PM_{10} to lie in the $PM_{2.5}$ fraction. The majority of TC was also

observed in particle size fraction $d_p < 0.49$ µm in Yosemite National Park, with 75% of TC in the submicron range (Herckes et al., 2006). Aerosols resulting from combustion have been observed in fine and ultrafine particles; the gasoline marker molecule coronene has been observed in aerosols smaller than 0.3µm in Phoenix (Cahill, 2013).

Several sources have been found to make up the coarse PM in Phoenix, including a prominent contribution of crustal soil, agricultural soil, and resuspended road and construction dusts. Previous studies in Pinal County, AZ, which lies southeast of Phoenix, show that PM_{10} is dominated in the summer by the coarse fraction ($PM_{10-2.5}$), which originated primarily from crustal material; $PM_{2.5}$ accounted for only 10-40% of PM_{10} (Clements et al., 2013). Additionally, increased crustal components in PM_{10} in the spring and fall are attributed to agricultural activity in these seasons (Clements et al., 2014). Crustal material can also contribute to $PM_{2.5}$, as it was found to dominate resuspended soils, comprising 63-100% of $PM_{2.5}$ and 44-91% of PM_{10} (Upadhyay et al., 2015).

Biological materials have been found in coarse PM in Phoenix, with the highest fractions present in the summer (Cahill, 2013). Additionally, both $PM_{2.5}$ and PM_{10} collected in an east Phoenix suburb show significant contributions from the direct injection of primary biological aerosol particles into the atmosphere (Jia & Fraser, 2011).

Higher TC concentrations were observed in all size fractions in January than in other sampling periods. Many factors have been previously observed to affect the concentration of PM in the greater Phoenix area. Brown and coworkers (2007) observed elevated $PM_{2.5}$ concentrations in the winter (December to February) compared to the summer months (March to May) as well as higher than average wintertime organic matter

concentrations. Cooler winter temperatures create a strong, low inversion layer nearly every morning, trapping local emissions in the valley. Additionally, winter emissions are exacerbated by higher populations of tourists and winter residents, contributing to increased carbon- and nitrogen-based emissions associated with motor vehicles and residential wood burning, and resulting in a visible urban haze (Brown et al., 2007; Ramadan et al., 2000; Solomon & Moyers, 1986). Increased gas-to-particle conversion can also elevate $PM_{2.5}$ concentrations (Brown et al., 2007). Cahill (2013) has also observed a seasonal pattern of combustion signatures, dominating in the winter months.

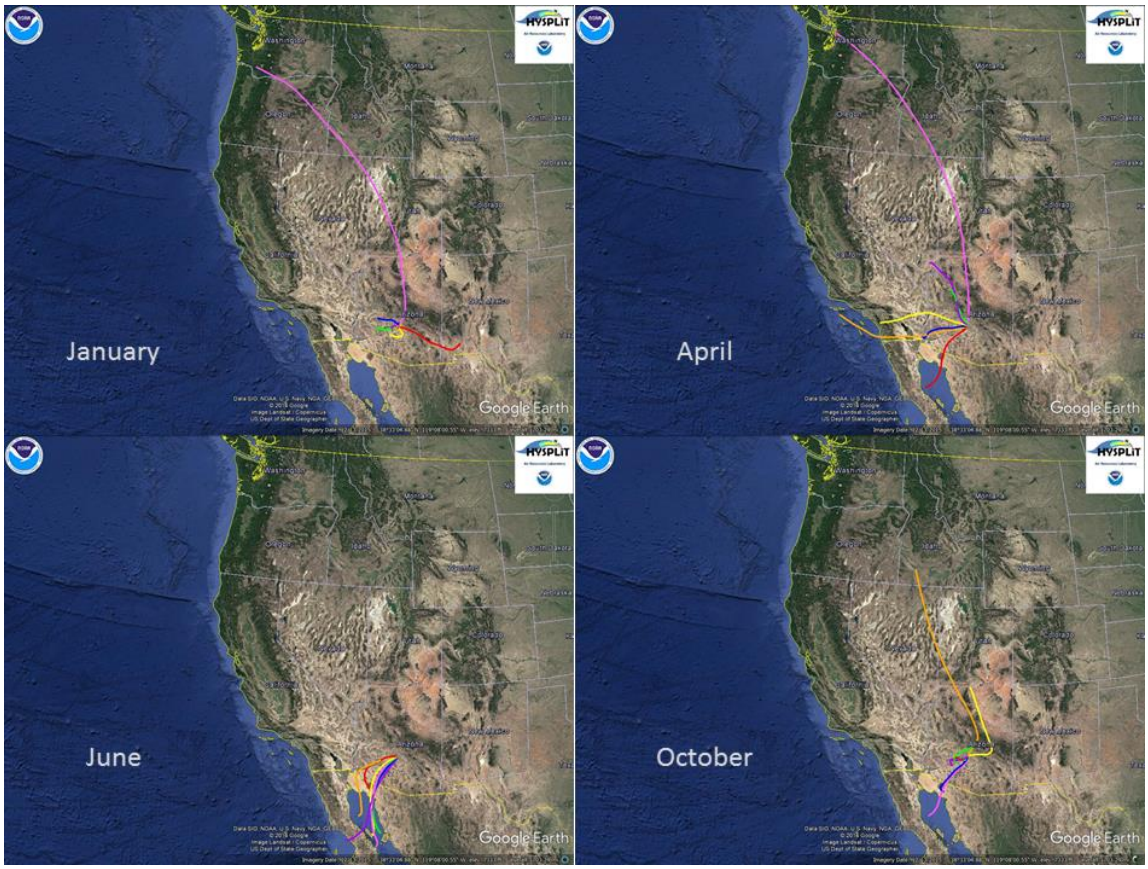

Figure 4.3. 24h HYSPLIT back trajectory analysis. For trajectories in each sampling period, red = day 1; orange = day 2; yellow = day 3; green = day 4; blue = day 5; purple = day 6; pink = day 7.

Analysis of back trajectories during the four sampling periods provides further insight into possible sources of PM (Figure 4.3). There is a dominance of local air mass influence during the sampling week in January, which corresponds to an increase in local anthropogenic emissions at that time. Long-range wind patterns originate mainly from the west in April and from the south in June, as the summer monsoon season begins. Air mass trajectories in October are more variable in both trajectory length and direction, and could imply a mixture of local anthropogenic influences and transported mineral dust and secondary PM.

Stable isotopic composition of total carbon.

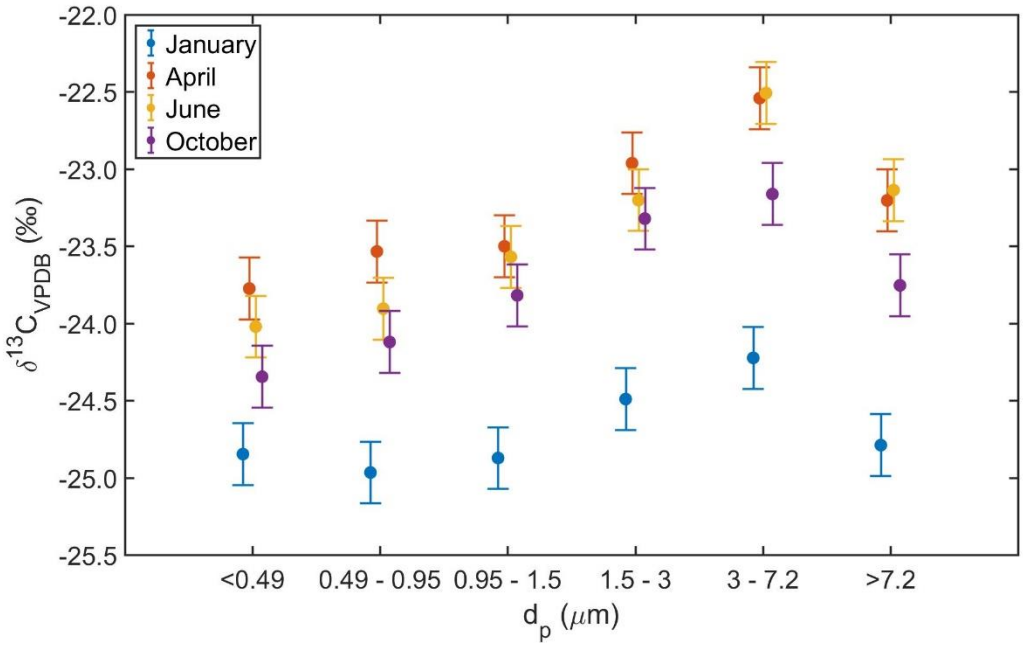

Figure 4.4. Stable carbon isotopic composition of total carbon during the four sampling periods.

The stable carbon isotopic composition of TC ($\delta^{13}C_{TC}$) in all samples is shown in Figure 4.4. Over the course of the campaign, $\delta^{13}C_{TC}$ ranged from -25.0‰ to -22.5‰. This is similar to ranges of $\delta^{13}C_{TC}$ values for $PM_{2.5}$ collected in cities in China (-26.84‰ to -23.13‰, Cao et al., 2011), PM_1 collected in Mexico City, Mexico (-30‰ to -22‰,

Marley et al., 2009), and PM_{10} collected in Grenada, Spain (-24.90‰ to -20.49‰, Mladenov et al., 2011), but slightly enriched in ^{13}C compared to bulk aerosol collected in Kathmandu, Nepal (-26.05‰ to -25.51‰, Shakya et al., 2010) and $PM_{2.5}$ collected in Paris, France (-26.5‰ ± 0.06‰, Widory et al., 2004). Since particle sources and the degree of secondary aerosol production are not uniform in all cities, some variation in $\delta^{13}C_{TC}$ is expected (Fisseha et al., 2009; Gensch et al., 2014; Gleason & Kyser, 1984; Goldstein & Shaw, 2003; Moura et al., 2008; Pichlmayer et al., 1998; Rudolph et al., 2003; Widory, 2006; Wozniak et al., 2012).

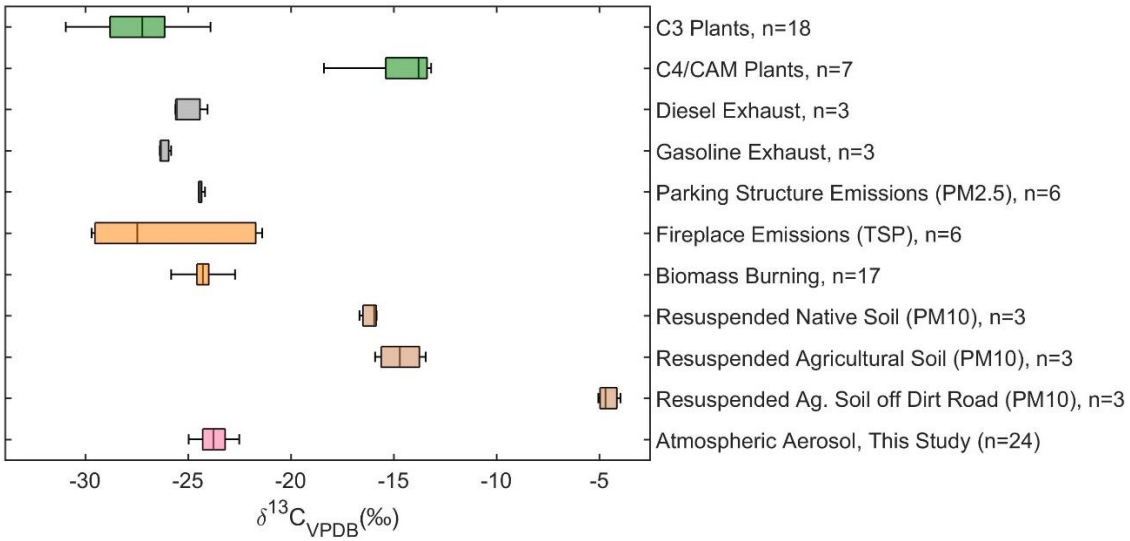

Figure 4.5. Total carbon isotopic composition of size-segregated aerosol samples and common local aerosol sources.

In order to compare the carbon isotopic composition of potential source materials to that of the aerosol samples collected in this study, local source materials were collected and analyzed. Figure 4.5 shows the results of $\delta^{13}C_{TC}$ analysis of these samples compared to the range of $\delta^{13}C_{TC}$ values for all aerosol samples collected in this study. The average $\delta^{13}C_{TC}$ of C_3 plant material was -27.3‰, and that of C_4 and CAM plants was 14.6‰, consistent with previous studies (Wozniak et al., 2012). The average $\delta^{13}C_{TC}$ of diesel and

gasoline tailpipe scrapings was -25.1‰ and -26.2‰, respectively; this result is contrary to other studies, which found diesel fuel to be depleted relative to gasoline (Fisseha et al., 2009; Widory et al., 2004). $PM_{2.5}$ emissions from a campus parking structure averaged -24.4‰, which is enriched relative to the gasoline tailpipe emissions. It is expected that most vehicles in the parking structure would use gasoline; the three tailpipe scrapings collected here may not have been a representative sample of vehicle emissions near campus.

Fireplace emissions were collected in the burning of three different fireplace materials: a firewood bundle, a Clean Flame compressed recycled paper log, and two Duraflame logs. The firewood and Clean Flame log were sampled under both flaming and smoldering conditions; results are indistinguishable within the instrumental uncertainty of 0.2‰. The average $\delta^{13}C_{TC}$ of emissions from firewood, the Clean Flame log, and the two Duraflame logs were, respectively, -21.6‰, -29.6‰, and -27.5‰. The emissions collected in biomass burning in northern Arizona and northern Colorado averaged -24.2‰ in $\delta^{13}C_{TC}$, indistinguishable from the parking structure emissions. The firewood emissions were the most enriched in ^{13}C of the materials sampled, while the Clean Flame and Duraflame logs were comparable to C_3 plants in $\delta^{13}C_{TC}$; however, the number of households that use natural firewood versus Clean Flame, Duraflame, or other types of fireplace material is not known. Additionally, inconsistencies in the profiles of both residential fires and wildfires have been observed and can be caused by variations in fuel, burn conditions, and the type of appliance used in burning (Lewis et al., 2003). It is expected that vehicle emissions and residential biomass burning would be major contributors to aerosol PM in the winter, while particles in the spring, summer, and fall

would be influenced to a greater degree by direct injection of biogenic material. Overall, the range in $\delta^{13}C_{TC}$ values of the samples collected are closest in range to vehicle emissions and C_3 plants, and also fall within the range of fireplace emissions (Figure 4.5).

The $\delta^{13}C_{TC}$ values of samples collected in January are 0.5 – 1.7‰ less than those in other sampling periods, indicating that total carbon is depleted in ^{13}C in the winter relative to other seasons. This could be caused in part by the long-range transport of aged carbonaceous particles from west and southwest of Phoenix. Increased photochemical activity has been observed by the presence of elevated secondary sulfate in fine PM in these warmer months (Brown et al., 2007; Lewis et al., 2003; Ramadan et al., 2000). When SOA-forming reactions that form CO_2 occur, the gaseous CO_2 released will be depleted in ^{13}C, causing the $\delta^{13}C$ of the total PM to increase (Aggarwal et al., 2013; Wang et al., 2012). This effect is observed in Figure 4.4, as all samples collected in April, June, and October are enriched in $\delta^{13}C$ relative to those collected in January.

Seasonal variations in $\delta^{13}C$ of carbonaceous particles could also be caused by changes in local particle sources in winter versus spring, summer, and fall. As stated earlier, the population of Phoenix is smaller in the spring, summer, and fall than in the winter, and warmer temperatures in the spring, summer, and fall eliminate the strong inversion that traps local emissions in the valley. Therefore, along with causing the seasonal changes in the concentration of carbonaceous PM observed in Figure 4.2, anthropogenic sources attributed to these factors will also have a smaller effect on $\delta^{13}C_{TC}$ in the spring, summer, and fall than in the winter. Changes in photosynthetic activity can also affect the $\delta^{13}C$ of PM, as many plants bloom in mild early spring weather.

Carbonate carbon.

A prominent distinction of Figure 4.4 is the increase in the $\delta^{13}C_{TC}$ of the samples with increasing particle size in all seasons, which reaches a maximum for particles in the 3 – 7.2 µm size range. ^{13}C-enriched coarse PM fractions have been observed in other studies as well (Cachier et al., 1985; Garbaras et al., 2009; Masalaite et al., 2015). Blown dust, including agricultural soil, native desert soil, paved and unpaved road dust, and construction materials, is known to be a major source of PM in the Phoenix area (Brown et al., 2007; Cahill, 2013; Lewis et al., 2003; Ramadan et al., 2000; Upadhyay et al., 2011) and in other locations (Manoli et al., 2002), and is a contributor to mineral dust, including carbonates, to coarse PM (Garbaras et al., 2009; López-Veneroni, 2009; Masalaite et al., 2015). The contribution of soil to $PM_{2.5}$ composition in Phoenix was found to be 25% by Brown and coworkers (2007) and 22 ± 2% by Lewis and coworkers (2003).

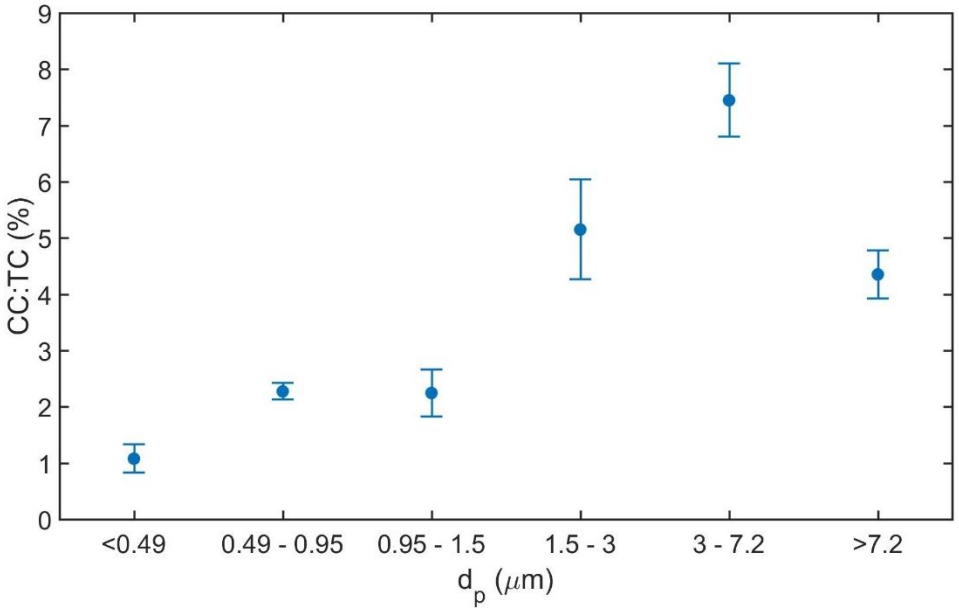

Figure 4.6. The percent of total carbon that is composed of carbonate carbon in samples collected in January.

The percent of TC that was measured to be carbonate carbon (CC) in samples collected in January is shown in Figure 4.6. During this sampling week, the TC of particles greater than 1.5 µm contains as much as 7.4% CC. The CC:TC ratio is as high as 10% for particle sizes 3 µm < d_p < 7.2 µm collected in April (Table 4.2). These values are less than a previous study which determined that coarse PM ($PM_{10-2.5}$) in Phoenix contains an average of 9% CC by thermal optical analysis of acidified filters (Turner et al., 2014). In comparing the profiles of Figure 4.4 and Figure 4.6, $\delta^{13}C_{TC}$ in January appears to increase as the ratio of CC:TC increases. The contribution of Saharan dust to PM_{10} in Granada, Spain has been attributed to higher $\delta^{13}C_{TC}$ values due to its carbonate content (Mladenov et al., 2011). It is therefore likely that the presence of CC has a significant effect on the $\delta^{13}C_{TC}$ of particles greater than 1.5 µm in diameter.

Table 4.2

Percent and carbon isotopic composition of carbonate in aerosol samples. Samples not shown were consumed prior to analysis. nss = available amount of sample not sufficient for analysis. The uncertainty in the last digit of the CC:TC percent ratio is shown in parentheses. The uncertainty in all $\delta^{13}C_{CC}$ results is 0.3‰.

Sampling Period	Particle Size Range	CC:TC (%)	$\delta^{13}C_{CC}$ (‰)
January	<0.49 µm	1.1(2)	nss
January	0.49µm - 0.95µm	2.3(1)	nss
January	0.95µm - 1.5µm	2.2(4)	nss
January	1.5µm - 3µm	5.2(9)	-8.2
January	3µm - 7.2µm	7.4(7)	-6.6
January	>7.2µm	4.4(4)	-7.5
April	<0.49 µm	5.5(4)	-5.2
April	3µm - 7.2µm	10(1)	-5.0
June	<0.49 µm	5.1(8)	-6.6
October	<0.49 µm	2.6(2)	nss
October	3µm - 7.2µm	7.1(5)	-6.3
October	>7.2µm	5.7(3)	-7.1

In order to test this, the carbon isotopic composition of CC ($\delta^{13}C_{CC}$) was measured and is shown in Table 4.2. $\delta^{13}C_{CC}$ values are highly enriched relative to $\delta^{13}C_{TC}$, ranging from -8.2‰ to -5.0‰ for all analyzed samples. These values are similar to airborne dust and soil samples analyzed elsewhere: $PM_{2.5}$ in the city of Xi'an in northwest China was found to have $\delta^{13}C_{CC}$ values of -8.3 ± 1.9‰ under normal ambient conditions (Cao et al., 2004; Cao et al., 2005). Other surveys of dust in various arid regions and plateaus in China range from -5.31‰ to 1.36‰ for aerosol collected in dust storms (Wang et al., 2005), -7.80‰ to -3.34‰ in resuspended dust and bulk soil

(Cao et al., 2008), and -8.2‰ to 0.5‰ in steppes and drylands in the Taklimakan Desert (Chen et al., 2016).

As seen in Figure 4.5, the average total carbon isotopic compositions of resuspended (PM_{10}) native soil, agricultural soil, and agricultural soil off of a dirt road were -16.2‰, -14.7‰, and -4.6‰, respectively. Due to the isotopic enrichment of these resuspended soils in ^{13}C as compared to other source materials, it is likely that soil is the major source of carbonates in the aerosol samples, particularly in size fractions with d_p greater than 1.5 µm.

In order to estimate the effects that biogenic and anthropogenic sources have on the $\delta^{13}C$ of collected samples (which would contribute OC and EC to aerosol), the combined carbon isotopic compositions of OC and EC ($\delta^{13}C_{OCEC}$) in samples collected in January were calculated using the relationship

$$\delta^{13}C_{TC} = f_{OCEC} \times \delta^{13}C_{OCEC} + f_{CC} \times \delta^{13}C_{CC} \quad (4.2)$$

and solving for $\delta^{13}C_{OCEC}$, where f_{CC} is the fraction of CC relative to TC and f_{OCEC} is the combined fraction of OC and EC relative to TC ($1 - f_{CC}$). The average $\delta^{13}C_{CC}$ of the three most coarse filters collected in January that were analyzed was used in this calculation, since the three finest particle size fractions (1.5 µm and below) did not contain sufficient amounts of carbonate for analysis.

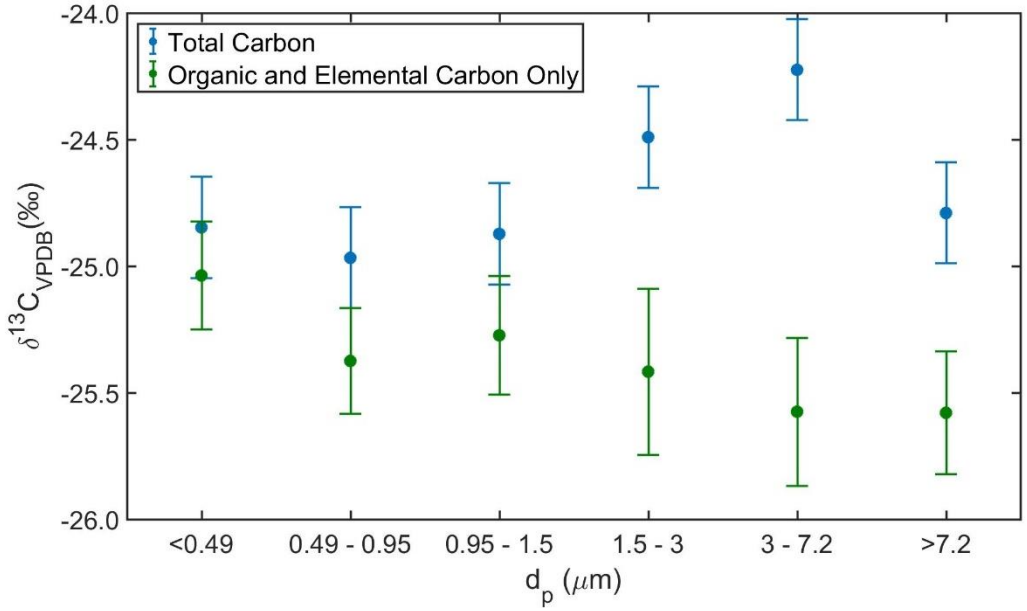

Figure 4.7. Carbon isotopic compositions of total carbon (blue) and combined organic and elemental carbon (green) in January.

Figure 4.7 compares the $\delta^{13}C$ of TC to that of only OC and EC in aerosol samples collected in January. Even though CC makes up less than 10% of the TC of each sample, its enrichment relative to bulk $\delta^{13}C_{TC}$ causes a significant shift in the $\delta^{13}C_{OCEC}$ of the three most coarse size fractions by up to 1.4‰. This data suggests that the $\delta^{13}C_{OCEC}$ of coarse PM may be depleted in ^{13}C relative to smaller particle size fractions. However, further analysis would be required to obtain $\delta^{13}C_{CC}$ values for all size modes before making this determination.

n-Alkanes.

Concentrations and carbon preference indices.

Table 4.3 contains the concentrations of identified *n*-alkanes ($C_{14}H_{30}$ to $C_{37}H_{76}$) in the size-segregated aerosol samples (limits of detection for each compound can be found in Appendix B, Table B7). The sum of the concentrations of all *n*-alkanes in each size fraction in all sampling periods is shown in Figure 4.8. Over 55% of total *n*-alkane mass

is found in particles less than 0.49 μm in diameter in all seasons, reaching as high as 69% in January. In contrast, 60% of TC in January was found in the size mode $d_p < 0.49$ μm, while the TC concentrations in $d_p < 0.49$ μm in April, June, and October were higher (68%, 69%, and 62%, respectively). The high concentration of *n*-alkanes in small particles could be due to their origination from chemical process such as vehicle exhaust, and may be intensified by high anthropogenic wintertime activity.

Table 4.3

n-*Alkane concentrations. <LOD = below limit of detection; see Table B7 for limits of detection of each species. * = A coeluting peak prohibited the integration of* n-$C_{19}H_{40}$ *in some samples.*

n-Alkane Concentration (ng/m^3)	January						April					
	<0.49 µm	0.49µm - 0.95µm	0.95µm - 1.5µm	1.5µm - 3µm	3µm - 7.2µm	>7.2µm	<0.49 µm	0.49µm - 0.95µm	0.95µm - 1.5µm	1.5µm - 3µm	3µm - 7.2µm	>7.2µm
$C_{14}H_{30}$	*<LOD*	*<LOD*	*<LOD*	*<LOD*	0.0058	*<LOD*	*<LOD*	0.0052	*<LOD*	0.0024	0.0040	*<LOD*
$C_{15}H_{32}$	0.217	*<LOD*	*<LOD*	0.0102	*<LOD*	*<LOD*	0.077	0.0075	0.0048	0.0006	*<LOD*	*<LOD*
$C_{16}H_{34}$	0.433	0.0335	0.0359	0.0183	0.0240	0.0128	0.132	0.0159	0.0170	0.0154	0.0124	0.0160
$C_{17}H_{36}$	0.056	0.0274	0.0226	0.0220	0.0196	0.0113	0.066	0.0135	0.0136	0.0114	0.0107	0.0099
$C_{18}H_{38}$	0.061	0.0039	0.0174	0.0109	0.0107	0.0160	0.126	0.0127	0.0095	0.0113	0.0108	0.0061
$C_{19}H_{40}$	0.116	0.0152	0.0176	0.0123	0.0146	0.0097	*	*	*	0.0081	0.00928	0.0068
$C_{20}H_{42}$	0.099	0.0132	0.0454	0.0123	0.0164	0.0154	0.070	0.0080	0.0055	0.0053	0.00766	0.0067
$C_{21}H_{44}$	0.128	0.0292	0.0265	0.0256	0.0295	0.0213	0.120	0.0177	0.0173	0.0151	0.01844	0.0148
$C_{22}H_{46}$	0.195	0.0449	0.0458	0.0390	0.0412	0.0357	0.118	0.0255	0.0223	0.0209	0.02376	0.0219
$C_{23}H_{48}$	0.212	0.0572	0.0637	0.0480	0.0529	0.0346	0.194	0.0496	0.0423	0.0375	0.04032	0.0331
$C_{24}H_{50}$	0.244	0.0392	0.0450	0.0283	0.0376	0.0438	0.092	0.0276	0.0216	0.0267	0.02601	0.0200
$C_{25}H_{52}$	0.778	0.0677	0.0793	0.0647	0.0610	0.0518	0.306	0.0427	0.0515	0.0467	0.05418	0.0368
$C_{26}H_{54}$	0.983	0.0797	0.0959	0.0810	0.0965	0.0390	0.228	0.0216	0.0275	0.0206	0.02592	0.0234
$C_{27}H_{56}$	1.809	0.0842	0.1115	0.0730	0.1413	0.0855	0.872	0.0746	0.0862	0.0810	0.08201	0.0752
$C_{28}H_{58}$	0.952	0.0462	0.0846	0.0340	0.0546	0.0518	0.145	0.01769	0.0247	0.0182	0.01641	0.0201
$C_{29}H_{60}$	1.966	0.1184	0.1626	0.1089	0.1842	0.1650	1.266	0.1105	0.1620	0.1539	0.15445	0.1290
$C_{30}H_{62}$	0.832	0.0513	0.0789	0.0586	0.0601	0.0729	0.326	0.0167	0.0225	0.0224	0.02096	0.0324
$C_{31}H_{64}$	1.850	0.1266	0.1350	0.1487	0.2391	0.2071	1.424	0.1119	0.1344	0.1017	0.14335	0.1319
$C_{32}H_{66}$	0.547	0.0297	0.0482	0.0275	0.0576	0.0588	0.200	0.0136	0.0144	0.0120	0.01623	0.0183
$C_{33}H_{68}$	0.668	0.0311	0.0486	0.0345	0.0533	0.0636	0.256	0.0182	0.0227	0.0161	0.01993	0.0248
$C_{34}H_{70}$	0.862	0.0299	0.0567	0.0843	0.180	0.139	0.664	0.0255	0.0164	0.0125	0.0368	0.0532
$C_{35}H_{72}$	0.957	0.0332	0.0639	0.0752	0.101	0.124	0.383	0.0181	0.0146	0.0215	0.0210	0.0321
$C_{36}H_{74}$	0.432	0.0306	0.0658	0.0826	0.097	0.152	0.215	0.0299	0.0130	0.0106	0.0442	0.0245
$C_{37}H_{76}$	0.409	*<LOD*	0.0660	0.0416	0.092	0.161	0.177	0.0181	0.0232	0.0128	0.0317	*<LOD*

Table 4.3 (continued)

n-*Alkane concentrations. <LOD = below limit of detection; see Table B7 for limits of detection of each species. * = A coeluting peak prohibited the integration of* n-$C_{19}H_{40}$ *in some samples.*

n-Alkane Concentration (ng/m^3)	June						October					
	<0.49 µm	0.49µm - 0.95µm	0.95µm - 1.5µm	1.5µm - 3µm	3µm - 7.2µm	>7.2µm	<0.49 µm	0.49µm - 0.95µm	0.95µm - 1.5µm	1.5µm - 3µm	3µm - 7.2µm	>7.2µm
$C_{14}H_{30}$	0.035	0.0025	*<LOD*	0.0017	0.0022	0.0057	*<LOD*	0.0081	0.0092	0.0119	*<LOD*	0.0138
$C_{15}H_{32}$	0.020	0.0025	0.0029	0.0020	0.0017	0.0043	*<LOD*	*<LOD*	*<LOD*	*<LOD*	0.0180	0.0093
$C_{16}H_{34}$	0.046	0.0067	0.0067	0.0061	0.0046	0.0087	0.148	0.0147	0.0136	0.0115	0.0190	0.0128
$C_{17}H_{36}$	0.052	0.0100	0.0103	0.0112	0.0080	0.0101	0.047	0.0103	0.0111	0.0115	0.0227	0.0118
$C_{18}H_{38}$	0.036	0.0064	0.0103	0.0020	0.0086	0.0054	0.030	0.0070	0.0089	0.0048	0.0119	0.0067
$C_{19}H_{40}$	0.048	*	*	*	*	*	*	*	*	*	*	*
$C_{20}H_{42}$	0.036	0.0049	0.0055	0.0050	0.0058	0.0047	0.065	0.0038	0.0035	0.0028	0.0049	0.0082
$C_{21}H_{44}$	0.062	0.0142	0.0161	0.0139	0.0119	0.0078	0.048	0.0084	0.0072	0.0048	0.0089	0.0086
$C_{22}H_{46}$	0.125	0.0224	0.0209	0.02566	0.0228	0.0246	0.061	0.0106	0.0102	0.0074	0.0140	0.0143
$C_{23}H_{48}$	0.155	0.0420	0.0396	0.04682	0.0473	0.0431	0.117	0.0144	0.0140	0.0141	0.0150	0.0196
$C_{24}H_{50}$	0.156	0.0504	0.0380	0.04847	0.0428	0.0303	0.116	0.0146	0.0189	0.0177	0.0233	0.0109
$C_{25}H_{52}$	0.309	0.1296	0.1197	0.14019	0.0978	0.0807	0.157	0.0329	0.0430	0.0244	0.0317	0.0490
$C_{26}H_{54}$	0.236	0.0865	0.0783	0.10266	0.0810	0.0508	0.175	0.0314	0.0248	0.0265	0.0202	0.0387
$C_{27}H_{56}$	0.518	0.1203	0.1255	0.1149	0.1169	0.1019	0.291	0.0468	0.0646	0.0558	0.0711	0.0792
$C_{28}H_{58}$	0.189	0.0267	0.0282	0.02729	0.0228	0.0241	0.115	0.0106	0.0197	0.0199	0.0261	0.0251
$C_{29}H_{60}$	1.071	0.1075	0.1510	0.14863	0.1581	0.1639	0.852	0.0755	0.1104	0.1065	0.1268	0.1143
$C_{30}H_{62}$	0.202	0.0122	0.0223	0.02261	0.0183	0.0185	0.261	0.0158	0.0256	0.0159	0.0230	0.0367
$C_{31}H_{64}$	1.302	0.0866	0.1209	0.14372	0.1621	0.1575	1.024	0.0821	0.1251	0.1156	0.1422	0.1404
$C_{32}H_{66}$	0.100	0.0121	0.0119	0.01153	0.0124	0.0133	0.197	0.0161	0.0210	0.0202	0.0236	0.0292
$C_{33}H_{68}$	0.278	0.0152	0.0174	0.01800	0.0212	0.0229	0.371	0.0242	0.0302	0.0292	0.0403	0.0366
$C_{34}H_{70}$	0.192	0.0054	0.0187	0.0085	0.0145	0.0121	0.324	0.0175	0.0256	0.0150	0.0315	0.0567
$C_{35}H_{72}$	0.117	0.0121	0.0158	0.0103	0.0131	0.0192	0.276	0.0146	0.0183	0.0141	0.0366	0.0406
$C_{36}H_{74}$	0.078	0.0099	0.0176	0.0063	0.0087	0.0200	0.132	0.0112	0.0123	0.0157	0.0222	0.0355
$C_{37}H_{76}$	0.105	*<LOD*	0.0061	0.0042	0.0119	0.0178	0.149	0.0103	0.0130	0.0139	0.0384	0.0366

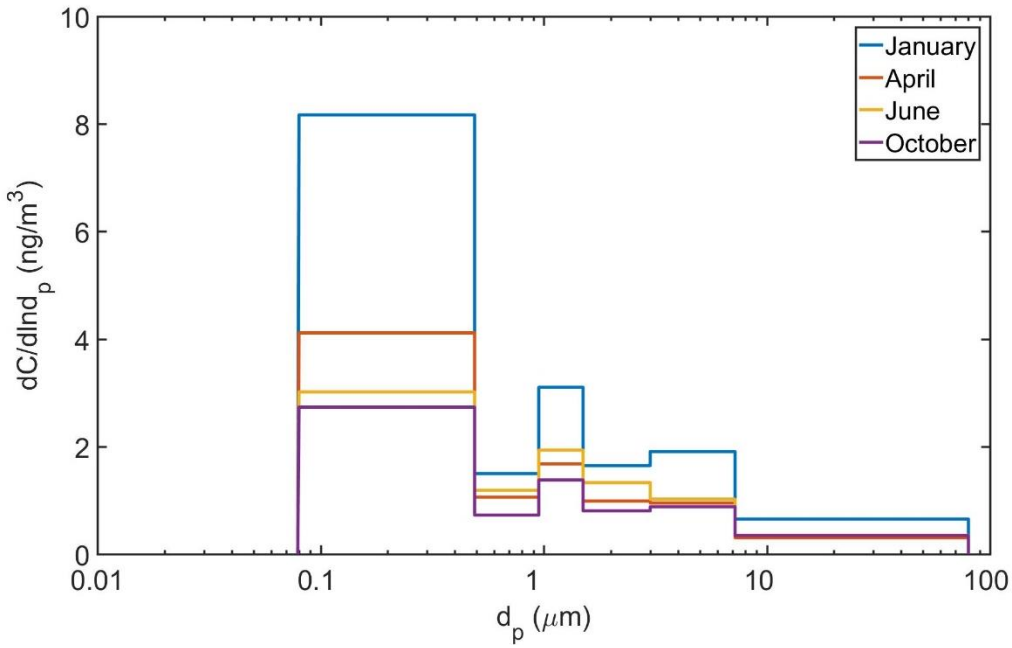

Figure 4.8. Size distributions of total detected *n*-alkanes during the four sampling periods.

The total concentration of *n*-alkanes over all size fractions in January is at least twice as high as in other sampling periods, which may be due to exacerbated wintertime anthropogenic emissions caused by strong inversion and a higher population in the winter compared to other seasons. This effect is stronger than what was seen for TC (Figure 4.2), where the total TC concentration in January over all size fractions was up to 80% larger than in other sampling periods. Accordingly, the percent of *n*-alkanes that are found in TC is highest in January (0.34%, compared to 0.32%, 0.27%, and 0.20% in April, June, and October, respectively).

In order to further evaluate the relative influence of biogenic and anthropogenic emissions in these samples, the carbon preference indices (CPI) were calculated as the ratio of the sum of the concentrations of odd-chain-length *n*-alkanes to the sum of the concentrations of even-chain-length *n*-alkanes,

$$CPI = \frac{\sum[C_{odd}]}{\sum[C_{even}]} \quad (4.3)$$

using *n*-alkanes ranging from $C_{26}H_{54}$ to $C_{35}H_{72}$, which are characteristic of higher plant wax (Simoneit, 1989). A CPI near unity would be indicative of anthropogenic emissions, and CPI values greater than one indicate an increasing influence of biogenic emissions.

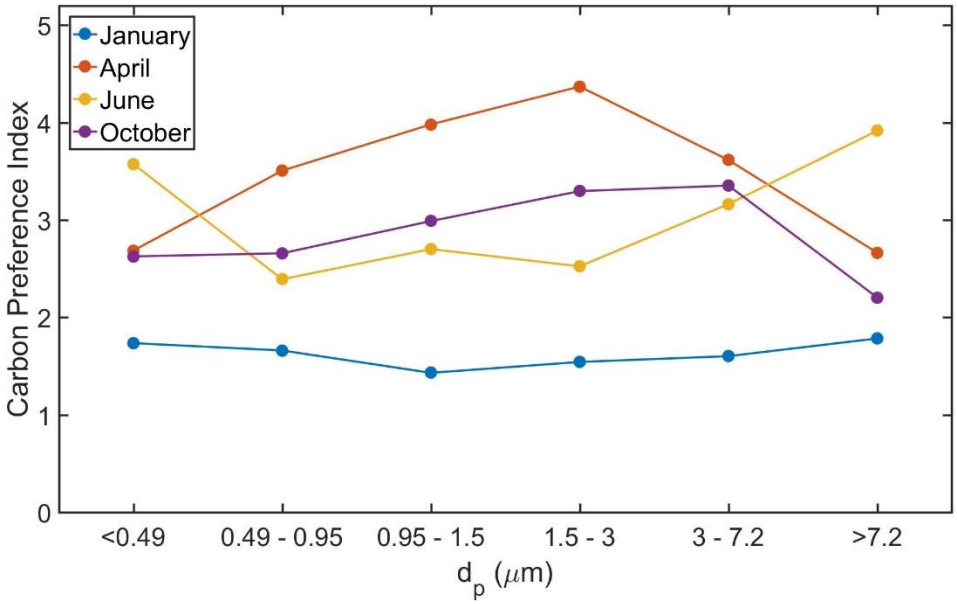

Figure 4.9. n-Alkane carbon preference indices.

Results of CPI calculations are shown in Figure 4.9. In January, CPI values in all size fractions are less than 2, indicative of the known dominance of anthropogenic emissions at this time. All CPI values in April, June, and October are greater than 2, which is typical in an urban environment experiencing a mix of biogenic and anthropogenic emissions (Simoneit, 1989). The CPI value exceeds 4 in April for particles in the size range of 1.5 – 3 µm. Many plants begin to bloom in early spring, and this could correspond to high pollen counts in this season. Previous work in Phoenix's east valley has found a significant contribution of primary biological aerosol particles in both $PM_{2.5}$ and PM_{10} (Jia & Fraser, 2011). Clements and coworkers (2014) has also found high

$PM_{2.5}$ concentrations in Pinal County in the spring associated with agricultural activity. $PM_{2.5}$ was mainly comprised of organic matter (37%); long-range transport of these aerosols to Phoenix could contribute to high CPI for fine particles.

In June and October, the CPI values across all size fractions remain elevated compared to January. The Sonoran and Chihuahuan desert regions in the southwest United States typically experience two rainy seasons, one in the autumn to early winter, and another in mid- to late-summer. Summer rains can promote the growth of plants in the summer and fall, which could be reflected in CPI measurements. Indeed, Whitford (2002) explains that autumn rains cause the germination of autumn ephemeral plants, which are mainly C_3, that bloom in the late winter to early spring. This is consistent with the high biogenic signal in the CPI of autumn. Summer ephemeral plants will germinate after the first intense rain storm of the summer and grow from late summer to the autumn. These plants mainly follow the C_4 photosynthetic pathway.

Compound-specific isotope analysis of* n-*alkanes.

The carbon isotopic composition of *n*-alkanes in all samples was determined (Table 4.4). Over all measurements, the $\delta^{13}C$ of *n*-alkanes ranges from -37.0‰ to -27.2‰, which is a depletion relative to $\delta^{13}C_{TC}$ of 4 – 14‰. *n*-Alkanes extracted from plants have been shown to be depleted in ^{13}C relative to total surface lipid extracts by an average of 3.6‰; *n*-alkane $\delta^{13}C$ values ranged from -38.8‰ to -30.7‰ for C_3 plants, -25.8‰ to -18.0‰ for C_4 plants, and -29.2‰ to -23.0‰ for CAM plants (Collister et al., 1994).

Table 4.4

n-*Alkane carbon isotopic compositions. nd = not detected.*

n-Alkane $\delta^{13}C_{VPDB}$ (‰)	Uncertainty in $\delta^{13}C_{VPDB}$ (‰)	January						April					
		<0.49 µm	0.49µm - 0.95µm	0.95µm - 1.5µm	1.5µm - 3µm	3µm - 7.2µm	>7.2µm	<0.49 µm	0.49µm - 0.95µm	0.95µm - 1.5µm	1.5µm - 3µm	3µm - 7.2µm	>7.2µm
$C_{24}H_{50}$	0.3	-31.6	-31.3	-32.2	-33.2	-30.3	-31.6	-30.6	-30.8	-31.1	-31.1	-31.0	-30.2
$C_{25}H_{52}$	0.5	-31.9	-31.1	-31.1	-32.1	-32.2	-32.8	-30.3	-31.3	-31.6	-31.5	-31.9	-32.0
$C_{26}H_{54}$	0.3	-30.8	-30.7	-31.8	-34.7	-32.0	-32.5	-31.3	-31.6	-31.0	-31.5	-31.2	-31.1
$C_{27}H_{56}$	0.6	-30.8	-33.1	-33.6	-35.1	-33.8	-33.6	-32.3	-34.0	-33.0	-33.1	-33.0	-34.0
$C_{28}H_{58}$	0.6	-31.2	-33.8	-33.3	-30.3	-32.5	-31.5	-29.7	-34.4	-33.1	-31.3	-30.2	-33.3
$C_{29}H_{60}$	0.6	-32.8	-33.0	-33.2	-35.7	-33.5	-34.8	-33.0	-35.3	-35.7	-34.4	-35.2	-33.9
$C_{30}H_{62}$	0.6	-31.8	n.d.	-35.7	-30.7	-32.2	-29.8	n.d.	n.d.	n.d.	n.d.	n.d.	n.d.
$C_{31}H_{64}$	0.6	-35.4	-34.9	-34.5	-34.5	-33.4	-33.6	-36.0	-35.8	-36.0	-32.0	-34.4	-35.6

Table 4.4 (continued)

n-*Alkane carbon isotopic compositions. nd = not detected.*

n-Alkane $\delta^{13}C_{VPDB}$ (‰)	Uncertainty in $\delta^{13}C_{VPDB}$ (‰)	June						October					
		<0.49 µm	0.49µm - 0.95µm	0.95µm - 1.5µm	1.5µm - 3µm	3µm - 7.2µm	>7.2µm	<0.49 µm	0.49µm - 0.95µm	0.95µm - 1.5µm	1.5µm - 3µm	3µm - 7.2µm	>7.2µm
$C_{24}H_{50}$	0.3	-32.4	-33.0	-34.9	-31.9	-31.3	-31.4	-32.2	-31.2	-30.5	-30.1	-30.6	-30.4
$C_{25}H_{52}$	0.5	-32.5	-33.0	-33.0	-32.8	-31.5	-30.9	-32.6	-30.5	-30.2	-32.4	-31.2	-31.4
$C_{26}H_{54}$	0.3	-36.2	-33.3	-34.1	-32.6	-31.0	-30.6	-31.8	-30.9	-32.0	-31.8	-30.6	-33.8
$C_{27}H_{56}$	0.6	-32.1	-34.5	-34.7	-33.7	-33.9	-32.0	-30.6	-32.5	-31.6	-32.5	-33.0	-33.4
$C_{28}H_{58}$	0.6	-29.7	-32.3	-27.2	-27.4	-29.9	-30.7	-30.5	-31.2	-33.6	-31.0	-28.0	-31.5
$C_{29}H_{60}$	0.6	-34.4	-34.6	-33.7	-37.0	-36.3	-34.9	-32.7	-32.5	-34.1	-32.0	-32.1	-33.8
$C_{30}H_{62}$	0.6	n.d.	n.d.	n.d.	n.d.	n.d.	n.d.	-32.5	n.d.	n.d.	n.d.	n.d.	n.d.
$C_{31}H_{64}$	0.6	-34.8	-33.5	-35.4	-36.2	-36.8	-35.0	-32.8	-34.8	-33.5	-32.0	-33.3	-32.3

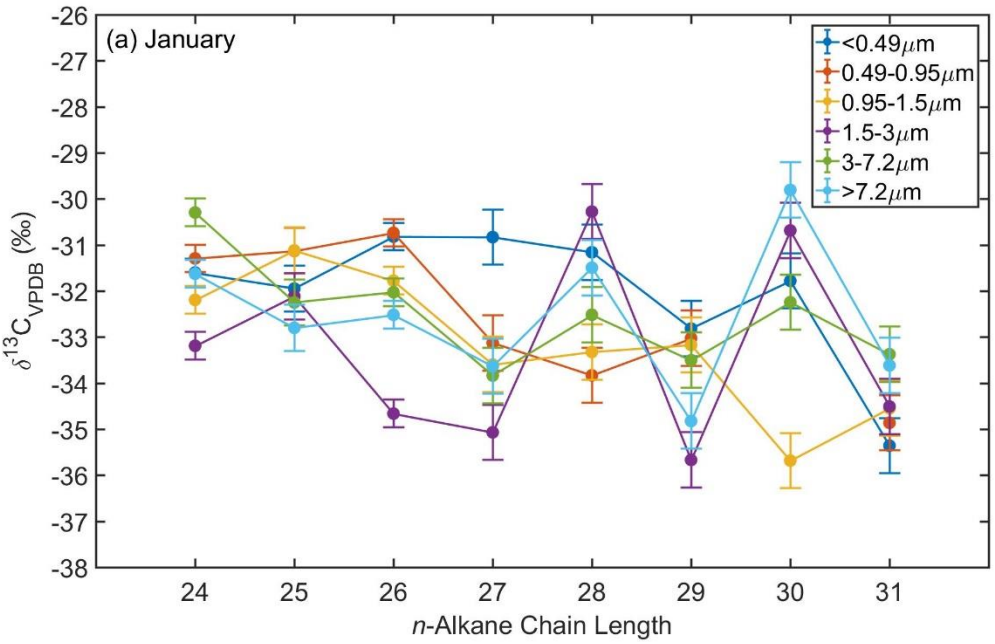
(a) January
<0.49μm
0.49-0.95μm
0.95-1.5μm
1.5-3μm
3-7.2μm
>7.2μm
δ13CVPDB (‰)
n-Alkane Chain Length

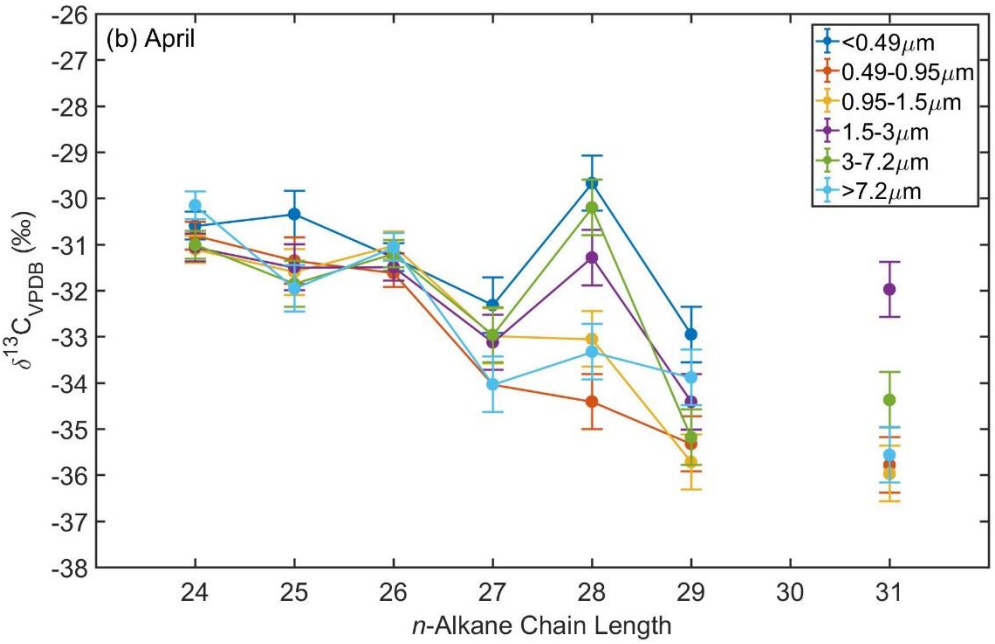
(b) April
<0.49μm
0.49-0.95μm
0.95-1.5μm
1.5-3μm
3-7.2μm
>7.2μm
δ13CVPDB (‰)
n-Alkane Chain Length

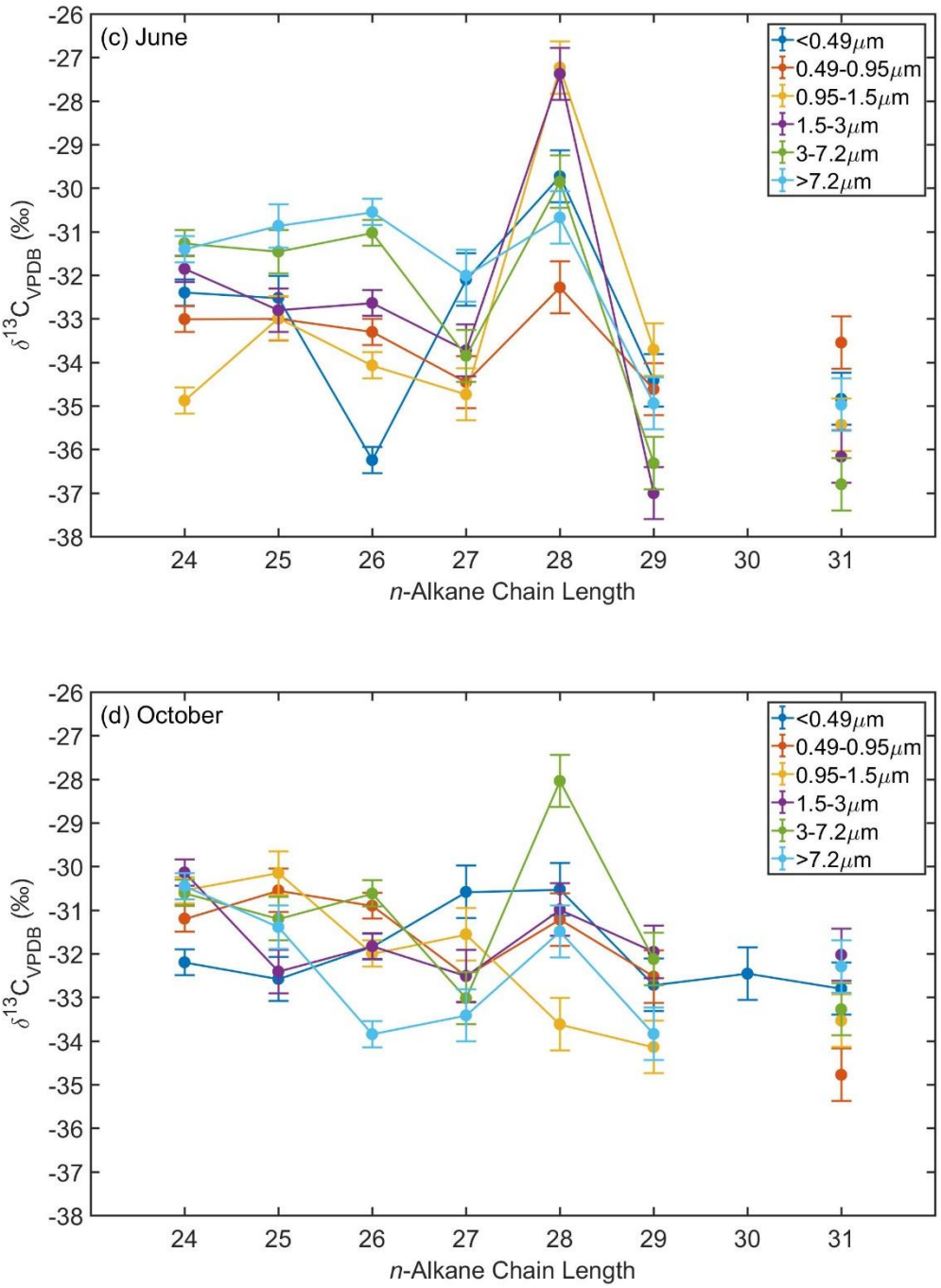

Figure 4.10. Carbon isotopic composition of individual *n*-alkanes collected in (a) January, (b) April, (c) June, and (d) October.

Figure 4.10 shows the $\delta^{13}C$ values of the *n*-alkanes collected in each size fraction in January, April June, and October. In the samples analyzed in this study, there is generally little difference in the $\delta^{13}C$ of $C_{24} – C_{26}$ *n*-alkanes in individual samples. In January, depletion of odd *n*-alkanes C_{27}, C_{29}, and C_{31} (by up to 4.6‰) and enrichment of even *n*-alkanes C_{28} and C_{30} (by up to 4.4‰) is apparent in coarser samples (> 1.5 µm), but this sawtooth pattern is weaker for samples < 1.5 µm (Figure 4.10a). In April and June, depletion of C_{29} and C_{31} is apparent in most samples (by up to 5.6‰ in April and 5.8‰ in June), while C_{28} is enriched in all samples collected in June (by up to 7.6‰) and two of the samples collected in April (1.6‰ in the < 0.49 µm fraction, 1.7‰ in the 3 µm – 7.2 µm fraction) (Figures 4.10b and 4.10c). C_{30} was not detected in April and June samples. In September, $\delta^{13}C$ values are scattered and exhibit a weak sawtooth pattern, with C_{28} enrichment only in samples >3µm and depletion of C_{29} and C_{31} in all size fractions except d_p < 0.49 µm (Figure 4.10d).

The sawtooth pattern in the $\delta^{13}C$ of *n*-alkanes C_{27} and above has been observed in other studies (Schefuß et al., 2003; Yamamoto & Kawamura, 2010), which attribute the isotopic depletion of odd-chain *n*-alkanes C_{27} and above to leaf wax sources, while non-leaf wax sources had an insignificant impact on $\delta^{13}C$ of these odd-chain *n*-alkanes. Notably, *n*-alkanes C_{29} and C_{31} were found to be the most depleted, and a moderate inverse correlation between $\delta^{13}C$ of these *n*-alkanes and the CPI of the sample was observed (Yamamoto & Kawamura, 2010). More scatter was observed in the $\delta^{13}C$ of long even chain *n*-alkanes, attributed to their low concentrations in plants making them susceptible to contamination (Schefuß et al., 2003). Interestingly, the $\delta^{13}C$ enrichment of even long-chain *n*-alkanes is not discussed in literature, though it is obvious in this study

that C_{28} is enriched relative to $C_{24} – C_{26}$ in some samples in this study. The cause of this enrichment is not clear, but may be interesting to investigate in future studies.

Based upon the range of $\delta^{13}C$ of *n*-alkanes analyzed in this study, it is likely that C_3 plants and fossil fuel emissions are dominant *n*-alkane sources, while C_4 and CAM plants would be minor sources of *n*-alkanes. No correlation was found between the CPI and $\delta^{13}C$ values of C_{29} or C_{31}, possibly due to the presence of known anthropogenic influences in the sampling location, which can include both fossil (vehicle) and non-fossil (residential wood-burning) emissions. There is a small seasonal shift apparent in June, in which the $\delta^{13}C$ range of $C_{24} – C_{26}$ *n*-alkanes is lower than in January, April, and October (-34.7‰ – -30.3‰, -32.0‰ – -30.2‰, and -33.8‰ – -30.1‰, respectively, compared to -36.2‰ – -30.6‰ in June). Also, the $\delta^{13}C$ range of $C_{27} – C_{31}$ *n*-alkanes in June is wider than in January, April, and October (-35.7‰ – -29.8‰, -36.0‰ – -29.7‰, and -34.8‰ – -28.0‰, respectively, compared to -37.0‰ – -27.2‰ in June). These observations could indicate that June samples are exhibiting the greatest dominance of C_3 emissions over fossil fuel emissions; however, an analysis of *n*-alkanes in local fossil emission sources and C_3 plant waxes would be necessary to make this distinction definitively.

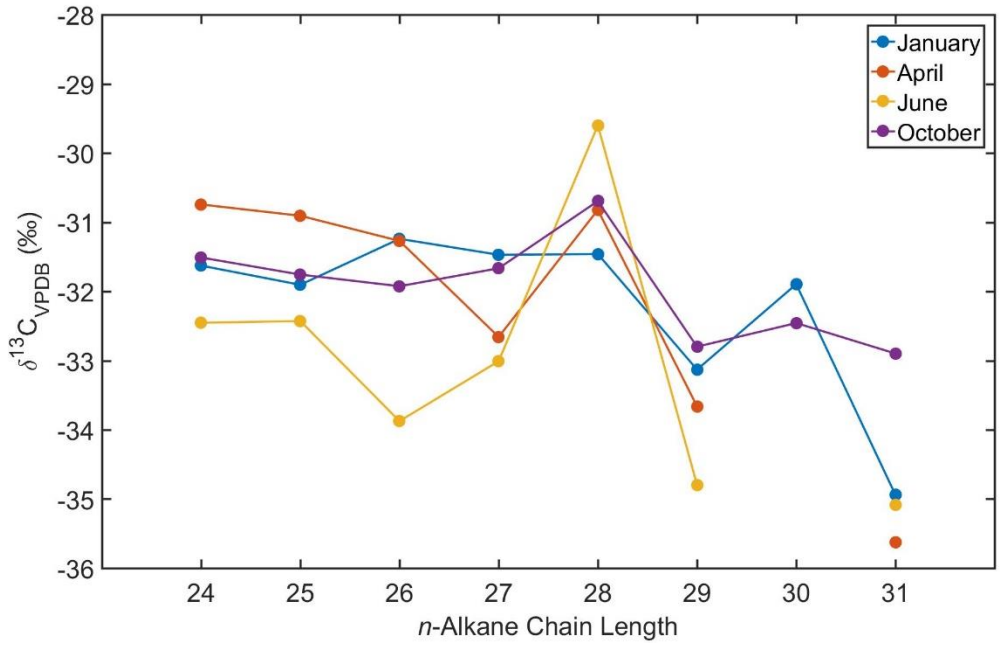

Figure 4.11. Average $\delta^{13}C$ of each *n*-alkane in total suspended particulates for each month.

Figure 4.11 shows the average $\delta^{13}C$ of n-alkanes during each sampling period, weighted by the *n*-alkane concentrations in each size fraction. Again, the average $\delta^{13}C$ of *n*-alkanes C_{24} – C_{26} in June are depleted (-32.5‰, -32.4‰, and -33.9‰ for C_{24}, C_{25}, and C_{26}) compared to January (-31.6‰, -31.9‰, and -31.2‰), April (-30.7‰, -30.9‰, and -31.3‰), and October (-31.5‰, -31.8‰, and -31.9‰). The average $\delta^{13}C$ of C_{28} in June (-29.6‰) is notably enriched relative to C_{24} – C_{26}, but enrichment is less apparent in other months. In October, the average $\delta^{13}C$ of C_{31} (-32.9‰) is greater than in January, April, or June (-34.9‰, -35.6‰, and -35.1‰, respectively). The average $\delta^{13}C$ of C_{29} is minimally enriched in October compared to other months. It is possible that the $\delta^{13}C$ enrichment in C_{31} in October is due to the growth of C_4 plants in the autumn caused by the summer rainy season (Whitford, 2002), as the $\delta^{13}C$ of total leaf wax and *n*-alkanes of C_4 plants is enriched relative to that of C_3 plants (Figure 4.5; Collister et al., 1994).

Previous studies have used the isotopic differences of *n*-alkanes in C_3 and C_4 plants to determine the relative contributions of these plant types in aerosols (Bendle et al., 2007; Huang et al., 2000; Simoneit, 1997). However, since the $\delta^{13}C$ ranges of *n*-alkanes from C_3 plants and fossil fuels are not distinguishable (Simoneit, 1997), sources apportionment using $\delta^{13}C$ of *n*-alkanes was not deemed suitable in an urban environment. Other studies have applied hydrogen isotope analysis (δ^2H) of *n*-alkanes to distinguish fossil and C_3 plant contributions to aerosol (Li et al., 2001; Yamamoto & Kawamura, 2010), since δ^2H of *n*-alkanes of fossil fuels and C_3 plants can be distinguished and δ^2H of *n*-alkanes in fossil fuels spans a wide range (up to 130‰ for different oils, Li et al., 2001). Still, the shift in the $\delta^{13}C$ of C_{31} observed in October shows some promise that the sources apportionment of plant material may be possible even in an urban environment.

Conclusions

The seasonal variations in the concentrations and isotopic compositions of total carbon, carbonate carbon, and *n*-alkanes in size-resolved atmospheric particulate matter collected in Phoenix, Arizona were studied. The carbon content of PM is heavily influenced by seasonal trends, including inversion, transport, population density, and photochemical activity, with samples collected in January exhibiting a dominant influence of anthropogenic emissions, especially in particles <0.49 μm, that are amplified by a low mixing layer. Biogenic emissions and photochemical activity have a greater influence in April, June, and October, as seen by the higher *n*-alkane CPI values and $\delta^{13}C_{TC}$ values compared to those in January in all size fractions. Variations in $\delta^{13}C_{TC}$ within a sampling period are caused by sources that generate PM in different size modes: soil and dust are more prevalent in particles greater than 1.5 μm, while anthropogenic

emissions would account for most particles smaller than 1.5 μm. CC has a significant enrichment effect on the $\delta^{13}C_{TC}$ of coarse particles, highlighting their importance in regions impacted by blown mineral dust.

n-Alkanes are isotopically depleted compared to TC, consistent with observations in other locations. The $\delta^{13}C$ values of *n*-alkanes likely exhibit a mixture of C_3 plant emissions and fossil fuel emissions, with C_4 plants contributing as well in October. Due to seasonal changes in dominant plants (C_3 in the late winter to early summer, C_4 in autumn), this location may be an interesting location for further studies of the $\delta^{13}C$ of urban *n*-alkanes; using both $\delta^{13}C$ and $\delta^{2}H$ measurements, source apportionment of fossil fuels, C_3 plants, and C_4 plants may be possible.

Acknowledgements

The author gratefully acknowledges Matthew Fraser for providing biomass samples from Higley, AZ and soil samples from Pinal County, AZ; Jeffrey Collett, Jr. for providing biomass burning samples from Ft. Collins; Marin Robinson for providing biomass burning samples from northern and eastern Arizona; Alyssa Sherry for assisting with fireplace emissions collection; Elizabeth Makings for aiding in plant identification; and Heather Throop for her help in determining plant photosynthetic cycles.

The author gratefully acknowledges the NOAA Air Resources Laboratory (ARL) for the provision of the HYSPLIT transport and dispersion model and READY website (http://www.ready.noaa.gov) used in this publication.

CHAPTER 5

AEROSOL INTERACTIONS WITH FOG IN URBAN AND SUBURBAN SITES IN NORTHEASTERN FRANCE

The Alsace region of France experiences autumnal radiation fog that can play an important role in local atmospheric chemistry and impacts air quality. Fog water studies were previously conducted in Strasbourg, the largest city and capital of the region, throughout the 1990's (Herckes et al., 2002; Millet et al., 1995; Millet et al., 1996; Millet et al., 1997). Comparisons of two droplet size fractions (2 – 6 μm and 6 – 8 μm) have found lower pH and higher concentrations of major ions in the smaller size fraction (Millet et al., 1996), as well as higher solubility of trace metals in the smaller droplet sizes (Millet et al., 1995). Both size fractions were found to have high concentrations of formate and acetate, attributed to automobile exhaust (Millet et al., 1997). A study of the change in composition of 5 – 8 μm droplets from 1990 – 1999 showed increasing pH and decreasing concentrations of major ions and trace metals, but could not attribute these changes to specific causes due to a lack of data for ambient particle and gas composition and concentration (Herckes et al., 2002).

Since temporal tends in the concentration of fog water were observed in the aforementioned studies, it would be interesting to see how the composition of fog water has continued to evolve. However, collection and analysis of fog water in Strasbourg ceased after 1999. Additionally, the tandem sampling of fog and particulate matter could provide additional information about the scavenging of aerosols by fog droplets and the effect of fog on the concentration and composition of particulate matter.

Previous studies of the components of atmospheric particles in Strasbourg have found strong seasonal and diurnal patterns in particulate matter concentrations and a prevalence of vehicular emissions as a major PM source. Abou Chakra and coworkers (2007) have found elevated genotoxic effects of $PM_{2.5}$ relative to PM_{10}, as well as higher genotoxic effects in the winter. A spatial heterogeneity was also observed, where genotoxic effects were elevated for those living near heavily trafficked areas compared to more industrial or residential areas. Another study concluded that most ultrafine particles in the center of Strasbourg were induced by traffic (Roth et al., 2008). Gas and particle phase concentrations of phenols and nitrophenols were found to exhibit seasonal trends, with the lowest concentrations in the spring. Additionally, diurnal variations corresponding to vehicular circulation were apparent year-round (Delhomme et al., 2010). Another study of PAH concentrations in PM_{10} also found seasonal trends, with the highest PAH concentrations in the winter, as well as diurnal variations dictated by vehicle emissions (Delhomme & Millet, 2012). Domestic heating was also found to contribute to particulate matter in the colder months (Delhomme et al., 2010; Delhomme & Millet, 2012).

In this field study, samples of particulate matter and fog were collected in the city of Strasbourg and a nearby suburb, Geispolsheim, in the fall of 2016. This chapter will focus on the analysis on $PM_{2.5}$ in Strasbourg and PM_{10} in Geispolsheim. OC and EC were quantified in these samples, and the stable carbon isotopic composition of total carbon ($\delta^{13}C_{TC}$) was measured. These measurements will provide insight on the fate of carbonaceous particles in multiphase systems, or systems in which fog, rain, or drizzle occur, through observations of the changes in particle concentration and isotopic

composition caused by aqueous phase scavenging. Results will also be compared to measurements from field campaigns performed in other heavily urbanized valleys, including the Po Valley of Italy and Central Valley of California. These inland valley locations experience high air pollution events in the autumn and winter due to strong inversions that trap emissions in the valleys, and they experience autumnal and winter radiation fog events, similar to Strasbourg. Additionally, the $\delta^{13}C_{TC}$ of particles collected in Strasbourg and Geispolsheim will be compared to $\delta^{13}C_{TC}$ measurements of $PM_{2.5}$ collected on the North American west coast to assess how differences in local particle sources affect the overall isotopic composition of atmospheric carbon. This work represents the first campaign studying the $\delta^{13}C$ of particles in Strasbourg and Geispolsheim, as well as the first campaign observing the effect of fog and rain events on the $\delta^{13}C$ of particulate matter.

Materials and Methods

Sample collection.

Samples were collected in the fall of 2016 in Strasbourg and Geispolsheim, located in the Alsace region of northeastern France (Figure 5.1). Both Strasbourg and Geispolsheim are located in the Rhine Valley, with the Vosges Mountains to the west and the Black Forest to the east. Strasbourg is an urban city containing shops, restaurants, residential areas, and the University of Strasbourg. Sampling was conducted on the balcony surrounding the University's Botanic Institute (48.5840°, 7.7663°, 30 m a.g.l.), which was situated approximately 3 km from major highways and industrial areas, 11 km from the regional airport, and 3.5 km from agricultural areas. Samples of $PM_{2.5}$ were collected using two Low Volume Samplers (2.3 m^3/h, Sven Leckel, Berlin, Germany)

equipped with prebaked (600°C overnight) 47 mm quartz fiber filters (Whatman QM-A, GE Healthcare Bio-Sciences, Marlborough, MA). Sampling was performed continuously from October 27, 2016 through December 15, 2016, with filters replaced 1 – 2 times daily when no fog events occurred. Five fog events occurred during this period; quartz filters were replaced at the beginning and end of each event.

(a)

(b)

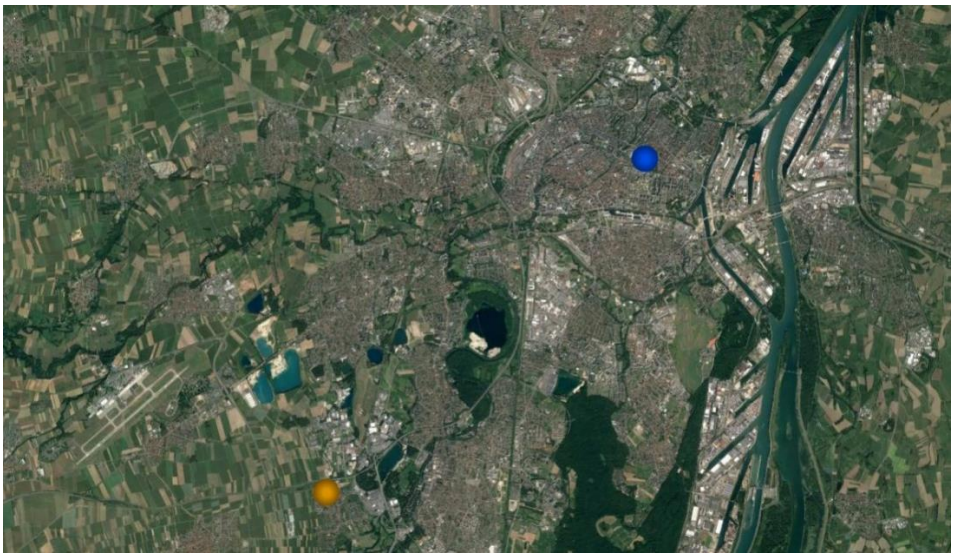

Figure 5.1. Maps featuring the location of the sampling sites. (a) Geispolsheim and Strasbourg are located in northeast France in the Rhine Valley. (b) The Geispolsheim sampling site (orange) is approximately 9 km southwest of the Strasbourg site (blue).

Fog water was collected using small stainless steel Caltech Active Strand Cloudwater Collectors (ss-CASCC2, Demoz et al., 1996). Only one ss-CASCC2 was available for the first three events, while two collectors were used simultaneously during the last two events. The start and end points of each event were determined when the visibility was estimated to be less than 500 m, using the belfry of the cathedral of Strasbourg as a visual reference. After collection, quartz filters were stored in prebaked aluminum foil at -20°C until analysis. Fog samples were filtered using prebaked quartz filters and frozen (-20°C) until analysis.

Geispolsheim is a suburban town located approximately 9 km southwest of Strasbourg with residential areas and two agricultural areas in the municipality. Sampling was conducted in a residential garden (48.5248°, 7.6806°, 4 m a.g.l.), which is 300 m from a highway, 800 m from two state roads, 300 m from a small commercial area, 4.5 km from the regional airport, and 6 km from industrial areas. Samples of PM_{10} were collected using a Sven Leckel Low Volume Sampler (2.3 m^3/h) equipped with prebaked (600°C overnight) 47 mm quartz fiber filters. Sampling was performed continuously from October 28, 2016 through November 2, 2016, with filters replaced 1-2 times daily when no fog events occurred. Two fog events occurred during this period; quartz filters were replaced at the beginning and end of each event. Fog water was collected using a ss-CASCC2. After collection, quartz filters were stored in prebaked aluminum foil at -20°C until analysis. Fog samples were filtered using prebaked quartz filters and frozen (-20°C) until analysis.

Sample analysis.

All aerosol samples were analyzed by thermal optical transmittance for organic carbon (OC), elemental carbon (EC), and total carbon (TC) concentrations using a Sunset Lab OC-EC Aerosol Analyzer (Birch & Cary, 1996). A variation of Sunset's "Quartz" TOT method was utilized. Variable time steps of 60 – 200 seconds were used during OC evolution, with temperature plateaus at 310°C, 475°C, 615°C, and 870°C. During EC evolution, the temperature was held at 550°C, 625°C, 700°C, 775°C, and 850°C for 45 seconds each, with a final hold at 870°C for 120 seconds. Quality control included the analysis of lab blanks, field blanks, replicate samples, and a sucrose standard, which was routinely within 10% of the known concentration.

A selection of samples were also fumed with concentrated hydrochloric acid (HCl) and analyzed using the above TOT method parameters in order to measure the amount of carbonate present in the samples (Cachier et al., 1989; Karanasiou et al., 2011). HCl fuming was performed by placing a 1.5 cm^2 filter punch into a clean glass petri dish and carefully placing 8 – 10 small drops (approximately 0.5 mm in diameter) around the filter without allowing the filter to come into contact with the acid. The petri dish was covered and the sample was fumed for 30 minutes. The sample was then removed from the petri dish and placed in a fume hood to allow residual HCl fumes to volatilize before analysis.

Isotopic measurements for $\delta^{13}C_{VPDB}$ of TC in PM samples were performed using a Costech Elemental Analyzer coupled to a Thermo Delta Plus Advantage Isotope Ratio Mass Spectrometer (EA-IRMS). The analytical uncertainty of samples analyzed on this method is reported at 0.2‰. NIST 2710 (Montana soil) was used as a linearity standard.

Three in-house glycine standards were used to perform and verify a two-point calibration from -39.6‰ to 15.7‰.

Isotopic measurements for $\delta^{13}C_{VPDB}$ of DOC fog samples were performed using an OI Analytical TOC Analyzer coupled to a Thermo Delta Plus Advantage Isotope Ratio Mass Spectrometer (TOC-IRMS). The analytical uncertainty of samples analyzed on this method is reported at 0.3‰. Potassium hydrogen phthalate (KHP, Sigma Aldrich, 99.95%) with a known isotopic composition was used as a linearity standard. Three in-house glycine standards were used to perform and verify a two-point calibration from -45.9‰ to 8.9‰.

Additionally, $PM_{2.5}$ samples collected in Bakersfield, CA in January and February 2013 were analyzed. OC and EC were quantified using the TOT method described above, and the $\delta^{13}C_{VPDB}$ of TC was measured.

Results and Discussion

Fog events in Strasbourg and Geispolsheim.

In total, fifteen fog events (five in Strasbourg, ten in Geispolsheim) were collected and analyzed. Table 5.1 reports the sampling times, pH, DOC, conductivity, $\delta^{13}C_{DOC}$, and major ions analyzed in each sample. The volume-weighted average DOC of fog was 23.3 ppmC (ranging from 7.8 – 37.7 ppmC) in Strasbourg and 21.8 ppmC (ranging from 8.6 – 43.1 ppmC) in Geispolsheim. The average pH of fog in Strasbourg was 6.8, which was less acidic than fog in Geispolsheim with an average pH of 6.0. Strasbourg fog in 2016 was much less acidic than in the early 1990's: the pH of fog ranged from 2.80 – 5.80 in 1991, 2.27 – 6.16 in 1992, 5.08 – 6.30 in 1993, and 2.40 – 5.50 in 1994 (Millet et al., 1997). From 1991 – 1999, the overall pH of fog was found to increase by approximately

1 pH unit, which was consistent with a decrease in SO_4^{2-} over the same time period (Herckes et al., 2002). In 1991, the average concentration of SO_4^{2-} in Strasbourg fog was 2,150 µeq/L (103 mg/L) in 5 – 8 µm droplets and 5,020 µeq/L (241 mg/L) in 2 – 6 µm droplets (Millet et al., 1996). In this study, the volume-weighted average concentration of SO_4^{2-} in Strasbourg fog was 18 mg/L.

Table 5.1

*Analysis results for fog collected in Strasbourg and Geispolsheim in 2016. Uncertainty in $\delta^{13}C$ measurements is 0.3‰. n.d. = not detected. * = not analyzed.*

Sample ID	Sampling Location	Start Date/Time	End Date/Time	Sampling Time (min)	Sample Volume (mL)	DOC (ppmC)	pH	Conductivity (µS/cm)
16S-1	Strasbourg	10/28/16 7:51 AM	10/28/16 10:51 AM	180	21.2	7.82	7.17	*
16S-2	Strasbourg	10/30/16 4:46 AM	10/30/16 11:42 AM	416	35.9	11.72	7.08	*
16S-3	Strasbourg	10/31/16 11:27 PM	11/1/16 7:33 AM	486	12.2	35.5	6.72	*
16S-4	Strasbourg	12/13/16 2:34 AM	12/13/16 10:26 AM	472	133.7	20.48	6.77	*
16S-5	Strasbourg	12/15/16 1:40 AM	12/15/16 11:56 AM	616	68.5	37.68	6.73	*
G16-1	Geispolsheim	10/16/16 2:25 AM	10/16/16 9:40 AM	435	92.5	13.64	6.12	105.8
G16-2	Geispolsheim	10/23/16 4:05 AM	10/23/16 7:35 AM	210	80.5	28.38	6.60	94.1
G16-3	Geispolsheim	10/27/16 5:40 AM	10/27/16 10:50 AM	310	94.0	13.18	6.12	101.3
G16-4	Geispolsheim	10/28/16 4:55 AM	10/28/16 11:05 AM	370	181.5	25.57	6.05	103.9
G16-5	Geispolsheim	10/30/16 4:25 AM	10/30/16 11:30 AM	425	101.5	43.14	6.06	170.6
G16-6	Geispolsheim	11/1/16 12:10 AM	11/1/16 10:05 AM	595	136.5	8.57	5.70	124.8
G16-7	Geispolsheim	12/6/16 10:00 PM	12/7/16 4:15 AM	375	56.5	23.88	5.62	138.7
G16-8	Geispolsheim	12/13/16 3:50 AM	12/13/16 9:05 AM	315	117.0	15.82	5.68	70.8
G16-9	Geispolsheim	12/15/16 2:20 AM	12/15/16 8:15 AM	355	73.0	25.32	*	*
G16-10	Geispolsheim	12/16/16 3:05 AM	12/16/16 7:40 AM	275	75.0	26.3	*	*

Table 5.1 (continued)

*Analysis results for fog collected in Strasbourg and Geispolsheim in 2016. Uncertainty in $\delta^{13}C$ measurements is 0.3‰. n.d. = not detected. * = not analyzed.*

Sample ID	$\delta^{13}C_{DOC}$ (‰)	F^- (mg/L)	Cl^- (mg/L)	NO_2^- (mg/L)	Br^- (mg/L)	NO_3^- (mg/L)	PO_4^{3-} (mg/L)	SO_4^{2-} (mg/L)	Na^+ (mg/L)	NH_4^+ (mg/L)	K^+ (mg/L)	Ca^{2+} (mg/L)
16S-1	-28.5	0.60	0.61	26.47	n.d.	10.09	3.40	24.44	3.78	10.80	1.29	11.43
16S-2	-26.5	0.72	2.29	0.84	n.d.	27.14	n.d.	15.27	6.77	11.35	0.99	2.35
16S-3	-26.9	1.11	2.31	2.14	n.d.	35.80	4.79	14.62	5.23	14.89	1.52	9.59
16S-4	-26.2	0.31	2.28	0.95	n.d.	35.63	0.59	14.35	6.43	13.98	0.64	1.05
16S-5	-27.0	0.87	3.11	4.38	n.d.	22.76	n.d.	26.33	4.60	20.52	1.36	1.78
G16-1	-26.9	0.13	5.77	1.88	n.d.	8.79	n.d.	10.02	4.06	6.38	0.83	1.92
G16-2	-25.7	0.19	0.49	1.83	n.d.	5.50	n.d.	8.25	2.11	8.01	0.47	3.50
G16-3	-26.3	0.21	0.74	1.87	n.d.	8.80	n.d.	16.26	2.21	8.24	1.05	3.25
G16-4	-25.9	0.08	1.11	1.98	0.52	16.28	n.d.	11.55	1.51	9.67	0.38	0.94
G16-5	-25.6	0.29	3.75	1.00	n.d.	45.26	n.d.	20.82	3.59	12.56	1.13	4.94
G16-6	-25.7	0.10	6.23	1.85	n.d.	28.50	n.d.	11.85	5.92	8.36	n.d.	1.04
G16-7	-25.6	0.97	5.66	0.37	n.d.	39.13	n.d.	22.24	2.09	13.89	2.09	4.49
G16-8	-25.4	0.68	1.72	0.70	n.d.	26.19	n.d.	8.84	0.45	11.19	0.38	0.04
G16-9	-26.1	0.47	1.64	2.36	n.d.	20.38	n.d.	14.16	0.43	14.14	0.77	0.04
G16-10	-26.0	1.33	1.09	2.88	n.d.	15.12	n.d.	9.42	1.69	11.59	0.60	0.07

Particulate matter in Strasbourg and Geispolsheim.

$PM_{2.5}$ samples were collected in Strasbourg from October 27, 2016 through December 15, 2016. PM_{10} samples were collected in Geispolsheim from October 28, 2016 through November 2, 2016. Sampling times and analysis results for all samples (OC, EC, and TC concentrations, and $\delta^{13}C_{TC}$) are detailed in Tables C1 and C2, respectively, of Appendix C. Using $PM_{2.5}$ data obtained from an air quality station in central Strasbourg monitored by ATMO Grand Est (http://www.atmo-grandest.eu/), organic matter (OM, calculated from the air concentration of OC and applying the multiplier of 1.4 for urban areas, Mancilla et al., 2015) was averaged to make up 34% of $PM_{2.5}$ in Strasbourg. The amount of OM falls within similar percentages of other locations. $PM_{1.5}$ collected in Aspvreten, a forest park in central Sweden, contained 43% OM; $PM_{1.5}$ from K-Puszta, a rural location in Hungary, contained 27% OM; and $PM_{1.5}$ from San Pietro Capofiume (in eastern Po Valley, a populous industrial and agricultural area) contained 21% OM (Zappoli et al., 1999). $PM_{2.5}$ collected in Yosemite National Park, however, contained an average of 70.6% OM (Malm et al., 2005), due to the high contribution of biomass burning and SOA sources (Bench, 2004; Engling et al., 2006).

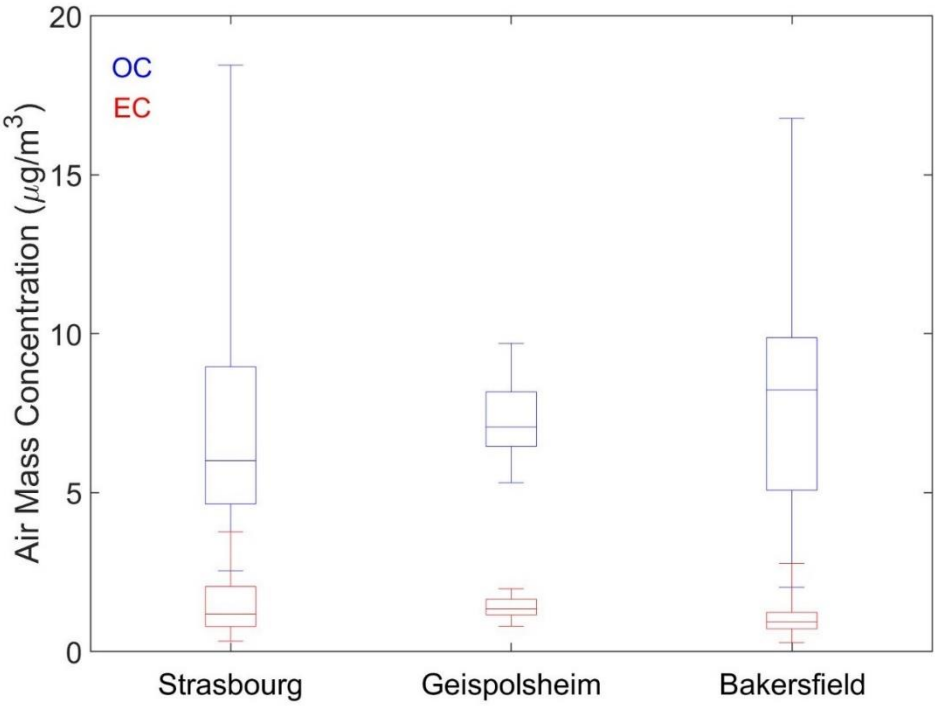

Figure 5.2. Box plots of OC and EC air mass concentrations in Strasbourg, Geispolsheim, and Bakersfield. The median, first and third quartiles, and minimum and maximum data points are visualized.

In Strasbourg, rain, fog, and frozen fog events occurred over the entire sampling period, while two fog events occurred during PM_{10} sampling in Geispolsheim. Figure 5.2 summarizes the concentrations of OC and EC when no multiphase events occurred. In Strasbourg, the median concentration of OC was 6 µg/m^3, ranging from 3 – 18 µg/m^3, and the median concentration of EC was 1.2 µg/m^3, ranging from 0.3 – 3.7 µg/m^3. In Geispolsheim, the median concentration of OC was 7 µg/m^3, ranging from 5 – 10 µg/m^3, and the median concentration of EC was 1.3 µg/m^3, ranging from 0.8 – 2.0 µg/m^3. These results are similar to other urbanized valley locations; in $PM_{2.5}$ collected in Bakersfield, CA, the median concentration of OC was 8 µg/m^3, ranging from 2 – 17 µg/m^3, and the median concentration of EC was 0.9 µg/m^3, ranging from 0.3 – 2.8 µg/m^3.

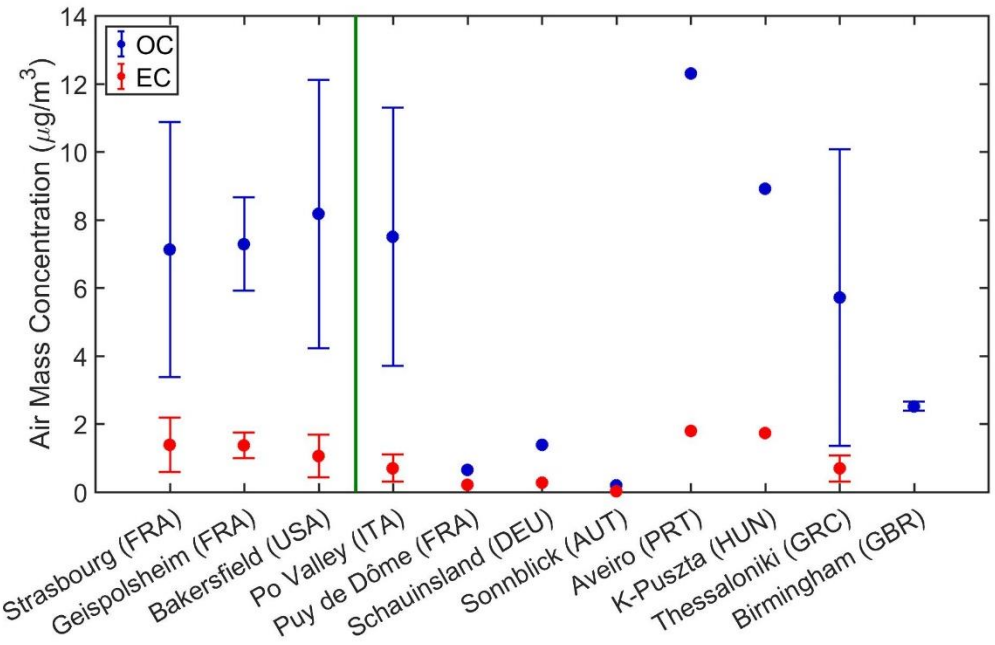

Figure 5.3. Plot of average OC and EC concentrations measured in urban and rural locations. Standard deviations are shown when available. Samples were collected in Strasbourg and Geispolsheim, France, and Bakersfield, CA (this study), the Po Valley, Italy (Decesari et al., 2001), Puy de Dôme, France, Schauinsland, Germany, Sonnblick, Austria, Aveiro, Portugal, and K-Puszta, Hungary (Gelencsér et al., 2007), Thessaloniki, Greece (Samara et al., 2014), and Birmingham, England (Yin et al., 2010).

Figure 5.3 shows the average concentrations of OC and EC in Strasbourg and Geispolsheim, as well as in other urban and rural locations. In $PM_{1.5}$ collected in the Po Valley, an urbanized area comparable to Strasbourg and Geispolsheim, the concentration of OC averaged 8 ± 4 μg/m^3, and the concentration of EC averaged 0.7 ± 0.4 μg/m^3 (Decesari et al., 2001). By contrast, $PM_{2.5}$ collected in the remote locations of Puy de Dôme, France, Schauinsland, Germany, and Sonnblick, Austria were found to have lower wintertime concentrations of OC and EC (respectively, 0.65 μg/m^3 OC, 0.21 μg/m^3 EC; 1.38 μg/m^3 OC, 0.28 μg/m^3 EC; 0.19 μg/m^3 OC, 0.02 μg/m^3 EC, Gelencsér et al., 2007), while $PM_{2.5}$ in the rural locations of Aveiro, Portugal and K-Puszta, Hungary contained comparable OC and EC concentrations in the winter (respectively, 12.3 μg/m^3 OC,

1.8 μg/m^3 EC; 8.91 μg/m^3 OC, 1.74 μg/m^3 EC, Gelencsér et al., 2007). Elevated OC and EC concentrations in Aveiro and K-Puszta were attributed to high incidences of biomass burning. $PM_{2.5}$ in Thessaloniki, Greece was found to contain an average of 5.72 μg/m^3 OC and 0.69 μg/m^3 EC (Samara et al., 2014). Wintertime urban background OC concentrations in $PM_{2.5}$ in Birmingham, England averaged 2.52 ± 0.13 μg/m^3 (Yin et al., 2010). Ambient OC and EC concentrations in Strasbourg and Geispolsheim are similar overall to other urbanized sampling locations, and are, as expected, higher than in remote locations.

Scavenging of carbonaceous particulate matter by fog.

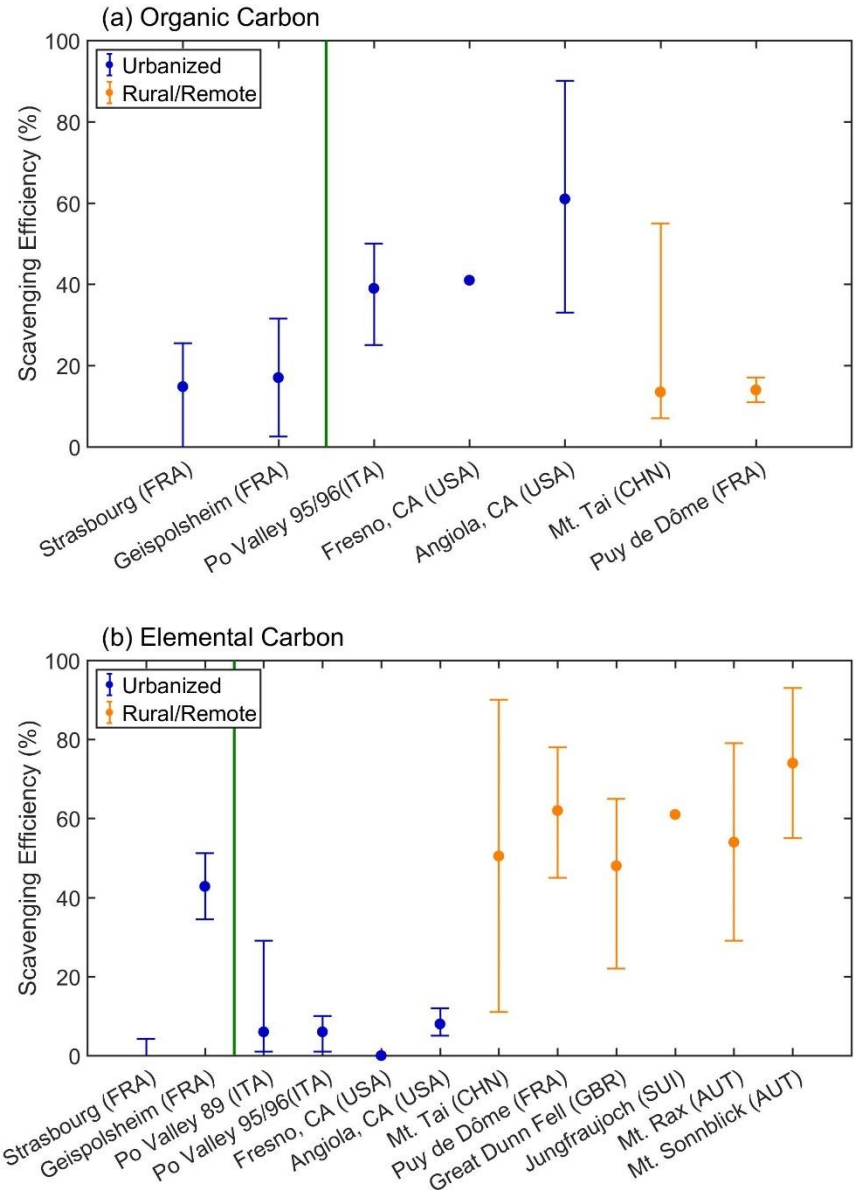

Figure 5.4. Scavenging efficiencies of (a) OC and (b) EC during fog events in Strasbourg and Geispolsheim, compared to OC and EC scavenging efficiencies in other urbanized and remote locations. Dots report the median or average value, and the error bars report the minimum and maximum observations, with the exception of Mt. Rax, where the error bars represent the standard deviations. Reported observations are from the Po Valley, Italy (Facchini et al., 1999; Hallberg et al., 1992), Angiola and Fresno, CA (Collett et al., 2008), Mt. Tai, China (Wang et al., 2011), Puy de Dôme, France (Sellegri et al., 2003), Great Dunn Fell, England (Gieray et al., 1997), Jungfraujoch, Switzerland (Cozic et al., 2007), Mt. Rax, Austria (Hitzenberger et al., 2001), and Mt. Sonnblick, Austria (Hitzenberger et al., 2000).

The scavenging efficiencies, defined as the fraction of PM incorporated into a fog droplet (Herckes et al., 2013), of OC and EC were calculated based upon the concentrations of particle phase OC and EC measured before and during the fog events. Figure 5.4 compares the OC and EC scavenging efficiencies of fog events in Strasbourg and Geispolsheim to measurements in other urbanized and remote locations. The scavenging efficiency of OC in Strasbourg averaged 15%, and ranged from negligible scavenging of OC to 26% of OC scavenged by fog. 2 – 32% of OC was scavenged during the two fog events in Geispolsheim. The OC scavenging efficiencies were more similar to those calculated in remote locations (Mt. Tai, Puy de Dôme) than in more urbanized locations (Po Valley, Fresno, Angiola). Scavenging of OC by fog is dependent on the polarity and water solubility of the organic species (Facchini et al., 1999) as well as the particle source (i.e., wood smoke vs. vehicle exhaust, Collett et al., 2008).

Overall, the scavenging of EC by fog in Strasbourg was negligible. However, the scavenging of EC in Geispolsheim ranged from 34 – 51%. The scavenging of EC in urbanized locations is generally low, due to the hydrophobic properties and small particle size of freshly emitted aerosols containing EC. All four studies in urbanized valley locations referenced in Figure 5.4b (Po Valley, Fresno, and Angiola) averaged 8% or lower scavenged EC. However, the average percent of EC scavenged by fog in rural and remote locations ranged from 48% at Great Dunn Fell (Gieray et al., 1997) to 74% at Mt. Sonnblick (Hitzenberger et al., 2000). In Geispolsheim, the wind originated primarily from the north during the 72 hours preceding each fog event (Figure 5.5), meaning that the air masses in Geispolsheim could contain aged particles originating in Strasbourg.

Aging of particles during transport could cause EC to become associated with oxidized material and larger particles that are more readily scavenged by the aqueous phase.

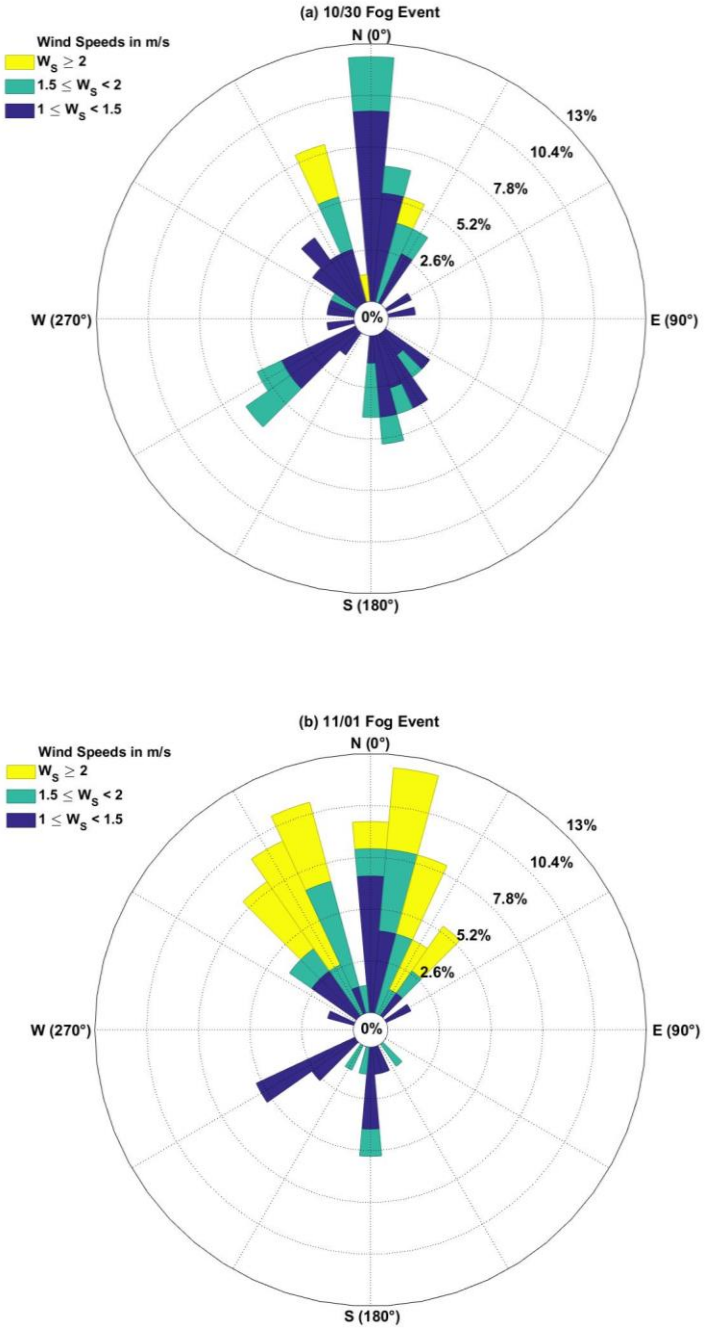

Figure 5.5. Wind roses depicting the wind direction 72h prior to two fog events in Geispolsheim, on (a) October 30 and (b) November 1. The wind primarily originated from the north before both fog events.

When a fog forms, it will scavenge carbonaceous material from both the gas and particle phases. Table 5.2 shows the change in concentration of particle phase OC when a fog forms, and the air equivalent concentration of the DOC of fog. During the fog event of October 28 (Sample 16S-1), the concentration of OC in $PM_{2.5}$ does not decrease as would be expected, but instead increases by 28%. Similarly, the concentration of EC during this event increases by 140%. It is possible that these high values were calculated due to the short sampling time of the fog (3 hours). In evaluating the scavenging efficiencies of fog, these data points were considered outliers and were not included in the discussion. During four of the fog events (16S-2, 16S-4, 16S-5, and G16-6), the [OC] of PM decreased by a greater value than the fog [DOC]. During event G16-5, the [DOC] of the fog was greater than the [OC] scavenged from the particle phase. Finally, during event 16S-3, the change in [OC] in $PM_{2.5}$ was negligible, but DOC was still present in the fog. Several factors could account for the variations in these observations. For fog events in which the [OC] scavenged from PM was higher than the [DOC] of fog, it is possible that water insoluble organic carbon was scavenged by the droplets. In the examples where the [DOC] of fog is higher than the [OC] scavenged from PM, gas-phase organic compounds may have been scavenged by the fog. A study and modeling of anthropogenically impacted fog (Davis, CA) compared to biogenically impacted fog (Whistler, BC) showed that aged (oxidized) air masses cause DOC to increase and cause the Henry's Law for DOC to increase such that more organic gases partition into the aqueous phase (Ervens et al., 2013). Concentrations of dissolved gases in fog in Angiola, CA were also found to be dependent on the size and lifetime of the droplets, and supersaturation of dissolved organic species caused by evaporation was observed (Ervens

et al., 2003). Additionally, droplet size can affect equilibrium of droplets with the gas phase due to variations in pH with droplet size, as was observed at Great Dunn Fell in England (Laj et al., 1997). Without measurements of gas-phase species in Strasbourg, elucidations of the mass balance of fog DOC is not possible.

Table 5.2

Comparison of OC concentrations in PM before and during fog, and the air equivalent DOC concentration in fog.

Sample ID	Sampling Location	OC, Pre-Fog PM ($\mu g/m^3$)	OC, Interstitial PM ($\mu g/m^3$)	OC Change, Pre-Fog - Interstitial PM ($\mu g/m^3$)	Fog DOC ($\mu g/m^3$)
16S-1	Strasbourg	4.82	6.15	-1.33	0.13
16S-2	Strasbourg	4.96	4.26	0.70	0.15
16S-3	Strasbourg	4.18	4.26	-0.08	0.13
16S-4	Strasbourg	7.14	5.60	1.54	0.42
16S-5	Strasbourg	11.18	8.33	2.85	0.30
G16-5	Geispolsheim	6.57	6.40	0.16	1.48
G16-6	Geispolsheim	6.31	4.32	1.99	0.28

$\delta^{13}C$ of particulate matter, no multiphase events.

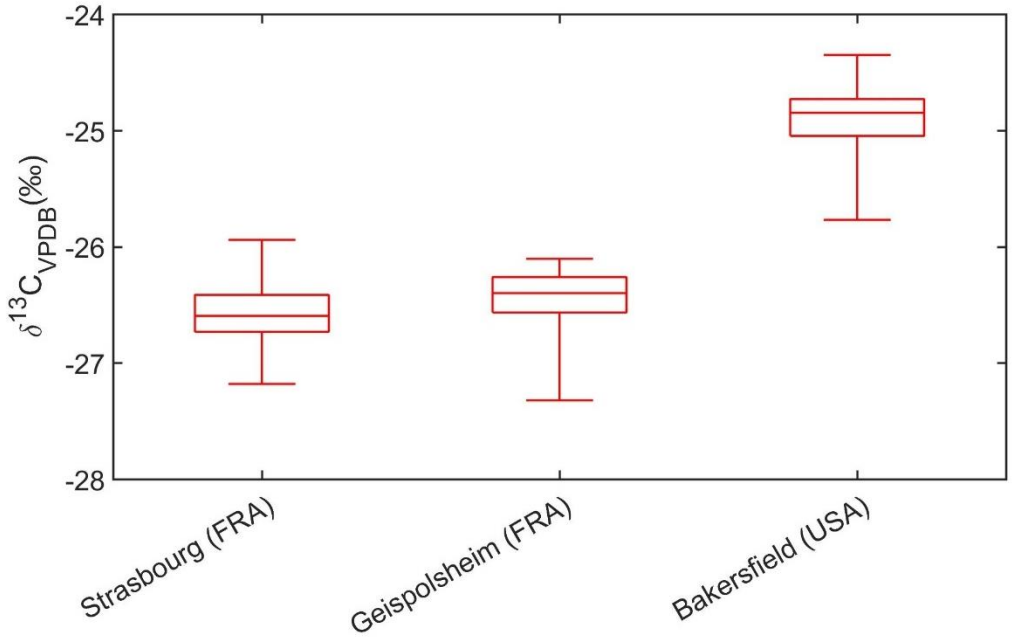

Figure 5.6. Box plots of the $\delta^{13}C_{TC}$ of atmospheric PM collected in Strasbourg, Geispolsheim, and Bakersfield.

Even though concentrations of OC and EC varied among sampling days, $\delta^{13}C_{TC}$ remained fairly consistent when no multiphase events occurred (Figure 5.6). The median $\delta^{13}C_{TC}$ in Strasbourg was -26.6‰, ranging from -27.2 – -25.9‰. In Geispolsheim, the median $\delta^{13}C_{TC}$ was -26.4‰, ranging from -27.3 – -26.1‰. In both locations, the difference between the first and third quartiles was 0.3‰. These results are consistent with the expectation that the formation of secondary organic aerosol is low in the autumn and winter. Photochemical reactions would cause a net decrease in $\delta^{13}C_{TC}$ due to the kinetic isotope effect in the formation of secondary organic aerosols (Fisseha et al., 2009), which would in turn cause greater variations in daily $\delta^{13}C_{TC}$ observations.

The average $\delta^{13}C_{TC}$ in both Strasbourg and Geispolsheim is depleted relative to that of Bakersfield, which is located in California's San Joaquin Valley. The median

$\delta^{13}C_{TC}$ of $PM_{2.5}$ in Bakersfield was -24.8‰, with a range of -25.8 – -24.4‰ and a difference of 0.3‰ between quartiles 1 and 3. Chapter 2 provides a comparison of atmospheric particulate matter $\delta^{13}C_{TC}$ of Strasbourg and Geispolsheim to other sampling locations in the western United States, Canada, and Mexico as well (Figure 2.2). The particulate matter collected in Strasbourg and Geispolsheim was found to be depleted in $\delta^{13}C_{TC}$ compared to these other urban locations, and similar to a biogenically influenced site (Whistler, BC). Studies of the $\delta^{13}C$ of primary aerosol sources have shown that diesel fuel is depleted in $\delta^{13}C$ relative to gasoline: In Paris, particles emitted by unleaded gasoline had an average $\delta^{13}C_{TC}$ of -24.2 ± 0.6‰, while those emitted by diesel had an average $\delta^{13}C_{TC}$ of -26.5 ± 0.5‰. (Widory et al., 2004). The greater use of diesel fuel in France could explain the depletion in $\delta^{13}C$ of the collected particles relative to Bakersfield. New diesel vehicles comprised 77% of new car sales in France in 2008, as opposed to 47% in 1995 (Schipper, 2011). Additionally, measurements of the ratios of select PAHs demonstrate that diesel fuel emissions are more prominent in PM_{10} in Strasbourg than gasoline (Delhomme & Millet, 2012). Conversely, diesel fuel accounts for 28% of fuel use in the United States (Gentner et al., 2012).

$\delta^{13}C$ of particulate matter in fog.

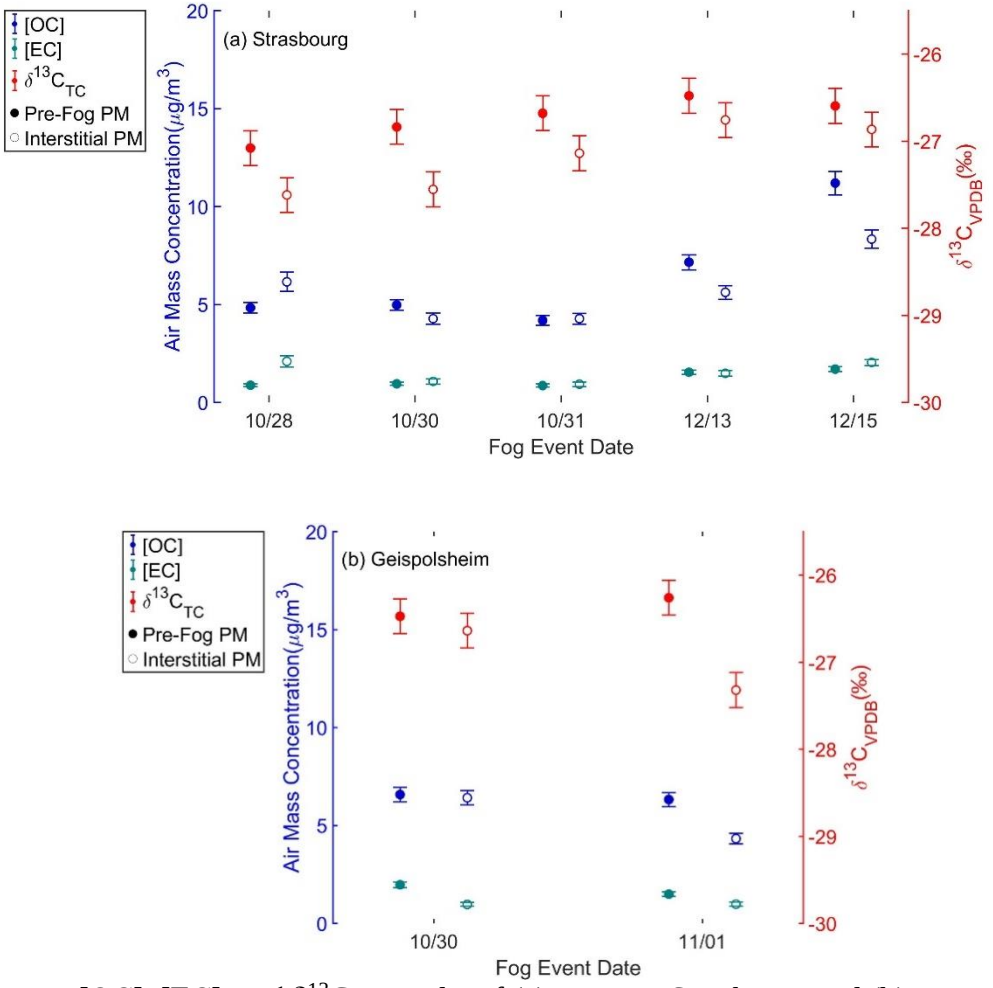

Figure 5.7. [OC], [EC], and $\delta^{13}C_{TC}$ results of (a) $PM_{2.5}$ in Strasbourg and (b) PM_{10} in Geispolsheim, immediately before a fog event (pre-fog PM) and during a fog event (interstitial PM).

Over the course of particle sampling, five fog events in Strasbourg and two fog events in Geispolsheim occurred. Figure 5.7 illustrates the effect of fog on $\delta^{13}C_{TC}$ and concentrations of OC and EC. In Strasbourg, $\delta^{13}C_{TC}$ of $PM_{2.5}$ was depleted by 0.3 – 0.7‰ during a fog event, relative to the particles collected in the time period immediately before the start of the event. In Geispolsheim, $\delta^{13}C_{TC}$ of PM_{10} during one fog event was depleted by 1.1‰. No depletion of $\delta^{13}C_{TC}$ was observed during the October 30th event in

Geispolsheim; however, this filter included aerosol collected for 4.5 hours before the 7-hour fog event, so an isotopic depletion effect may be diluted. This sample will therefore not be included in the discussion.

These results suggest that preferential particle scavenging by the fog might be occurring, which would result in carbon enriched in $\delta^{13}C_{TC}$ being incorporated into droplets and carbon depleted in $\delta^{13}C_{TC}$ remaining in the particle phase. Additionally, if preferential scavenging by fog is occurring in Strasbourg, it is likely size-dependent, with large particles enriched in $\delta^{13}C_{TC}$ relative to small particles: if larger particles are scavenged more readily than small particles, the remaining interstitial particles would display an overall depletion in $\delta^{13}C_{TC}$.

Previous studies have shown that the $\delta^{13}C_{TC}$ of particles in larger size modes tends to be heavier than smaller particles. As discussed in Chapter 4, the $\delta^{13}C_{TC}$ of particles > 1.5 μm in Tempe, AZ was higher than the $\delta^{13}C_{TC}$ of particles < 1.5 μm, due to the presence of carbonate in the coarser size fractions. Masalaite and coworkers (2015) collected particles in eleven size-segregated fractions from 0.056 – 18 μm in Vilnius, Lithuania and found the coarse fractions (> 1 μm) to be enriched relative to the fine fractions (< 1 μm), on average (-26 ± 1‰, versus -28.0 ± 0.9‰, respectively). The enrichment in $\delta^{13}C$ of coarse particles was attributed to a combination of carbonates in the coarse fraction, variations in particle source among size fractions (with fossil contributions in fine particles and non-fossil contributions in coarse particles), and the enrichment in $\delta^{13}C$ that results when fine particles aggregate into coarse particles in aqueous-phase chemical processing.

The size-dependent scavenging of particulate matter by fog has long been a subject of study. Bator & Collett (1997) found that there was a difference in chemical composition of small (4 – 23 μm) and large (> 23 μm) cloud droplets, which could be attributed to differences in the composition of large primary aerosols and small accumulation-mode aerosols. Herckes and coworkers (2002) found that TOC concentrations in small fog droplets (in the range of 6 – 17 μm) were higher than in large droplets (> 17 μm) collected in Angiola, CA, on average by a factor of 2.8, possibly due to the formation of small droplets on smaller particles that contain more carbonaceous material than large particles. Collett and coworkers (2008) also observed that wood smoke particles were more efficiently scavenged by fog in Angiola and Fresno than those of vehicle exhaust, which suggests that the lifetime of wood smoke particles is limited relative to motor vehicle exhaust particles. This study also suggests that differences in OC and EC scavenging could result from differences in size distributions of these species. In measuring the hygroscopic growth of particles at Great Dunn Fell, Svenningsson and coworkers (1997) measured higher growth factors and a greater soluble fraction for larger particles (265 nm) than smaller particles (50 nm).

Strasbourg is situated along the Rhine River, whose banks are composed of loess (Salomons, 1975; Swineford & Frye, 1955; Taylor et al., 1983). The loess along the Rhine consists of particles in a wide size range, from greater than 44 μm to less than 2 μm, and particles in the size fraction below 2 μm can to contain up to 40% calcium carbonate (Swineford & Frye, 1955). Carbonate therefore has the potential to be incorporated into $PM_{2.5}$. Additionally, carbonate minerals are highly enriched in $\delta^{13}C$ relative to organic and elemental carbon; specifically, carbonate analyzed at the Rhine-

Meuse estuary in the Netherlands ranged in $\delta^{13}C$ from -3.6 – -0.6‰ (Salomons, 1975). Therefore, as discussed in Chapter 3, carbonate carbon content as low as 2% of the total carbon could potentially impact the $\delta^{13}C_{TC}$ of a sample. A selection of $PM_{2.5}$ samples were consequently selected for carbonate analysis by acidification by HCl fuming to remove carbonate and subsequent TOT analysis; results are shown in Table 5.3. In some samples, a decrease of up to 1 μg/cm^2 in the measured load of TC on a filter is observed, which is equivalent to a loss of 1 – 5% of carbon with acid fuming. This, however, is not the case for all samples, and for those samples that do decrease in TC when acid treated, the change in mass is not significant when the uncertainty in the measurements is considered. Because small filters (47 mm) were used in sample collection, there is insufficient sample to perform the carbonate quantification method outlined in Chapter 3. There is also insufficient sample to perform acid treatment of the PM_{10} samples collected in Geispolsheim, but because the coarse mode was collected here, there is a greater potential for loess carbonate to impact these samples. While the presence of carbonate in these samples cannot be confirmed, it cannot be ruled out as a constituent of $PM_{2.5}$ in Strasbourg.

Table 5.3

Results of acid treatment of select $PM_{2.5}$ filters collected in Strasbourg for the determination of carbonate concentration. Results are shown as micrograms of carbon per square centimeter of filter.

Sample ID	Total Carbon ($\mu g/cm^2$)	Total Carbon Uncertainty ($\mu g/cm^2$)	Total Carbon, HCl Fumed ($\mu g/cm^2$)	Total Carbon, HCl Fumed Uncertainty ($\mu g/cm^2$)
SA04	21.6	1.3	21.3	1.3
SA13	22.7	1.3	21.6	1.3
SA41	20.8	1.2	20.7	1.2
SA55	23.2	1.4	23.0	1.4
SA72	21.7	1.3	21.0	1.3
SA78	22.4	1.3	22.4	1.3
SA84	33.9	1.9	35.1	2.0

In sum, the preferential scavenging of particles enriched in $\delta^{13}C_{TC}$ could be due to a number of factors. Size-dependent scavenging could play a role, as particles in different size fractions have different compositions and originate from different primary aerosol sources. As discussed in Chapter 2, different source materials could potentially have different $\delta^{13}C$ values, but this factor is location-dependent; a study of the isotopic compositions of local source materials in Strasbourg and Geispolsheim and a source apportionment of local aerosols would be necessary to make these determinations. The presence of carbonate, which is enriched in $\delta^{13}C$ relative to OC and EC, could cause the $\delta^{13}C_{TC}$ of interstitial particles to become depleted if particles containing carbonate are scavenged.

$\delta^{13}C$ of particulate matter in rain and frozen fog.

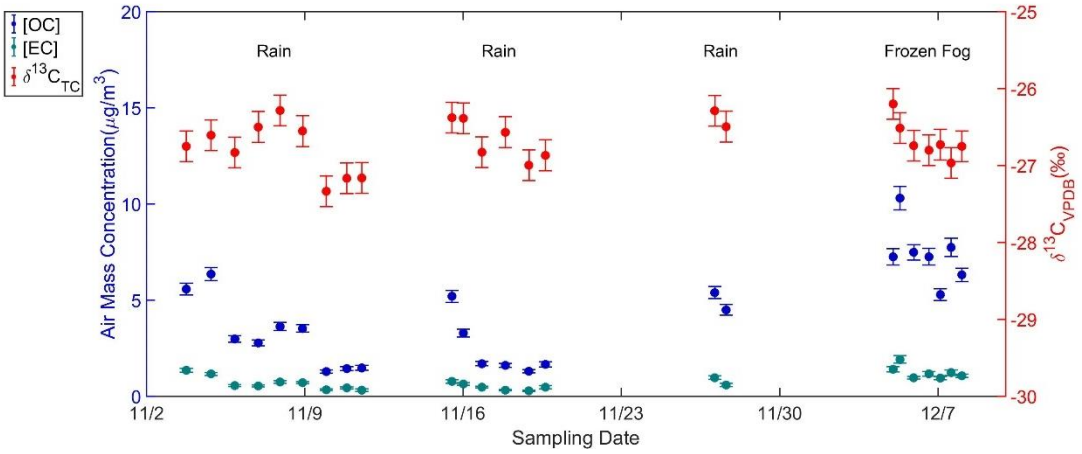

Figure 5.8. [OC], [EC], and $\delta^{13}C_{TC}$ results of three periods of rain on November 3 – November 11, November 15 – November 19, and November 26 – November 27, and a period of frozen fog on December 4 – December 8.

Three periods of rain occurred over the course of $PM_{2.5}$ sampling in Strasbourg. Figure 5.8 depicts a time series of these events. Significant scavenging of both OC and EC occurred during each event. During the period of rain from November 3 – November 11, [OC] decreased from 5.6 µg/m^3 to 1.5 µg/m^3, and [EC] decreased from 1.4 µg/m^3 to 0.3 µg/m^3. From November 15 – November 19, [OC] decreased from 5.2 µg/m^3 to 1.7 µg/m^3, and [EC] decreased from 0.8 µg/m^3 to 0.5 µg/m^3. From November 26 – November 27, [OC] decreased from 5.4 µg/m^3 to 4.5 µg/m^3, and [EC] decreased from 1.0 µg/m^3 to 0.6 µg/m^3. During each of these periods, a depletion in $\delta^{13}C_{TC}$ of $PM_{2.5}$ was also observed: $\delta^{13}C_{TC}$ decreased from -26.8‰ to -27.2‰ from November 3 – November 11, -26.4‰ to -26.9‰ from November 15 – November 19, and -26.3‰ to -26.5‰ from November 26 – November 27. During wet deposition, large particles would be scavenged more readily than small particles as rain droplets fall (Lim et al.,1991). As previously discussed with reference to the scavenging of particles by fog, isotopic differences with

particle size caused by differences in primary source material would result in an isotopic depletion of interstitial aerosol when large, isotopically enriched particles are scavenged. The removal of ^{13}C-enriched large particles through wet deposition could therefore explain the depletion in $\delta^{13}C_{TC}$ during these events.

Among all rain events, there is a significant correlation between the $\delta^{13}C_{TC}$ and the concentrations of OC and TC. These relationships are shown in Figure 5.9. There is a correlation between [OC] and $\delta^{13}C_{TC}$ of 0.64 ($p < 0.01$), and a correlation between [TC] and $\delta^{13}C_{TC}$ of 0.61 ($p < 0.01$). These results indicate that, as particles are scavenged by wet deposition and air mass concentrations decrease, the $\delta^{13}C$ of the particles also decreases. This data provides further evidence of the selective scavenging of particles enriched in ^{13}C. No significant correlation was observed between [EC] and $\delta^{13}C_{TC}$ ($r = 0.40$, $p > 0.1$). The majority of primary aerosols from vehicle emissions would be found in the submicron size range (Morawska et al., 1998), and since freshly emitted EC from would be found in small hydrophobic particles (Herckes et al., 2013), it would not be readily or consistently scavenged by wet deposition.

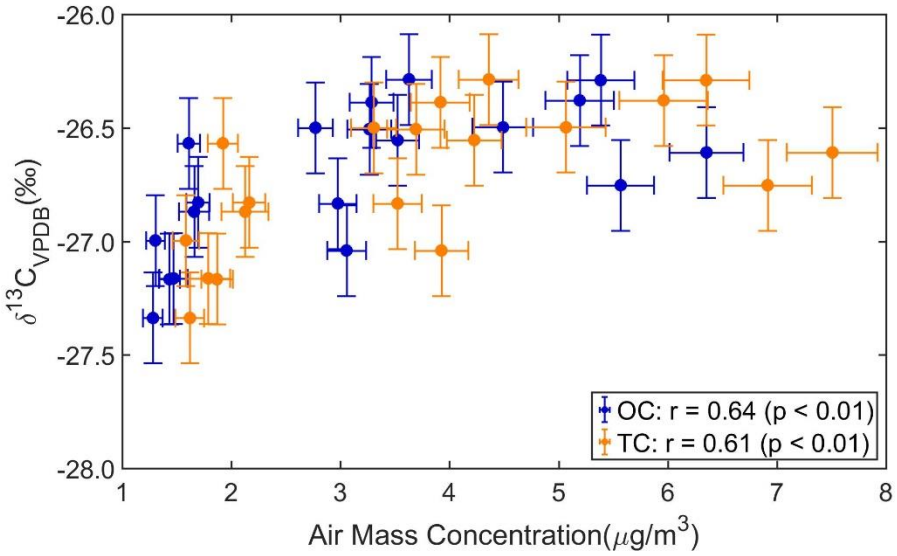

Figure 5.9. Correlation between air mass concentrations of OC and TC, and $\delta^{13}C_{TC}$ during periods of rain in Strasbourg.

A period of frozen fog occurred from December 4 – December 8 and is also depicted in Figure 5.8. While no consistent changes in OC or EC concentrations were apparent, the $\delta^{13}C_{TC}$ of $PM_{2.5}$ decreased significantly, from -26.2‰ to -26.8‰. It is possible that during this period, isotopically enriched particles were scavenged as condensation nuclei into particles greater than 2.5 µm in size. Meanwhile, anthropogenic particles from vehicle exhaust and wood burning would continue to be emitted as $PM_{2.5}$ into the atmosphere (Delhomme et al., 2010; Delhomme & Millet, 2012). This could account for a change in $\delta^{13}C_{TC}$ while no changes in particle concentration were apparent.

Conclusions

Samples of particulate matter and fog were collected in Strasbourg and Geispolsheim, France in the fall of 2016. Particulate matter samples were analyzed for [OC], [EC], and $\delta^{13}C_{TC}$, and fog samples were analyzed for pH, DOC, conductivity, $\delta^{13}C_{DOC}$, and major ions. The composition of fog in Strasbourg has changed over time,

with higher pH values and lower concentrations of SO_4^{2-} than in the 1990s. [OC] and [EC] concentrations of particulate matter fell in similar ranges to other urbanized valley locations, including Bakersfield, CA and the Po Valley in Italy. The scavenging of elemental carbon was negligible in Strasbourg but high in Geispolsheim, possibly due to the transport of aged aerosol from Strasbourg to Geispolsheim. Scavenging of organic carbon was moderate in both locations.

The $\delta^{13}C_{TC}$ of particulate matter was found to be consistent over time in both locations when no weather events occurred, but particles were isotopically depleted in the presence of fog due to preferential scavenging of larger isotopically enriched particles. Rain events also appeared to selectively scavenge isotopically enriched carbon, possibly due to isotopic differences with particle size. The $\delta^{13}C_{TC}$ of particulate matter in Strasbourg and Geispolsheim was also found to be depleted relative to the $\delta^{13}C_{TC}$ of particles collected in urban locations in the western United States, possibly due to differences in the use of diesel and gasoline fuel.

While the results of this study indicate that preferential particle scavenging is occurring by both fog and rain, further work is necessary to determine the exact cause of the observed isotopic depletion of interstitial particles. Since it is possible that fine (< 2 μm) loess particles that contain calcium carbonate could be present in $PM_{2.5}$, future studies should attempt to measure the fraction of TC that is carbonate. The carbonate measurement method introduced in Chapter 3 could be utilized if samples were collected for longer periods of time (greater than 24 h) to increase sample load, or a high-volume sampler that collects PM samples on large filter sheets (8 x 10 inches) could be deployed in place of a low-volume sampler. The use of a high-volume sampler could also make it

possible to perform $\delta^{13}C$ analysis of the carbonate carbon in the samples. Additionally, particle sources, transport, and atmospheric lifetimes can affect the size of particles and their hygroscopic properties, affecting particle scavenging efficiencies by fog. Source apportionment studies could aid in elucidating the most prominent sources of OC and EC in Strasbourg and Geispolsheim, and isotopic analysis of primary sources could help identify the types of particles that would most likely be scavenged by fog.

CHAPTER 6

ANALYSIS OF TIME-RESOLVED FOG EVENTS ON THE SOUTHERN CALIFORNIA COAST

The study of the organic composition of fog is relatively new and only became a field of interest in the 1990s (Herckes et al., 2013 and references therein). Measurements of the total organic carbon (TOC) or dissolved organic carbon (DOC) present in fog are now common (Capel et al., 1990; Collett et al., 2008; Erel et al., 1993; Ervens et al., 2013; Herckes et al., 2002; Reyes-Rodríguez et al., 2009), as are measurements of individual organic species (Boris et al., 2016; Boris et al., 2018; Löflund et al., 2002; Raja et al., 2008). However, there are currently no published studies on the carbon isotopic composition ($\delta^{13}C_{DOC}$) of the organics in fog water.

Conversely, water isotopes have been used extensively in literature to determine the relative contributions of rain and fog waters to local ecosystem hydrology (Corbin et al., 2005; Dawson, 1998; Fischer & Still, 2007; Ingraham & Matthews, 1988; Ingraham & Matthews, 1990; Schmid et al., 2011; Scholl et al., 2007; Scholl et al., 2011). For example, using $\delta^{18}O$ and $\delta^{2}H$ data, fog drip was shown to contribute to the recharge of shallow groundwater in northern Kenya (Ingraham & Matthews, 1988). In northern California, Ingraham & Matthews (1990) also found the relative isotopic compositions of fog, rain, and groundwater to be dependent upon their respective sources and atmospheric processing. Fog water was isotopically depleted relative to its source due to the isotopic fractionation during evaporation, which causes vapor to be depleted in $\delta^{18}O$ and $\delta^{2}H$ relative to liquid. Rain was isotopically depleted compared to fog due to Rayleigh distillation that occurs when clouds rain-out as they travel over the oceans. The isotope

composition of groundwater fell between fog and rain; since the $\delta^{18}O$ and $\delta^{2}H$ values of groundwater did not appear to model the evaporation of rain water, an input of fog drip was presumed.

Rundel and coworkers (1991) extensively described the importance of fog as a source of water to plants in the Atacama and Peruvian Deserts. Several subsequent studies have focused on studying the isotope signatures of fog and cloud water with the aim of distinguishing and quantifying the deposition of each water source. Using isotope data, Dawson (1998) showed that fog water is an important source of water for plants in California's redwood forests, especially during seasons with less rain. Similar results were obtained by Corbin and coworkers (2005) through the use of a mixing model to determine the use of fog water during drought in coastal prairie grasses in northern California. Scholl and coworkers (2007) found cloud water to contribute up to 46% of precipitation at sites on Maui, HI by utilizing a mixing model of cloud water and rain water.

Some recent studies have focused on using fog stable isotope information to analyze $\delta^{18}O$ and $\delta^{2}H$ in relation to droplet size, temporal evolution, temperature and altitude changes, and fog origin. The stable isotopes of clouds collected at Schmücke are detailed by Spiegel and coworkers (2012a, 2012b). This campaign showed that collection of fog water with a CASCC does not cause artificial isotope fractionation, and there is no variation in $\delta^{18}O$ and $\delta^{2}H$ among different droplet sizes (Spiegel et al., 2012a). Additionally, droplets were found to equilibrate quickly with the surrounding vapor, anywhere from less than 1/10 of one second to under one minute, with smaller droplets equilibrating more quickly. The temporal evolution of $\delta^{18}O$ and $\delta^{2}H$ during 13 cloud

events was also discussed (Spiegel et al., 2012b). Each fog event was found to evolve uniquely, with either increasing, decreasing, or increasing then decreasing $\delta^{18}O$ and $\delta^{2}H$. Changes in $\delta^{18}O$ and $\delta^{2}H$ were found to be caused either by temperature changes, which affect the isotopic equilibrium of condensation, or changes in the air mass that feeds the cloud. Another study of fog collected in the Swiss Alps (Michna et al., 2015) found fog to form a meteoric water line steeper than the global meteoric water line (GMWL), indicating that condensation processes were relevant: Stratus clouds formed by re-condensation during frontal passages are often observed at the site. Seasonal changes in the deuterium excess were also observed, with lower deuterium excess in the more humid spring than in the drier autumn months. A campaign sampling fog water throughout the Namib Desert in Africa (Kaseke et al., 2017; Kaseke et al., 2018) found that fog across the region was isotopically distinct, based upon the type of fog and the water source (for example, advective fog from air masses originating over the ocean versus radiation fog forming from local rivers, aquifers, and rainfall).

In this work, the temporal evolution of stable isotopes of fog water ($\delta^{18}O$ and $\delta^{2}H$) and the stable isotopes of dissolved organic carbon ($\delta^{13}C_{DOC}$) during four fog events will be discussed. Isotopic data will be compared to other common measurements of fog composition (such as TOC, LWC, and trace organics) to determine how isotopic information can complement these measurements when evaluating the evolution of a fog event. $\delta^{13}C_{DOC}$ measurements are expected to provide information about compositional changes to fog constituents, while $\delta^{18}O$ and $\delta^{2}H$ are expected to provide information about the meteorological factors that affect fog formation. At the time of writing, no articles discussing the $\delta^{13}C_{DOC}$ of fog samples have been published.

Materials and Methods

Sample collection.

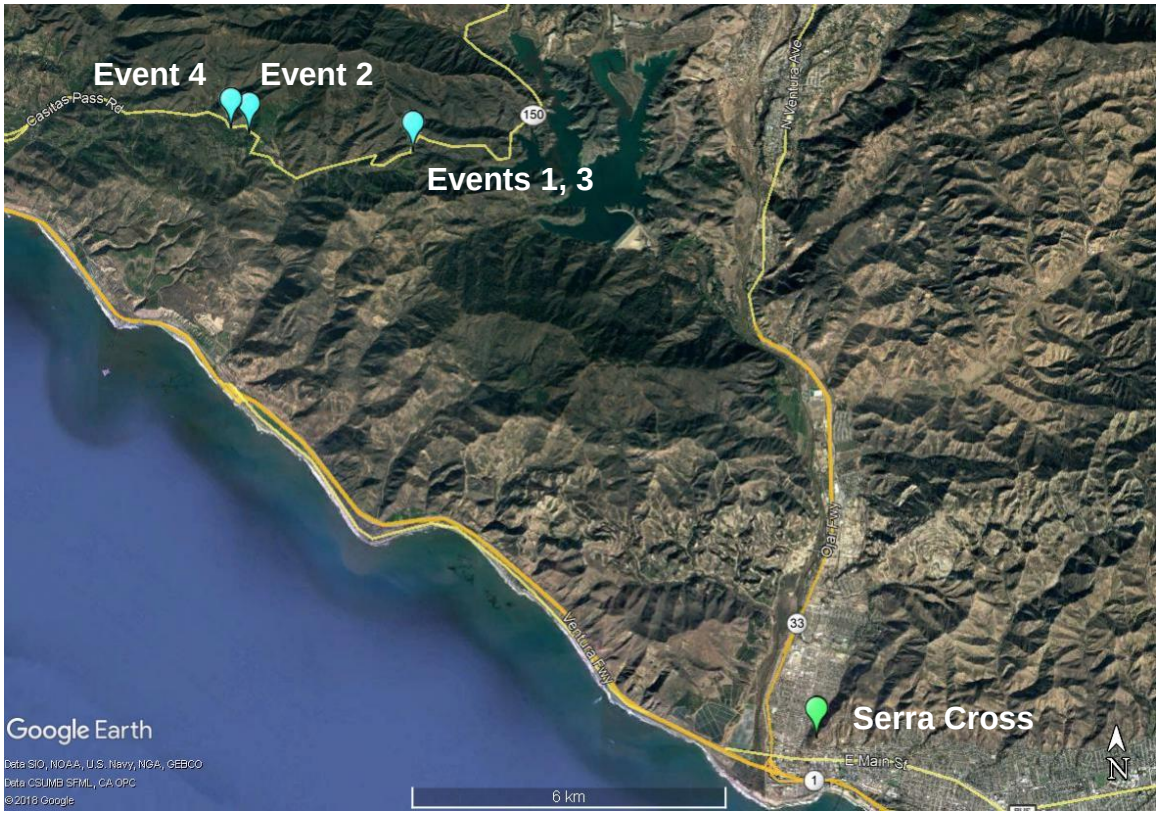

Figure 6.1. Map of fog and particulate matter sampling sites. The sites of fog events 1 – 4 along Highway 150 (Casitas Pass) are labeled in light blue. Serra Cross, the site of PM sampling, is labeled in green.

Fog samples were collected at Casitas Pass, north of Ventura, CA and inland of the Santa Barbara Channel, from June 8 – 14, 2015 (Figure 6.1). Four fog events occurred on the mornings of June 11 – 14 that offered sufficient sample for chemical analysis (hereafter referred to as events one through four). Fog events one and three were captured at the summit of Casitas Pass (34.3863, -119.3809, 350 m a.s.l.), event two from below the summit along Highway 150 near an avocado grove (34.3896, -119.4158, 290 m a.s.l.), and event four from a location along Highway 150 near an orange grove (34.3904, -119.4197, 250 m a.s.l.). All sampling sites were on gravel pull-offs along

Highway 150, 2 – 10 m from the road. Motor vehicle traffic was infrequent from 10:00 pm – 4:00 am (during most sampling periods) and increased somewhat through the final morning hours of each fog sampling period.

Two Caltech Active Strand Cloudwater Collectors (CASCCs, Demoz et al., 1996) were used to collect fog water. One stainless steel CASCC (ss-CASCC, Herckes et al., 2002) was used to collect samples for organic analyses, and one smaller Teflon collector (CASCC2) was used to collect samples for analyses of ions and trace metals. The samplers were run in tandem during each event, with collection bottles replaced every 1 – 2 hours to obtain time resolution. A total of 19 samples from four fog events were collected; sampling dates and times are reported in Table 6.1. Samples were massed and pH was measured on-site immediately after collection. Measurements of pH, TOC, inorganic ions, and organic species have been previously reported (Boris et al., 2018).

Table 6.1

Isotopic measurements performed on fog water samples.

	Start Date	Start Time	End Time	$\delta^{13}C_{VPDB}$ (‰)	$\delta^{13}C_{VPDB}$ unc (‰)	$\delta^{2}H_{VSMOW}$ (‰)	$\delta^{2}H_{VSMOW}$ unc (‰)	$\delta^{18}O_{VSMOW}$ (‰)	$\delta^{18}O_{VSMOW}$ unc (‰)
	10-Jun	22:05	0:05	-25.3	0.3	-24.6	0.2	-3.67	0.03
	11-Jun	0:05	2:05	-26.5	0.3	-24.8	0.2	-3.74	0.05
Event 1	11-Jun	2:05	4:05	-26.2	0.3	-26.2	0.2	-3.84	0.04
	11-Jun	4:05	6:05	-26.6	0.3	-28.2	0.5	-4.32	0.06
	11-Jun	6:05	8:05	-26.5	0.3	-29.2	0.6	-4.69	0.07
	12-Jun	2:00	3:00	-25.2	0.3	-11.3	0.2	-2.36	0.07
Event 2	12-Jun	3:00	4:00	-26.0	0.3	-11.5	0.5	-2.13	0.05
	12-Jun	4:00	6:00	-26.2	0.3	-11.6	0.2	-1.97	0.05
	12-Jun	6:00	8:00	-26.1	0.3	-11.5	0.1	-1.78	0.06
	12-Jun	21:30	23:30	-24.4	0.3	-13.4	0.1	-2.06	0.04
	12-Jun	23:30	1:30			-12.6	0.3	-1.93	0.07
Event 3	13-Jun	1:30	3:30	-24.6	0.3	-12.2	0.3	-1.77	0.07
	13-Jun	3:30	5:30						
	13-Jun	5:30	7:30	-25.4	0.3	-13.0	0.3	-1.76	0.03
	14-Jun	0:50	1:50	-25.6	0.3	-5.4	0.3	-0.87	0.08
	14-Jun	1:50	2:50	-24.6	0.3	-6.9	0.2	-1.55	0.05
Event 4	14-Jun	2:50	3:50	-24.8	0.3	-7.5	0.5	-1.7	0.1
	14-Jun	3:50	4:50	-25.6	0.3	-9.2	0.1	-1.94	0.04
	14-Jun	4:50	6:50	-25.6	0.3	-10.2	0.5	-2.02	0.06

Atmospheric particulate matter samples were collected at Serra Cross Park in Ventura, CA (34.2846, -119.2962) (Figure 6.1). Collection was performed using a Tisch high-volume aerosol sampler (1.13 m^3/min), which was equipped with a $PM_{2.5}$ impaction stage. Both $PM_{2.5}$ and $PM_{>2.5}$ were collected onto prebaked (600°C for a minimum 12 h) quartz fiber filters and were stored in aluminum foil at -20°C. Two field blanks were collected over the sampling period. Sampling dates and times are reported in Table 6.2.

Table 6.2

Isotopic measurements performed on PM samples. The uncertainty in all $\delta^{13}C$ measurements is 0.2‰.

Start Date	Start Time	End Date	End Time	$\delta^{13}C_{VPDB}$ $PM_{2.5}$ (‰)	$\delta^{13}C_{VPDB}$ $PM_{>2.5}$ (‰)
7-Jun	0:00	7-Jun	7:01	-25.8	-24.9
7-Jun	8:00	7-Jun	16:00	-25.0	-24.8
7-Jun	20:00	8-Jun	7:00	-25.6	-24.8
8-Jun	20:33	9-Jun	7:00	-25.5	-25.6
9-Jun	8:28	9-Jun	20:15	-25.6	-25.7
9-Jun	21:01	10-Jun	6:58	-26.4	-24.6
10-Jun	7:16	10-Jun	20:30	-25.1	-26.4
10-Jun	20:50	11-Jun	6:50	-25.0	-24.6
11-Jun	9:30	11-Jun	19:30	-25.1	-25.0
11-Jun	21:00	12-Jun	7:00	-25.0	-24.6
13-Jun	9:00	13-Jun	19:00	-25.6	-24.7

Sample analysis.

Fog samples were filtered through a prebaked quartz filter for isotopic analysis of dissolved organic carbon (DOC). Isotopic measurements for $\delta^{13}C_{VPDB}$ of DOC of fog samples were performed using an OI Analytical TOC Analyzer coupled to a Thermo Delta Plus Advantage Isotope Ratio Mass Spectrometer (TOC-IRMS). The analytical uncertainty of samples analyzed on this method is reported at 0.3‰. Potassium hydrogen phthalate (KHP) with a known isotopic composition was used as a linearity standard. Three in-house glycine standards were used to perform and verify a two-point calibration from -39.6‰ to 15.7‰.

Isotopes of $\delta^{2}H_{VSMOW}$ and $\delta^{18}O_{VSMOW}$ of fog water were measured using a Los Gatos Research DLT-100 Liquid Water Isotope Analyzer (LWIA). Results are reported as the average and standard deviation of five replicate injections of each sample.

Measurements were calibrated to the Vienna Standard Mean Ocean Water (VSMOW) scale using five water standards with known isotopic compositions ranging from -154.3‰ to 108.7‰ for $\delta^{2}H_{VSMOW}$ and -19.5‰ to 12.34‰ for $\delta^{18}O_{VSMOW}$.

All particulate matter samples were analyzed by thermal optical transmittance for total carbon (TC) concentrations using a Sunset Lab OC-EC Aerosol Analyzer (Birch & Cary, 1996). A variation of Sunset's "Quartz" TOT method was used. Variable time steps of 60-200 seconds were used during OC evolution, with temperature plateaus at 310°C, 475°C, 615°C, and 870°C. During EC evolution, the temperature was held at 550°C, 625°C, 700°C, 775°C, and 850°C for 45 seconds each, with a final hold at 870°C for 120 seconds. Quality control included the analysis of lab blanks, field blanks, replicate samples, and a sucrose standard, which was routinely within 10% of the known concentration.

Isotopic measurements for $\delta^{13}C_{VPDB}$ of TC in particulate matter were performed using a Costech Elemental Analyzer coupled to a Thermo Delta Plus Advantage Isotope Ratio Mass Spectrometer (EA-IRMS). The analytical uncertainty of samples analyzed on this method is reported at 0.2‰. NIST 2710 (Montana soil) was used as a linearity standard. Three in-house glycine standards were used to perform and verify a two-point calibration from -39.6‰ to 15.7‰.

Results and Discussion

$\delta^{13}C_{VPDB}$ of DOC in fog water samples.

The $\delta^{13}C$ of DOC ($\delta^{13}C_{DOC}$) was measured in 17 of 19 fog water samples (Table 6.1). Event 3 had a particularly low liquid water content, and two of the five samples collected during this event did not yield enough water for carbon isotope analysis. The

volume weighted average $\delta^{13}C_{DOC}$ of Events 1 – 4, respectively, were -26.2‰, -26.0‰, -24.8‰, and -25.2‰. As discussed in Chapter 2, the $\delta^{13}C_{DOC}$ of fog collected in Casitas Pass is similar to that of fog collected Davis, another urban sampling site in California.

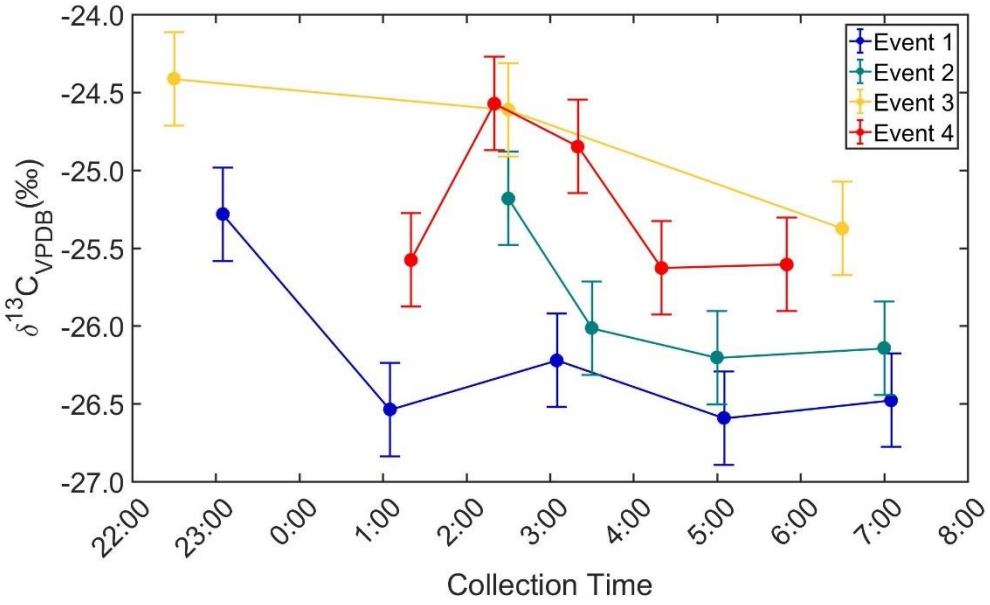

Figure 6.2. Changes in $\delta^{13}C_{DOC}$ of each fog event over time. Points represent the midpoint of the collection time for each sample. Lines connecting the points are for visual aid. Of the five samples collected during Event 3, only the first, third, and fifth yielded enough sample for $\delta^{13}C_{DOC}$ analysis. See Table 6.1 for sampling details.

With the exception of the first sample collected in Event 4, over the course of each fog event, the $\delta^{13}C_{DOC}$ decreased over time (Figure 6.2). The magnitude of this depletion in $\delta^{13}C$ was 1.2‰ for Event 1, and 1.0‰ for Events 2 – 4. Changes in $\delta^{13}C_{DOC}$ are caused by isotope fractionation processes, which, as discussed in Chapter 2, could either be physical or chemical. Chemical processes would include reactions occurring within droplets to form aqueous SOA material, while physical processes include the scavenging and deposition of organic matter. In the next sections, these possibilities will

be explored through comparisons with the organic and inorganic composition of fog water.

Total organic carbon and liquid water content.

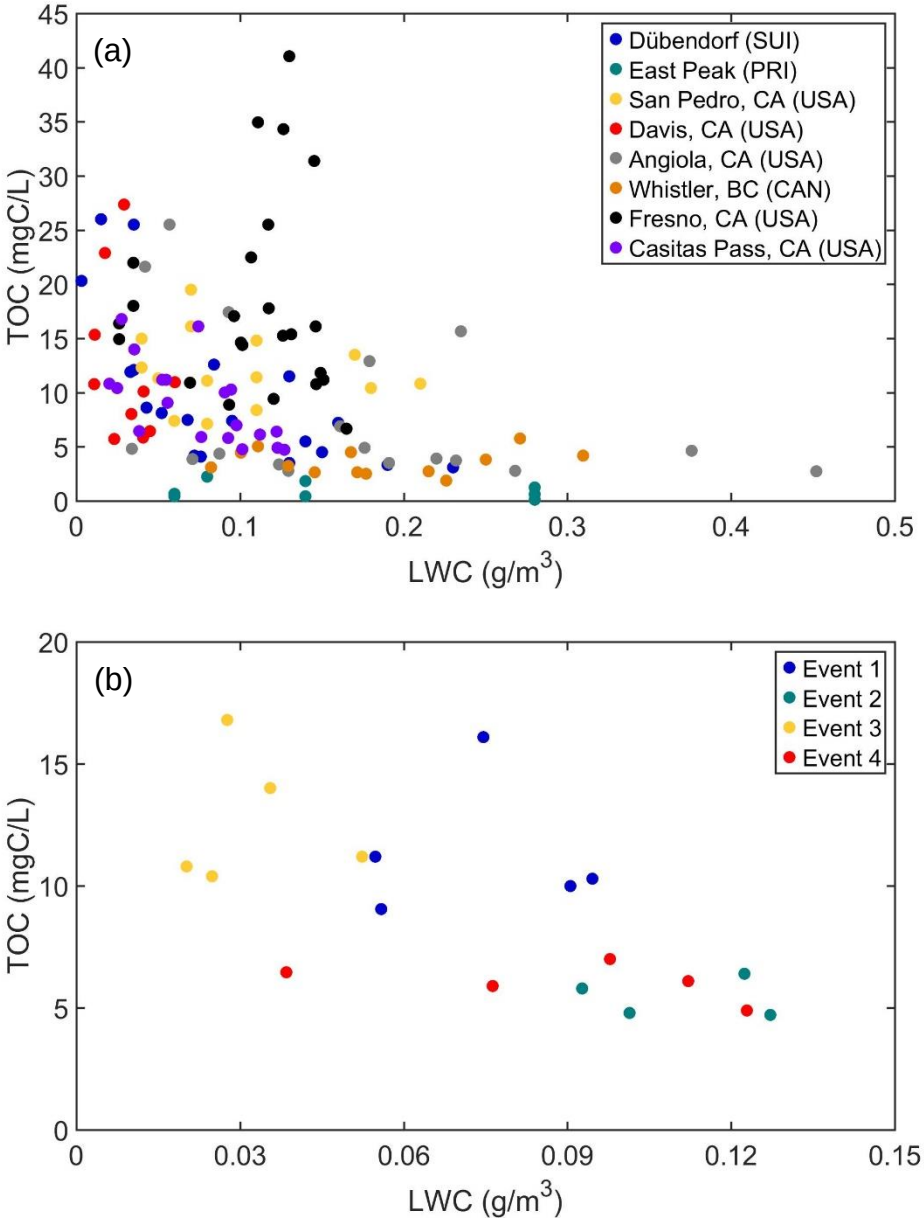

Figure 6.3. TOC or DOC measured in fog water as a function of liquid water content. (a) Studies were conducted in Dübendorf, Switzerland (Capel et al., 1990), East Peak, Puerto Rico (Reyes-Rodríguez et al., 2009), San Pedro, CA (Erel et al., 1993), Davis, CA (Ervens et al., 2013), Angiola, CA (Herckes et al., 2002), Whistler, British Columbia (Ervens et al., 2013), Fresno, CA (Collett et al., 2008), and Casitas Pass, CA (this study). (b) TOC vs. LWC in Casitas Pass (this study), classified by event.

Measurements of DOC and LWC are commonly made and compared in fog water studies. Figure 6.3a shows measured DOC or TOC versus LWC at various sites, including this study. An inverse relationship was observed between TOC and LWC in Casitas Pass fog ($r = -0.655$, $p < 0.01$) that appears to be nonlinear. Figure 6.3b shows this relationship between TOC and LWC in Casitas Pass fog, classified by event. The fog events appear to be clustered, showing that preexisting atmospheric conditions (for example, relative humidity and concentration of particles) may have an impact on the composition of a fog. An inverse relationship was also observed between TOC and LWC for samples collected in Angiola, CA (Herckes et al. 2002), and was also nonlinear, likely due to the effect of soluble gases and the variability in atmospheric particle concentrations before each event.

In general, there are no clear relationships between organics and LWC among all sites shown in Figure 6.3a. Some sites do exhibit characteristics that reflective of the sampling location. In remote locations, such as East Peak, Puerto Rico (Reyes-Rodríguez et al., 2009) and Whistler, British Columbia (Ervens et al., 2013), the organic carbon concentrations are lower than in urban locations; The DOC of all samples at East Peak are less than 3 mgC/L, and the TOC of all samples collected in Whistler are less than 6 mgC/L. The TOC of fog in urban locations in California (San Pedro, Erel et al., 1993; Davis, Ervens et al., 2013; and Fresno, Collett et al., 2008) are higher than in East Peak or Whistler, with a minimum TOC among the three locations of 6 mgC/L and maximum of 41 mgC/L. None of these individual sites, however, exhibit significant correlations between TOC and LWC. Additionally, no generalizations on the relationship between TOC and LWC can be made among all locations.

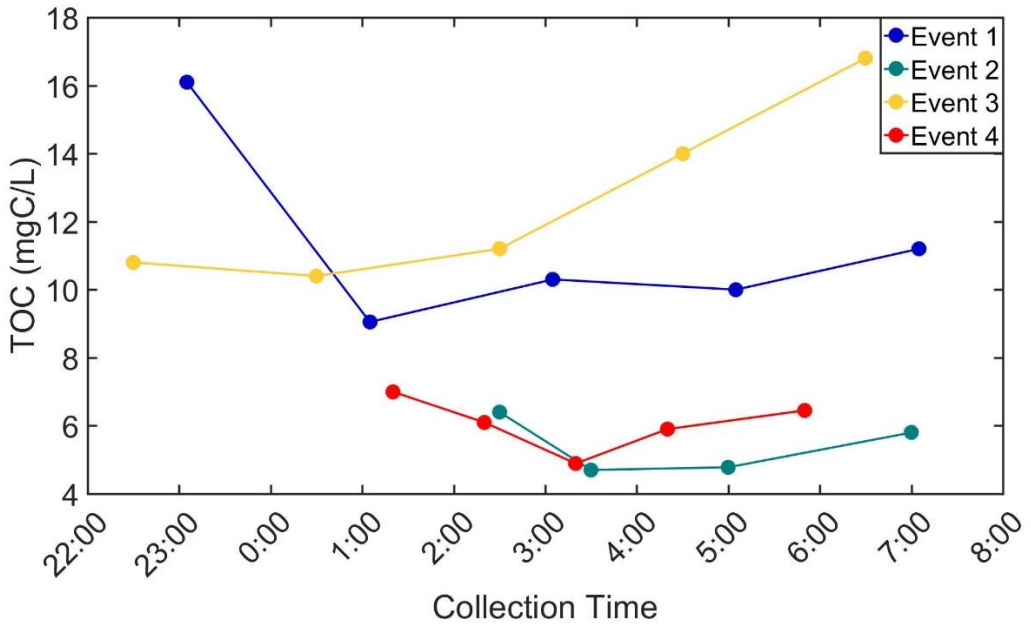

Figure 6.4. Changes in [TOC] of each fog event over time. Points represent the midpoint of the collection time for each sample. Lines connecting the points are for visual aid. See Table 6.1 for sampling details.

Figure 6.4 shows the evolution of [TOC] over time during each fog event. In general, the [TOC] first decreases over time, then increases. This trend would explain the negative correlation observed between [TOC] and LWC: As a fog forms, the LWC increases, then decreases as the fog dissipates. The inverse trend in [TOC] would therefore be explained by a dilution effect.

Previous studies have made comparisons among the concentrations of inorganic fog constituents and LWC (Aleksic & Dukett, 2010; Elbert et al., 2000, 2002; Kasper-Giebl, 2002; Straub et al., 2012). In general, a tenuous inverse relationship between inorganics and LWC exists due to dilution effects that decrease solute concentrations with droplet growth, but the relationship is not linear and is complicated by the uptake of soluble gases and particle scavenging efficiency, both of which are dependent on droplet size and LWC.

In this study, no correlation between $\delta^{13}C_{DOC}$ and TOC was observed. While the TOC concentration decreases then increases over time, the $\delta^{13}C_{DOC}$ only decreases. Therefore, $\delta^{13}C_{DOC}$ is not impacted by dilution effects.

Organic species.

In terms of the presence of individual organic species of these fog samples, many similarities to other studies exist. Several organic acids (notably, lactic, acetic, propionic, formic, pyruvic, valeric, glutaric, succinic, malonic, maleic, oxalic, and methanesulfonic acids) were quantified; the breadth and concentrations of these acids indicate a notable presence of oxidized organic matter that could originate from aqueous- or gas-phase chemistry. Among the identified carboxylic acids, formic acid, acetic acid, and oxalic acid dominate in concentration, making up 3.40%, 3.74%, and 3.54%, respectively, of TOC (Boris et al., 2018). These small acids were also found in fog collected on Baengnyeong Island, South Korea (Boris et al., 2016), Mt. Rax, Austria (Löflund et al., 2002), and Gulf Coast sites in Baton Rouge, LA and Houston, TX (Raja et al., 2008).

There is a correlation between $\delta^{13}C_{DOC}$ and pyruvate ($r = 0.563$, $p < 0.02$) and $\delta^{13}C_{DOC}$ and malonate ($r = 0.564$, $p < 0.02$), but not with any other measured organic species. Pyruvate and malonate, along with methanesulfonate and glutarate, correlate with oxalate, suggesting that these acids are formed through similar oxidation processes (Boris et al., 2018). The lack of correlation of $\delta^{13}C_{DOC}$ with organic species implies that carbon isotope information cannot provide a generalization of overall fog composition, origin, or reactivity, and changes in $\delta^{13}C_{DOC}$ are not reflected in aqueous SOA material formation.

Inorganic species.

As the Casitas Pass sampling sites were located within 6 km of the Pacific Ocean, sea spray was expected to be a significant source of PM. The mean value of the Cl^-/Na^+ ratio was 1.1 (Boris et al., 2018), confirming the influence of sea spray aerosols; the expected ratio of sea spray is 1.16 (Keene et al., 1986). Consistent correlations of sea spray ions with $\delta^{13}C_{DOC}$ were found: Na^+ ($r = 0.486$, $p < 0.05$), Mg^{2+} ($r = 0.516$, $p < 0.05$), Ca^{2+} ($r = 0.494$, $p < 0.05$), and Cl^- ($r = 0.501$, $p < 0.05$). Sea spray elements are generally associated with larger particle size modes (Ault et al., 2013; Junge, 1972), which would be scavenged more readily and would deposit quicker than particles in the accumulation mode. $\delta^{13}C_{DOC}$ might therefore be used as a parameter to evaluate the scavenging and deposition of particles. Figure 6.5 outlines the process by which $\delta^{13}C_{DOC}$ could change based on particle scavenging and deposition. As described in Chapter 4 and in other studies (Chalbot et al., 2014; Masalaite et al., 2015), $\delta^{13}C$ of particles varies among particle sizes due to differences in sources that contribute to PM in different size modes, and larger particles tend to be enriched in $\delta^{13}C$ relative to small particles. As a fog forms, larger particles are scavenged more readily than small particles, which would result in ^{13}C-enriched particles becoming incorporated in the aqueous phase. Droplets formed on large condensation nuclei are larger than droplets formed around smaller condensation nuclei (Svenningsson et al., 1997), and larger ($\delta^{13}C$-enriched) droplets would then be deposited either gravitationally or by turbulent deposition faster than small droplets (Collett et al., 2008; Collett et al., 2001). The remaining fog would become increasingly depleted in $\delta^{13}C_{DOC}$. Over time, the particles available to act as condensation nuclei would become lighter in $\delta^{13}C$, further driving the $\delta^{13}C_{DOC}$ of the fog to become

depleted. This depletion of interstitial particles during a fog event was observed in $PM_{2.5}$ collected in Strasbourg in Chapter 5.

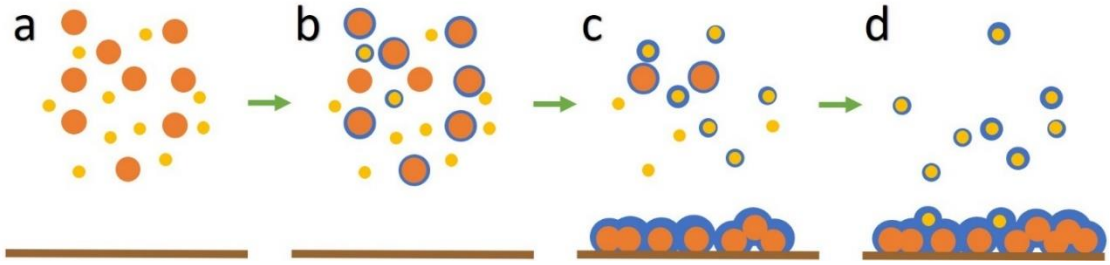

Figure 6.5. A simplified schematic illustrating the temporal scavenging and deposition of particles over the course of a fog event. (a) Large (orange) and small (yellow) particles are present before a fog. (b) As a fog forms (blue), larger particles are preferentially scavenged as cloud condensation nuclei. (c) As LWC increases, large droplets formed around large particles deposit, and particle scavenging continues. (d) Growing droplets continue to deposit, and small particles are scavenged more frequently as large particles are removed from the atmosphere.

$PM_{2.5}$ and $PM_{>2.5}$ were collected in Ventura, CA at Serra Cross during this campaign. As shown in Figure 6.6, $PM_{>2.5}$ is enriched in $\delta^{13}C_{TC}$ relative to $PM_{2.5}$ in eight of 11 samples, though some of the differences between coarse and fine particles are small. The number of samples collected in this location thus far is limited, and more sampling and isotopic analysis of size-segregated particles would be needed to determine the rate of occurrence of $\delta^{13}C_{TC}$-enriched large particles, and under what conditions (i.e., temporal, meteorological) enriched large particles occur.

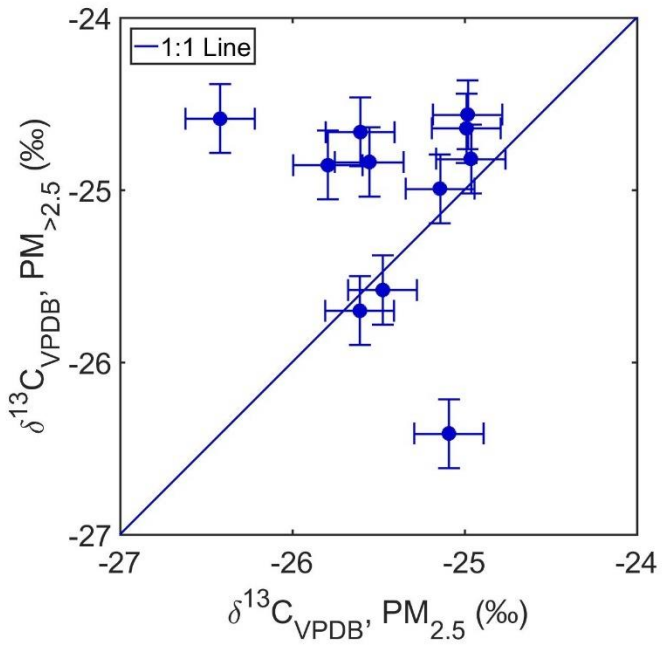

Figure 6.6. A comparison of the $\delta^{13}C_{TC}$ of coarse ($PM_{>2.5}$) and fine ($PM_{2.5}$) particle size fractions collected in Ventura, CA in June 2015. a 1:1 line is included for visual aid.

$\delta^{2}H$ and $\delta^{18}O$ of fog water.

Studies of the composition of fog are generally quite difficult, as fog is a dynamic system. Along with the continuous formation and evaporation of droplets and the scavenging of PM and VOCs, changes in meteorological conditions, such as temperature, relative humidity, and the movement of air masses, can affect fog composition. Isotope analysis of water droplets will be used to evaluate these effects.

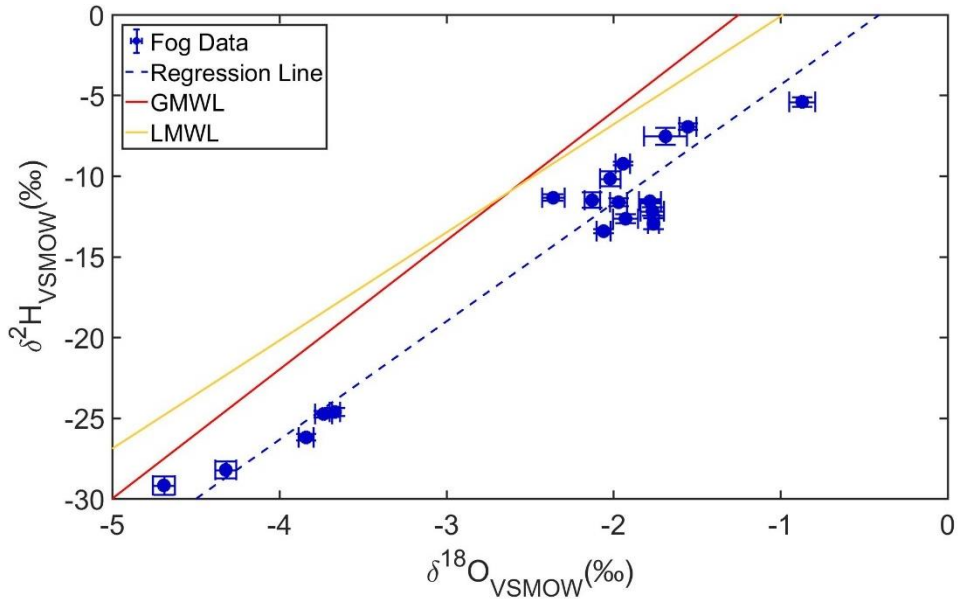

Figure 6.7. δ^2H versus $\delta^{18}O$ of fog water samples. The line for orthogonal regression analysis, as well as the LMWL (Fischer & Still, 2007) and GMWL, are included for reference. The fog samples fall below both the GMWL and LMWL.

The δ^2H and $\delta^{18}O$ of fog water samples are plotted in Figure 6.7. δ^2H is plotted as a function of $\delta^{18}O$ in order to compare these samples to other meteoric water lines. The samples collected at Casita's Pass form a Cloud Water Line (CWL) with the equation $\delta^2H = 7.3 \times \delta^{18}O + 3.0 \times 10^{-3}$, calculated by orthogonal regression. The slope of this line is greater than that of a reported local meteoric water line (LMWL) of mixed rain and fog samples collected on the nearby Channel Islands ($\delta^2H = 6.7 \times \delta^{18}O + 6.6 \times 10^{-3}$, Fischer & Still, 2007), but less than the global meteoric water line (GMWL, $\delta^2H = 8 \times \delta^{18}O + 10 \times 10^{-3}$). Both of these lines are plotted in Figure 6.7 for reference. The fog data falls below the GMWL, as it does in other studies of coastal fog (Ingraham & Matthews, 1990; Kaseke et al., 2018; M. Scholl et al., 2011). Inland and mountain fogs have been found to fall above the GMWL, due to water recycling and precipitation during transport (Ingraham & Matthews, 1988; Spiegel et al., 2012b). The deuterium excess for the fog

collected in Casitas Pass (3‰) is lower than that for the Channel Island study (6.6‰) and the GMWL (10‰). Spiegel and coworkers (2012b) observed that a low deuterium excess could represent early-stage condensation. The low deuterium excess in Casitas Pass fog could be indicative of minimal transport of the air masses feeding the fog.

The isotope effects observed throughout the hydrologic cycle are effected by myriad processes, including evaporation, condensation, temperature, relative humidity, the distance traveled by an air mass, and changes in the water vapor feeding a cloud (Gat, 1996; Spiegel et al., 2012b). Evaporation that occurs as rain falls causes the rain droplets to become isotopically enriched relative to the cloud; these samples generally display a slope less than 8 and a smaller deuterium excess, (Gat, 1996), as is evident in the Meteoric Water Line observed in the Channel Islands relative to the GMWL. However, since the resulting vapor is isotopically depleted, subsequent rains become isotopically depleted and would have a greater deuterium excess (Dansgaard, 1964).

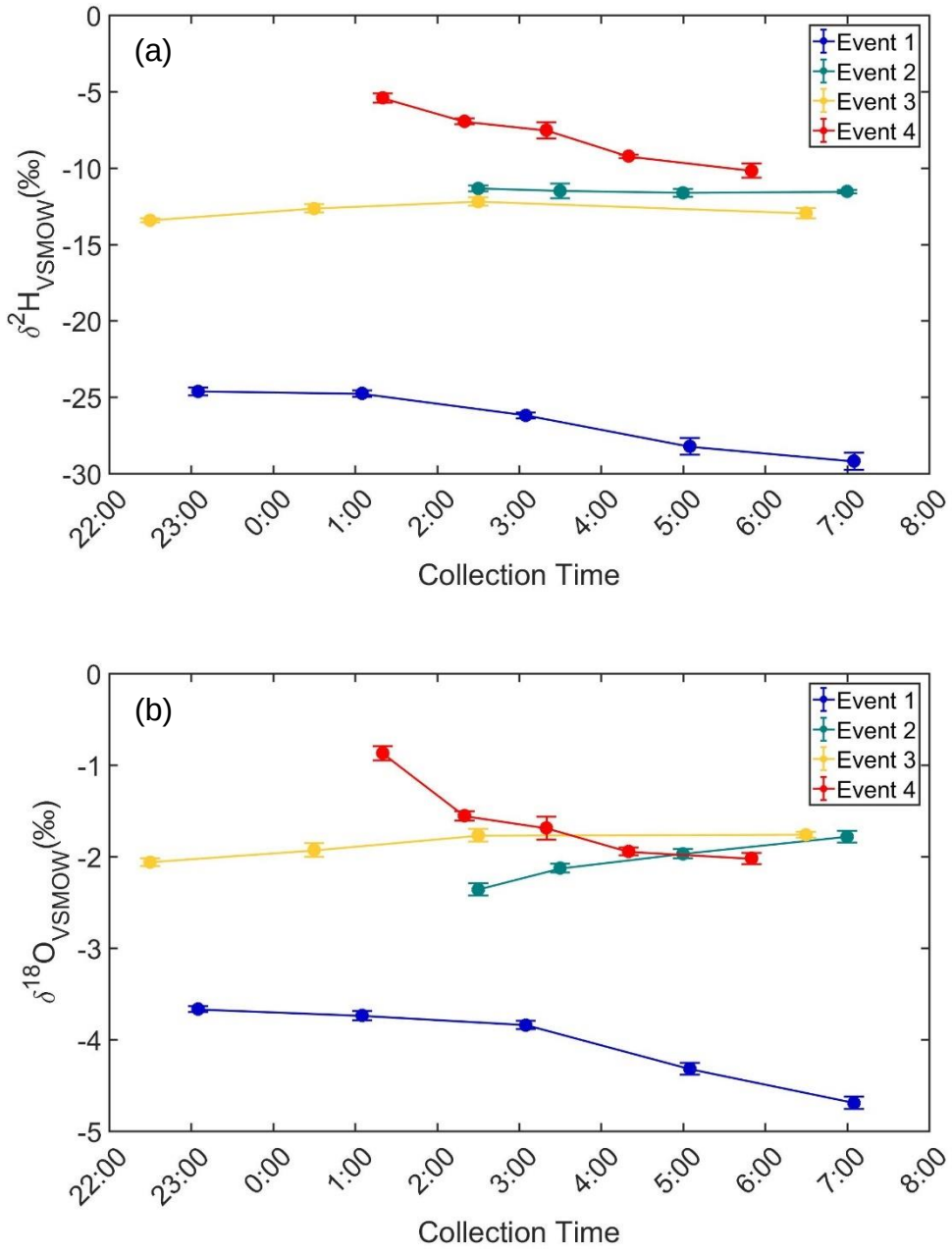

Figure 6.8. Changes in (a) δ^2H and (b) $\delta^{18}O$ of each fog event over time. Points represent the midpoint of the collection time for each sample. Lines connecting the points are for visual aid. The fourth of five samples collected during Event 3 was not aliquoted for δ^2H and $\delta^{18}O$ analysis. See Table 1 for sampling details.

Figure 6.8 shows the temporal evolution of δ^2H and $\delta^{18}O$ for each fog event. δ^2H and $\delta^{18}O$ are well correlated among all events ($r = 0.975$, $p < 0.001$). The volume-

weighted average of δ^2H for events 1 – 4, respectively, is -26.6 ± 0.3‰, -11.5 ± 0.2‰, -12.7 ± 0.3‰, and -7.7 ± 0.3‰, with a range in values of -29.2‰ – -5.4‰. The volume-weighted average of $\delta^{18}O$ for events 1 – 4, respectively, is -4.0 ± 0.1‰, -2.0 ± 0.1‰, -1.8 ± 0.1‰, and -1.6 ± 0.1‰, with a range in values of -4.7‰ – -0.9‰. These values fall well within range of other published studies of fog globally, which range from -71 – +13‰ for δ^2H and -10.4 – +2.7‰ for $\delta^{18}O$ (Scholl et al., 2011). δ^2H and $\delta^{18}O$ are notably depleted in event 1 relative to events 2 – 4. This is likely due to the occurrence of rain in the days before event 1; rain-out of air masses prior to a fog event causes isotopic depletion due to depleted rain water, modeled by Rayleigh distillation (Gat, 1996; Spiegel et al., 2012b).

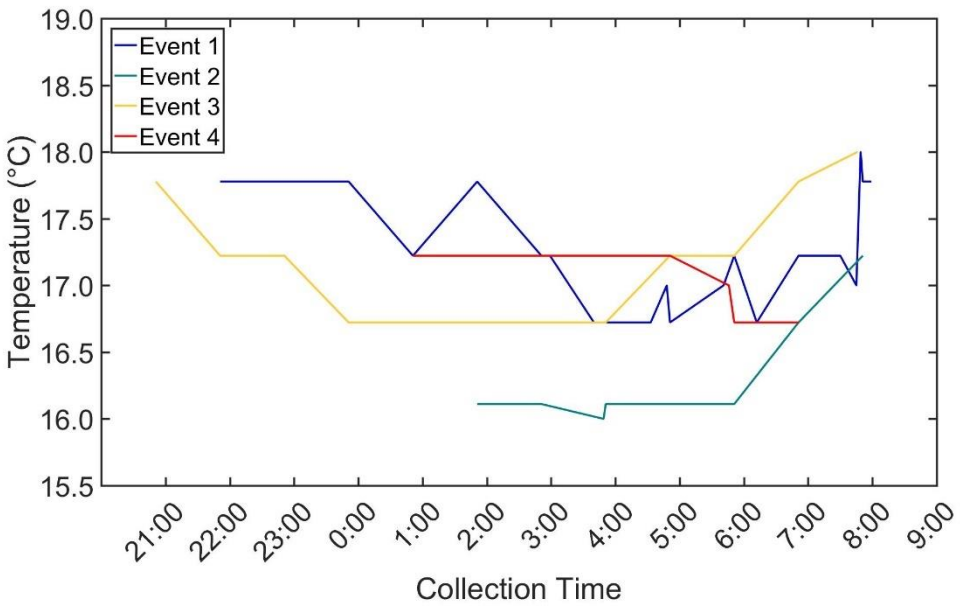

Figure 6.9. Temperatures measured in Oxnard, CA during each fog event.

During each of the fog events at Casitas Pass, the δ^2H and $\delta^{18}O$ behave differently over time. From the start to end of fog collection in Event 1, δ^2H decreased by 4.6‰, and $\delta^{18}O$ decreased by 1.0‰. During Event 2, δ^2H increased by 0.2‰, and $\delta^{18}O$ increased by

0.6‰. During Event 3, δ^2H increased by 0.5‰, and $\delta^{18}O$ increased by 0.3‰. During Event 4, δ^2H decreased by 4.8‰ and $\delta^{18}O$ decreased by 1.1‰. Figure 6.9 plots the temperature during each fog event, recorded at a nearby weather station in Oxnard, CA (https://www.wunderground.com/history/daily/us/ca/oxnard/KOXR). Over the course of Event 1, the temperature drops approximately 1.5 degrees, which may have caused the observed depletion in δ^2H and $\delta^{18}O$. The temperature during Event 2 was fairly stable until 6:00 AM, when the temperature increased by one degree. Over the course of Event 3, the temperature first decreased from 18°C to 17°C from 9:00 PM to midnight, then increased again to 18°C starting at 5:00AM. The enrichment in δ^2H and $\delta^{18}O$ during Events 2 and 3 are somewhat mirrored towards the end of each of these events by the change in temperature at the end of sample collection. Similarly, the temperature during Event 4 is steady at 17°C until 6:00 AM, and then decreases by 0.5°C; however, the δ^2H and $\delta^{18}O$ become depleted throughout Event 4. It is possible that changes in the air mass feeding the fog could cause the observed changes in δ^2H and $\delta^{18}O$ during Events 2 – 4. Figure 6.10 shows the back trajectories of the air masses calculated using HYSPLIT. Over the course of Event 2, the origin of the air masses shifted from west to east. During Event 3, there is a shift from west to east between midnight and 2:00 AM. During Event 4, the air mass trajectories shift from long-range to local transport.

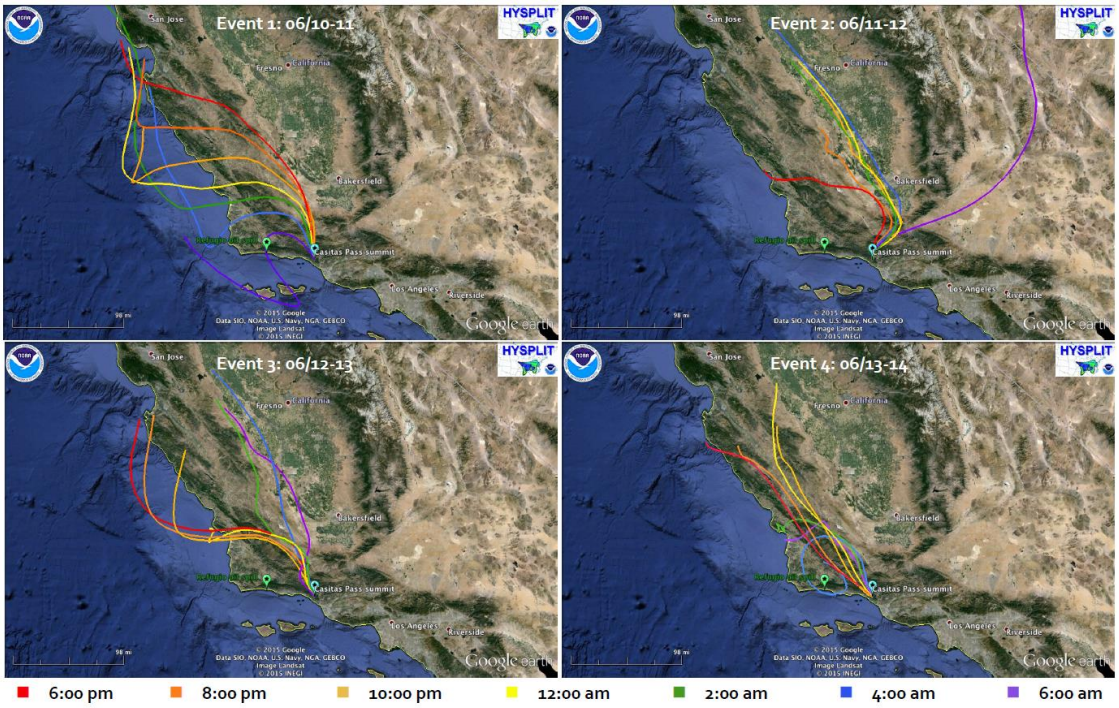

Figure 6.10. HYSPLIT back trajectory analysis. From Boris et al., 2018.

There is a positive correlation between $\delta^{13}C$ and each of the water isotopes ($\delta^{2}H$: $r = 0.594$, $p < 0.02$; $\delta^{18}O$: $r = 0.588$, $p < 0.02$). As the condensed phase is generally enriched in $\delta^{2}H$ and $\delta^{18}O$ relative to vapor due to equilibrium isotope effects, it would be interesting to observe if isotopically enriched water condenses and deposits sooner than depleted water, similarly to the way that $\delta^{13}C$-enriched fog is scavenged and deposited faster than $\delta^{13}C$-depleted fog (Figure 6.5). This may be a phenomenon akin to Rayleigh distillation, as isotopically enriched water condenses and is rained out of a cloud before isotopically depleted water. If so, it may be possible for $\delta^{2}H$ and $\delta^{18}O$ to be used as tracers in analyzing the scavenging and deposition of organic PM by fog in conjunction with $\delta^{13}C$.

Only one field study currently exists that evaluates the temporal evolution of fog or cloud events (Spiegel et al., 2012a, 2012b). This study, conducted at the summit of

Schmüke in Germany, modeled thirteen cloud vents and found two major causes of temporal changes in isotopic composition during an event: changes in meteorological conditions (such as temperature or relative humidity), or changes in the composition of the air mass feeding the cloud. In the cases where temperature affected $\delta^{2}H$ and $\delta^{18}O$, increases in temperature caused isotopic enrichment, and decreases in temperature caused isotopic depletion. However, no overarching consistent trends in the temporal evolution of fog were concluded from this study.

Cloud events at Schmüke and Casitas Pass, however, may not be directly comparable, since the environmental conditions and transport time of the clouds/fog are different. Additionally, air masses that travel longer distances are more subject to isotopic depletion through Rayleigh distillation (Spiegel et al., 2012b); fog and cloud is generally more enriched in coastal areas or lower latitudes (Scholl et al., 2011).

Conclusions

Compositional changes in time-resolved fog events collected in Casitas Pass, CA were studied. TOC and LWC were inversely correlated, and the relationship was not linear. Comparisons of TOC vs. LWC during each event showed that the events were clustered, indicating that dilution plays a role in TOC concentration. The fog samples also contained organic species found in other locations, and correlations among oxidized species imply similarities in their oxidation pathways.

$\delta^{13}C_{DOC}$ of the fog samples decreased over time during each event, but did not correlate consistently with organic species. There was, however, a correlation $\delta^{13}C_{DOC}$ with ions associated with sea spray. This observation shows that $\delta^{13}C_{DOC}$ may be useful in observing fog scavenging and deposition, as aerosols associated with sea spray are

generally coarse and are scavenged and deposited more readily than fine, anthropogenically-derived particles.

The isotopes of fog water (δ^2H and $\delta^{18}O$) form a CWL ($\delta^2H = 7.3 \times \delta^{18}O + 3.0 \times 10^{-3}$) that falls below the GMWL and a LMWL calculated from mixed fog and rain on the Channel Islands (Fischer & Still, 2007). Both the slope and deuterium excess of the CWL are consistent with fog that has not undergone synoptic scale transport. The changes in δ^2H and $\delta^{18}O$ during each event may exhibit influence from both changes in temperature and changes in the air masses feeding the fog. Based upon the correlation of δ^2H and $\delta^{18}O$ with $\delta^{13}C_{DOC}$, there is a possibility that water isotopes could be indicators of droplet deposition, similar to Rayleigh distillation observed in rainout. It may be interesting in future studies to focus on this possible relationship between water isotopes and $\delta^{13}C_{DOC}$.

Overall, these multiphase atmospheric systems are dynamic and highly complex. Measurements of stable isotopes add a breadth of new information that can lead to a better understanding of fog scavenging, evolution, and deposition.

CHAPTER 7

SUMMARY AND FUTURE WORK

The major goal of this work is to understand the processing of organic particulate matter by fog and clouds. Particulate matter has a pronounced effect on our climate and causes negative health outcomes. Reactions that occur in atmospheric waters can form new secondary aerosol material from gas-phase species or primary organic aerosols; it is therefore important to understand these reactions, as well as how organic material is scavenged and deposited, so that climate and health effects can be assessed. Stable isotope systems are used to study these processes because primary sources of aerosols and gas-phase species have distinguishable isotopic compositions, and isotope fractionation occurs in both physical and chemical processes. Measurements of stable isotopes can be used to track all aspects of atmospheric processing, from particle scavenging, reactions that form secondary organic aerosol material, and particle deposition. Stable isotopes of carbonaceous material ($\delta^{13}C$) have been used widely in studying volatile and particle phase atmospheric chemistry, but studies on how organic matter is processed by fog have not been previously conducted. Here, field studies are used to determine the isotopic composition of carbonaceous particles in several locations, and assess how the particles are effected by fog through changes in $\delta^{13}C$.

Chapter 2 provided an overview of carbon isotope signatures of primary organic aerosol sources collected and analyzed for this study as well as several examples from literature. The $\delta^{13}C$ of particulate matter, the $\delta^{13}C$ of the DOC of fog, and the comparison of the $\delta^{13}C$ of coexisting fog and interstitial particles were also discussed. It was hypothesized that both the $\delta^{13}C_{TC}$ of particulate matter and the $\delta^{13}C_{DOC}$ of fog would

reflect the $\delta^{13}C$ signatures of primary aerosol sources, but that the $\delta^{13}C_{DOC}$ of fog would differ from the $\delta^{13}C_{TC}$ of coexisting interstitial particles since the scavenging of particles and gases by fog is selective based upon the chemical composition of carbonaceous atmospheric constituents. The $\delta^{13}C_{TC}$ of particulate matter was found to reflect the $\delta^{13}C$ of primary aerosol sources expected for each sampling site; the $\delta^{13}C_{TC}$ of particles collected in the cities of Davis, Bakersfield, and Ventura, CA, and Monterrey, MX, all fall within similar ranges, while the $\delta^{13}C_{TC}$ of particulate matter in Whistler, BC was depleted in comparison due to the dominance of primary biogenic emissions in this rural location. $\delta^{13}C_{TC}$ of particulate matter collected in Tempe, AZ was enriched compared to other urban locations due to the presence of carbonates in blown dust prevalent in the desert, while the $\delta^{13}C_{TC}$ of particles collected in the cities of Strasbourg and Geispolsheim were depleted relative to cities in North America due to the greater influence of diesel fuel emissions relative to gasoline emissions. The $\delta^{13}C_{DOC}$ of fog also mirrored these results, as fog from Davis and Casitas Pass, CA contained DOC with similar isotopic composition, and the $\delta^{13}C_{DOC}$ of fog from Whistler was depleted in comparison. Fog collected on Baengnyeong Island, South Korea was enriched in $\delta^{13}C_{DOC}$ due to the influence of marine organic carbon. The $\delta^{13}C_{DOC}$ of fog collected in the cities of Strasbourg and Metz, France were again depleted relative to fog in California, but the $\delta^{13}C_{DOC}$ of fog from suburban towns of Geispolsheim and Erstein was variable, possibly due to the influence of both urban and agricultural transported particles in these locations. The comparison of the $\delta^{13}C_{DOC}$ of fog and $\delta^{13}C_{TC}$ of interstitial particles does show that the two are indeed dissimilar, but the isotopic changes that occur in scavenging are not the same in French sites versus those in the United States and Canada. Future work

should focus on measuring the isotopic fractionation that occurs in the particle and aqueous phases, as well as the gas phase, as a fog forms so that all of the processes that affect the $\delta^{13}C_{DOC}$ of fog can be understood.

In Chapter 3, a new method to quantify carbonate in particulate matter samples was developed and tested for accuracy, precision, and reproducibility. Due to restrictions on filter size, sample homogeneity, and filter material, existing methods of carbonate quantification are not suitable for all particulate matter samples. Here, the CO_2 released from a filter upon acidification in a sealed jar is measured at ambient pressure. The amount of filter analyzed can be customized to up to 24 cm^2 depending on the particle load to decrease detection limits. The amount of sodium bicarbonate added to a clean quartz filter was measured within 15% of the known mass, and triplicate analyses of particulate matter samples resulted in a median standard deviation within 8% of the measured carbonate concentration. For particulate matter samples collected in locations with high concentrations of carbonate (such as Tempe, AZ, discussed in Chapter 4), this method can be used to determine whether carbonate is a significant contributor to $\delta^{13}C_{TC}$.

Chapter 4 discussed the quantification and measurement of $\delta^{13}C$ of the total carbon and *n*-alkanes present in particulate matter in Tempe, AZ. It was hypothesized that seasonal differences in the concentration and $\delta^{13}C$ of total carbon and *n*-alkanes would be observed based on changes in weather conditions and particle sources. It was found that the $\delta^{13}C_{TC}$ was heavily influenced by seasonal trends, including inversion, transport, population density, and photochemical activity. January exhibited dominant anthropogenic influences, while April, June, and October had a more prominent influence of biogenic emissions, based on differences in $\delta^{13}C_{TC}$ and *n*-alkane CPI values. Within a

sampling period, variations in $\delta^{13}C_{TC}$ were caused by sources that generate particles in different size modes (soil and dust in particles greater than 1.5 μm, and anthropogenic emissions in particles smaller than 1.5 μm). Carbonate in coarse particles was shown to have the most significant impact on the observed differences in $\delta^{13}C_{TC}$ of coarse and fine particles. The $\delta^{13}C$ values of *n*-alkanes exhibited a mixture of C_3 plant emissions and fossil fuel emissions, and C_4 plants may also have contributed in October due to the seasonal changes in dominant plant types in the American southwestern deserts. Future studies should focus on seasonal measurements of both $\delta^{13}C$ and $\delta^{2}H$ of *n*-alkanes in particulate matter and major *n*-alkane sources (such as vehicle exhaust, C_3 plants, and C_4 plants) to work toward a more complete source apportionment of urban *n*-alkane emissions.

Chapter 5 discussed the first study of interactions between fog (and other multiphase systems, including rain) and particulate matter using $\delta^{13}C$ in two sites in northeastern France, Strasbourg and Geispolsheim. It was hypothesized that fog and rain would affect the $\delta^{13}C_{TC}$ of particles, due to their selective scavenging of coarse particles. Concentrations of organic and elemental carbon were found to be consistent with other urbanized valley locations (Bakersfield, CA and the Po Valley, Italy). Scavenging of organic carbon was similar to other urban locations. The scavenging of elemental carbon was negligible in Strasbourg but high in Geispolsheim, possibly due to the transport of aged aerosol from Strasbourg to Geispolsheim. The $\delta^{13}C_{TC}$ of particulate matter was found to be consistent over time in both Strasbourg and Geispolsheim when no weather events occurred, but particles were isotopically depleted in the presence of fog and rain due to preferential scavenging of larger, isotopically enriched particles. While the results

of this study indicate that preferential particle scavenging by both fog and rain occurred, further work is necessary to determine the exact cause of the observed isotopic depletion of interstitial particles. Since it is possible that fine (< 2 μm) loess particles that contain calcium carbonate could be present in $PM_{2.5}$, future studies should attempt to quantify the carbonate in particulate matter. A longer sample collection time using a low-volume sampler could make it possible to quantify carbonate using the method developed in Chapter 3, but the use of a high-volume sampler (as was used to collect particulate matter in Chapter 4) could provide enough sample to both quantify CC and analyze the $\delta^{13}C$ of carbonate.

Chapter 6 discussed the temporal evolution of fog collected in Casitas Pass, on the southern California coast. This is the first study performed on the $\delta^{13}C_{DOC}$ of time-resolved fog samples. The stable isotopes of fog water ($\delta^{18}O$ and $\delta^{2}H$) and dissolved organic carbon ($\delta^{13}C_{DOC}$) during four fog events were measured and compared to other common measurements of fog composition to determine how isotopic information can complement these measurements when evaluating the evolution of a fog event. It was hypothesized that $\delta^{13}C_{DOC}$ measurements would provide information about compositional changes to fog constituents, while $\delta^{18}O$ and $\delta^{2}H$ would provide information about the meteorological factors that affect fog formation. The $\delta^{13}C_{DOC}$ of the fog samples were found to decrease over time during each event. There was no correlation between $\delta^{13}C_{DOC}$ and TOC; TOC of fog and the liquid water content were, however, found to have a nonlinear inverse relationship, likely caused by the dilution of fog droplets over the duration of a fog. Therefore, dilution did not impact $\delta^{13}C_{DOC}$. Additionally, correlations among oxidized organic species measured in the fog imply similarities in their oxidation

pathways; however, there was no consistent correlation between these species and $\delta^{13}C_{DOC}$, indicating that $\delta^{13}C_{DOC}$ is not a metric of aqueous SOA material formation. A correlation was observed between $\delta^{13}C_{DOC}$ and ions associated with sea spray, indicating that $\delta^{13}C_{DOC}$ may be useful in observing fog scavenging and deposition; aerosols associated with sea spray are generally coarse and are scavenged and deposited more readily than fine particles. The isotopes of fog water ($\delta^{2}H$ and $\delta^{18}O$) form a cloud water line with the equation $\delta^{2}H = 7.3 \times \delta^{18}O + 3.0 \times 10^{-3}$. This line falls below the global meteoric water line and is consistent with fog that has not undergone synoptic scale transport. The changes in $\delta^{2}H$ and $\delta^{18}O$ during each event may exhibit influence from both changes in temperature and changes in the air masses feeding the fog. Based upon the correlation of $\delta^{2}H$ and $\delta^{18}O$ with $\delta^{13}C_{DOC}$, there is a possibility that principles of Rayleigh distillation may be used as indicators of fog evolution and droplet deposition.

REFERENCES

Abou Chakra, O. R., Joyeux, M., Nerrière, E., Strub, M. P., & Zmirou-Navier, D. (2007). Genotoxicity of organic extracts of urban airborne particulate matter: An assessment within a personal exposure study. *Chemosphere*, *66*(7), 1375–1381. http://doi.org/10.1016/j.chemosphere.2006.06.066

Aggarwal, S. G., & Kawamura, K. (2008). Molecular distributions and stable carbon isotopic compositions of dicarboxylic acids and related compounds in aerosols from Sapporo, Japan: Implications for photochemical aging during long-range atmospheric transport. *Journal of Geophysical Research: Atmospheres*, *113*, 1–13. http://doi.org/10.1029/2007JD009365

Aggarwal, S. G., Kawamura, K., Umarji, G. S., Tachibana, E., Patil, R. S., & Gupta, P. K. (2013). Organic and inorganic markers and stable C-, N-isotopic compositions of tropical coastal aerosols from megacity Mumbai: sources of organic aerosols and atmospheric processing. *Atmospheric Chemistry and Physics*, *13*(9), 4667–4680. http://doi.org/10.5194/acp-13-4667-2013

Aleksic, N., & Dukett, J. E. (2010). Probabilistic relationship between liquid water content and ion concentrations in cloud water. *Atmospheric Research*, *98*(2–4), 400–405. http://doi.org/10.1016/j.atmosres.2010.08.003

Annual Estimates of the Resident Population: April 1, 2010 to July 1, 2016. (n.d.). Retrieved February 1, 2018, from https://factfinder.census.gov/faces/tableservices/jsf/pages/productview.xhtml.

Ault, A. P., Moffet, R. C., Baltrusaitis, J., Collins, D. B., Ruppel, M. J., Cuadra-Rodriguez, L. A., Zhao, D., Guacso, T. L., Ebben, C. J., Geiger, F. M., Bertram, T. H., Prather, K. A., & Grassian, V. H. (2013). Size-Dependent Changes in Sea Spray Aerosol Composition and Properties with Different Seawater Conditions. *Environmental Science and Technology*, *47*(11), 5603–5612. http://doi.org/10.1021/es400416g

Bator, A., & Collett, J. L. (1997). Cloud chemistry varies with drop size. *Journal of Geophysical Research: Atmospheres*, *102*(D23), 28071–28078. http://doi.org/10.1029/97JD02306

Bench, G. (2004). Measurement of Contemporary and Fossil Carbon Contents of $PM_{2.5}$ Aerosols: Results from Turtleback Dome, Yosemite National Park. *Environmental Science and Technology*, *38*(8), 2424–2427. http://doi.org/10.1021/es035161s

Bender, M. M. (1971). Variations in the $^{13}C/^{12}C$ ratios of plants in relation to the pathway of photosynthetic carbon dioxide fixation. *Phytochemistry*, *10*, 1239–1244.

Bendle, J., Kawamura, K., Yamazaki, K., & Niwai, T. (2007). Latitudinal distribution of terrestrial lipid biomarkers and *n*-alkane compound-specific stable carbon isotope ratios in the atmosphere over the western Pacific and Southern Ocean. *Geochimica et Cosmochimica Acta*, *71*(24), 5934–5955. http://doi.org/10.1016/j.gca.2007.09.029

Benn, T., Herckes, P., & Westerhoff, P. (2012). *Fullerenes in environmental samples: C_{60} in atmospheric particulate matter*. *Comprehensive Analytical Chemistry* (1st ed., Vol. 59). Elsevier B.V. http://doi.org/10.1016/B978-0-444-56328-6.00010-4

Birch, M. E., & Cary, R. A. (1996). Elemental Carbon-Based Method for Monitoring Occupational Exposures to Particulate Diesel Exhaust. *Aerosol Science and Technology*, *25*(3), 221–241. http://doi.org/10.1080/02786829608965393

Boris, A. J., Lee, T., Park, T., Choi, J., Seo, S. J., & Collett, J. L. (2016). Fog composition at Baengnyeong Island in the eastern Yellow Sea: Detecting markers of aqueous atmospheric oxidations. *Atmospheric Chemistry and Physics*, *16*(2), 437–453. http://doi.org/10.5194/acp-16-437-2016

Boris, A. J., Napolitano, D. C., Herckes, P., Clements, A. L., & Collett, J. L. (2018). Fogs and Air Quality on the Southern California Coast. *Aerosol and Air Quality Research*, *18*, 224–239. http://doi.org/10.4209/aaqr.2016.11.0522

Brown, S. G., Frankel, A., Raffuse, S. M., Roberts, P. T., Hafner, H. R., & Anderson, D. J. (2007). Source apportionment of fine particulate matter in Phoenix, AZ, using positive matrix factorization. *Journal of the Air & Waste Management Association (1995)*, *57*(6), 741–752. http://doi.org/10.3155/1047-3289.57.6.741

Brown, S. G., Herckes, P., Ashbaugh, L., Hannigan, M. P., Kreidenweis, S. M., & Collett, J. L. (2002). Characterization of organic aerosol in Big Bend National Park, Texas. *Atmospheric Environment*, *36*(38), 5807–5818. http://doi.org/10.1016/S1352-2310(02)00578-2

Cachier, H., Bremond, M., & Buat-Menard, P. (1989). Determination of atmospheric soot carbon with a simple thermal method. *Tellus, 41B*, 379–390.

Cachier, H., Buat-Menard, P., Fontugne, M., & Chesselet, R. (1986). Long-range transport of continentally-derived particulate carbon in the marine atmosphere : Evidence from stable carbon isotope studies. *Tellus*, *38B*, 161–177. http://doi.org/10.1111/j.1600-0889.1986.tb00184.x

Cachier, H., Buat-Menard, P., Fontugne, M., & Rancher, J. (1985). Source terms and source strengths of the carbonaceous aerosol in the tropics. *Journal of Atmospheric Chemistry*, *3*(4), 469–489. http://doi.org/10.1007/BF00053872

Cahill, T. M. (2013). Annual cycle of size-resolved organic aerosol characterization in an urbanized desert environment. *Atmospheric Environment*, *71*, 226–233. http://doi.org/10.1016/j.atmosenv.2013.02.004

Cao, J., Chow, J. C., Tao, J., Lee, S., Watson, J. G., Ho, K., Wang, G., Zhu, C., & Han, Y. (2011). Stable carbon isotopes in aerosols from Chinese cities: Influence of fossil fuels. *Atmospheric Environment*, *45*(6), 1359–1363. http://doi.org/10.1016/j.atmosenv.2010.10.056

Cao, J. J., Lee, S. C., Zhang, X. Y., Chow, J. C., An, Z. S., Ho, K. F., Watson, J. G., Fung, K., Wang, Y. Q., & Shen, Z. X. (2005). Characterization of airborne carbonate over a site near Asian dust source regions during spring 2002 and its climatic and environmental significance. *Journal of Geophysical Research D: Atmospheres*, *110*(3), 1–8. http://doi.org/10.1029/2004JD005244

Cao, J. J., Zhu, C. S., Chow, J. C., Liu, W. G., Han, Y. M., & Watson, J. G. (2008). Stable carbon and oxygen isotopic composition of carbonate in fugitive dust in the Chinese Loess Plateau. *Atmospheric Environment*, *42*(40), 9118–9122. http://doi.org/10.1016/j.atmosenv.2008.09.043

Cao, J., Wang, Y., Zhang, X., Lee, S., Ho, K., Cao, Y., & Li, Y. (2004). Analysis of carbon isotopes in airborne carbonate and implications for aeolian sources. *Chinese Science Bulletin*, *49*(15), 1637–1641. http://doi.org/10.1007/BF03184135

Capel, P. D., Gunde, R., Zürcher, F., & Giger, W. (1990). Carbon Speciation and Surface Tension of Fog. *Environmental Science and Technology*, *24*(5), 722–727. http://doi.org/10.1021/es00075a017

Carlton, A. G., Turpin, B. I., Altieri, K. E., Seitzinger, S. P., Mathur, R., Roselle, S. J., & Weber, R. J. (2008). CMAQ model performance enhanced when in-cloud secondary organic aerosol is included: Comparisons of organic carbon predictions with measurements. *Environmental Science & Technology*, *42*(23), 8798–802. Retrieved from http://www.ncbi.nlm.nih.gov/pubmed/19192800

Cary, B. (2017). Sunset Laboratory Inc., Personal Communication.

Chalbot, M.-C. G., Brown, J., Chitranshi, P., Gamboa da Costa, G., Pollock, E. D., & Kavouras, I. G. (2014). Functional characterization of the water-soluble organic carbon of size-fractionated aerosol in the southern Mississippi Valley. *Atmospheric Chemistry and Physics*, *14*(12), 6075–6088. http://doi.org/10.5194/acp-14-6075-2014

Chen, B., Cui, X., & Wang, Y. (2016). Regional prediction of carbon isotopes in soil carbonates for Asian dust source tracer. *Atmospheric Environment*, *142*, 1–8. http://doi.org/10.1016/j.atmosenv.2016.07.029

Chen, B., Jie, D., Shi, M., Gao, P., Shen, Z., Uchida, M., Zhou, L., Liu, K., & Kitagawa, H. (2015). Characteristics of ^{14}C and ^{13}C of carbonate aerosols in dust storm events in China. *Atmospheric Research*, *164–165*, 297–303. http://doi.org/10.1016/j.atmosres.2015.06.003

Chow, J. C., & Watson, J. G. (2002). $PM_{2.5}$ carbonate concentrations at regionally representative Interagency Monitoring of Protected Visual Environment sites. *Journal of Geophysical Research Atmospheres*, *107*(21), 6-1–6-9. http://doi.org/10.1029/2001JD000574

Chow, J. C., Watson, J. G., Crow, D., Lowenthal, D. H., & Merrifield, T. (2001). Comparison of IMPROVE and NIOSH Carbon Measurements. *Aerosol Science and Technology*, *34*(1), 23–34. http://doi.org/10.1080/02786820119073

Clarke, A. G., & Karani, G. N. (1992). Characterization of the Carbonate Content of Atmospheric Aerosols. *Journal of Atmospheric Chemistry*, *14*, 119–128.

Clements, A. L., Fraser, M. P., Upadhyay, N., Herckes, P., Sundblom, M., Lantz, J., & Solomon, P. A. (2014). Chemical characterization of coarse particulate matter in the Desert Southwest - Pinal County Arizona, USA. *Atmospheric Pollution Research*, *5*, 52–61. http://doi.org/10.5094/apr.2014.007

Clements, A. L., Fraser, M., Upadhyay, N., Herckes, P., Sundblom, M., Lantz, J., & Solomon, P. (2013). Characterization of summertime coarse particulate matter in the Desert Southwest–Arizona, USA. *Journal of the Air & Waste Management Association*, *63*(7), 764–772. http://doi.org/10.1080/10962247.2013.787955

Collett, J. L., Herckes, P., Youngster, S., & Lee, T. (2008). Processing of atmospheric organic matter by California radiation fogs. *Atmospheric Research*, *87*(3–4), 232–241. http://doi.org/10.1016/j.atmosres.2007.11.005

Collett, J. L., Sherman, D. E., Moore, K. F., Hannigan, M. P., & Lee, T. (2001). Aerosol Particle Processing and Removal by Fogs: Observations in Chemically Heterogeneous Central California Radiation Fogs. *Water, Air, and Soil Pollution: Focus*, *1*(5–6), 303–312.

Collister, J. W., Rieley, G., Stern, B., Eglinton, G., & Fry, B. (1994). Compound-Specific $\delta^{13}C$ Analyses of Leaf Lipids from Plants with Differing Carbon Dioxide Metabolisms, *21*(6), 619–627.

Corbin, J. D., Thomsen, M. A., Dawson, T. E., & D'Antonio, C. M. (2005). Summer water use by California coastal prairie grasses: Fog, drought, and community composition. *Oecologia*, *145*(4), 511–521. http://doi.org/10.1007/s00442-005-0152-y

Cozic, J., Verheggen, B., Mertes, S., Connolly, P., Bower, K., Petzold, A., Baltensperger, U., & Weingartner, E. (2007). Scavenging of black carbon in mixed phase clouds at the high alpine site Jungfraujoch. *Atmospheric Chemistry and Physics*, *7*(7), 1797–1807. http://doi.org/10.5194/acp-7-1797-2007

Criado, J. M., & Ortega, A. (1992). A study of the influence of particle size on the thermal decomposition of $CaCO_3$ by means of constant rate thermal analysis. *Thermochimica Acta*, *195*, 163–167. http://doi.org/10.1016/0040-6031(92)80059-6

Dansgaard, W. (1964). Stable isotopes in precipitation. *Tellus*, *16*(4), 436–468. http://doi.org/10.3402/tellusa.v16i4.8993

Dawson, T. E. (1998). Fog in the California redwood forest: Ecosystem inputs and use by plants. *Oecologia*, *117*(4), 476–485. http://doi.org/10.1007/s004420050683

Decesari, S., Facchini, M. C., Matta, E., Lettini, F., Mircea, M., Fuzzi, S., Tagliavini, E., & Putaud, J. (2001). Chemical features and seasonal variation of fine aerosol water-soluble organic compounds in the Po Valley, Italy. *Atmospheric Environment*, *35*, 3691–3699. http://doi.org/10.1016/S1352-2310(00)00509-4

Delhomme, O., & Millet, M. (2012). Characterization of particulate polycyclic aromatic hydrocarbons in the east of France urban areas. *Environmental Science and Pollution Research*, *19*(5), 1791–1799. http://doi.org/10.1007/s11356-011-0701-3

Delhomme, O., Morville, S., & Millet, M. (2010). Seasonal and diurnal variations of atmospheric concentrations of phenols and nitrophenols measured in the Strasbourg area, France. *Atmospheric Pollution Research*, *1*(1), 16–22. http://doi.org/10.5094/APR.2010.003

Demoz, B. B., Collett, J. L., & Daube, B. C. (1996). On the caltech active strand cloudwater collectors. *Atmospheric Research*, *41*(1), 47–62. http://doi.org/10.1016/0169-8095(95)00044-5

Elbert, W., Hoffmann, M. R., Krämer, M., Schmitt, G., & Andreae, M. O. (2000). Control of solute concentrations in cloud and fog water by liquid water content. *Atmospheric Environment*, *34*(7), 1109–1122. http://doi.org/10.1016/S1352-2310(99)00351-9

Elbert, W., Hoffmann, M. R., Krämer, M., Schmitt, G., & Andreae, M. O. (2002). Reply to Discussion on "Control of solute concentrations in cloud and fog water by liquid water content." *Atmospheric Environment*, *36*, 1909–1910. http://doi.org/10.1016/S1352-2310(99)00351-9

Engling, G., Herckes, P., Kreidenweis, S. M., Malm, W. C., & Collett, J. L. J. (2006). Composition of the fine organic aerosol in Yosemite National Park during the 2002 Yosemite Aerosol Characterization Study. *Atmospheric Environment*, *40*(16), 2959–2972. http://doi.org/10.1016/j.atmosenv.2005.12.041

Erel, Y., Pehkonen, S. O., & Hoffmann, M. R. (1993). Redox chemistry of iron in fog and stratus clouds. *Journal of Geophysical Research*, *98*(D10), 18423. http://doi.org/10.1029/93JD01575

Ervens, B. (2015). Modeling the Processing of Aerosol and Trace Gases in Clouds and Fogs. *Chemical Reviews*, *115*(10), 4157–4198. http://doi.org/10.1021/cr5005887

Ervens, B., Herckes, P., Feingold, G., Lee, T., Collett, J. L., & Kreidenweis, S. M. (2003). On the drop-size dependence of organic acid and formaldehyde concentrations in fog. *Journal of Atmospheric Chemistry*, *46*(3), 239–269. http://doi.org/10.1023/A:1026393805907

Ervens, B., Wang, Y., Eagar, J., Leaitch, W. R., Macdonald, A. M., Valsaraj, K. T., & Herckes, P. (2013). Dissolved organic carbon (DOC) and select aldehydes in cloud and fog water: The role of the aqueous phase in impacting trace gas budgets. *Atmospheric Chemistry and Physics*, *13*(10), 5117–5135. http://doi.org/10.5194/acp-13-5117-2013

Facchini, M. C., Fuzzi, S., Zappoli, S., Andracchio, A., Gelencsér, A., Kiss, G., Krivácsy, Z., Mészáros, E., Hansson, H., Alsberg, T., & Zebühr, Y. (1999). Partitioning of the organic aerosol component between fog droplets and interstitial air. *Journal of Geophysical Research: Atmospheres*, *104*(D21), 26821–26832. http://doi.org/10.1029/1999JD900349

Fischer, D. T., & Still, C. J. (2007). Evaluating patterns of fog water deposition and isotopic composition on the California Channel Islands. *Water Resources Research*, *43*(4), 1–13. http://doi.org/10.1029/2006WR005124

Fisseha, R., Saurer, M., Jäggi, M., Siegwolf, R. T. W., Dommen, J., Szidat, S., Samburova, V., & Baltensperger, U. (2009). Determination of primary and secondary sources of organic acids and carbonaceous aerosols using stable carbon isotopes. *Atmospheric Environment*, *43*(2), 431–437. http://doi.org/10.1016/j.atmosenv.2008.08.041

Folinsbee, L. J. (1993). Human health effects of air pollution. *Environmental Health Perspectives*, *100*(12), 45–56. Retrieved from http://www.pubmedcentral.nih.gov/articlerender.fcgi?artid=1519570&tool=pmcentrez&rendertype=abstract

Garbaras, A., Rimselyte, K., Kvietkus, K., & Remeikis, V. (2009). $\delta^{13}C$ values in size-segregated atmospheric carbonaceous aerosols at a rural site in Lithuania. *Lithuanian Journal of Physics*, *49*(2), 229–236.

Gat, J. R. (1996). Oxygen and Hydrogen Isotopes in the Hydrologic Cycle. *Annual Review of Earth and Planetary Sciences*, *24*, 225–262. http://doi.org/10.1146/annurev.earth.24.1.225

Gelencsér, A., May, B., Simpson, D., Sánchez-Ochoa, A., Kasper-Giebl, A., Puxbaum, H., Casiero, A., Pio, C., & Legrand, M. (2007). Source apportionment of $PM_{2.5}$ organic aerosol over Europe: Primary/secondary, natural/anthropogenic, and fossil/biogenic origin. *Journal of Geophysical Research Atmospheres*, *112*(23), 1–12. http://doi.org/10.1029/2006JD008094

Gensch, I., Kiendler-Scharr, A., & Rudolph, J. (2014). Isotope ratio studies of atmospheric organic compounds: Principles, methods, applications and potential. *International Journal of Mass Spectrometry*, *365–366*, 206–221. http://doi.org/10.1016/j.ijms.2014.02.004

Gentner, D. R., Isaacman, G., Worton, D. R., Chan, A. W. H., Dallmann, T. R., Davis, L., Liu, S., Day, D. A., Russell, L. M., Wilson, K. R., Weber, R., Guha, A., Harley, R. A., & Goldstein, A. H. (2012). Elucidating secondary organic aerosol from diesel and gasoline vehicles through detailed characterization of organic carbon emissions. *Proceedings of the National Academy of Sciences*, *109*(45), 18318–18323. http://doi.org/10.1073/pnas.1212272109/-/DCSupplemental.www.pnas.org/cgi/doi/10.1073/pnas.1212272109

Gieray, R., Wieser, P., Engelhardt, T., Swietlicki, E., Hansson, H. C., Mentes, B., Orsini, D., Martinsson, B., Svennigsson, B., Noone, K. J., & Heintzenberg, J. (1997). Phase partitioning of aerosol constituents in cloud based on single-particle and bulk analysis. *Atmospheric Environment*, *31*(16), 2491–2502. http://doi.org/10.1016/S1352-2310(96)00298-1

Gleason, J. D., & Kyser, T. K. (1984). Stable isotope compositions of gases and vegetation near naturally burning coal. *Nature*, *307*(19), 254–257.

Goldstein, A. H., & Shaw, S. L. (2003). Isotopes of volatile organic compounds: An emerging approach for studying atmospheric budgets and chemistry. *Chemical Reviews*, *103*(12), 5025–48. http://doi.org/10.1021/cr0206566

Gorka, M., Rybicki, M., Simoneit, B. R. T., & Marynowski, L. (2014). Determination of multiple organic matter sources in aerosol PM_{10} from Wroclaw, Poland using molecular and stable carbon isotope compositions. *Atmospheric Environment*, *89*, 739–748. http://doi.org/10.1016/j.atmosenv.2014.02.064

Hallberg, A., Ogren, J. A., Noone, K. J., Heintzenberg, J., Berner, A., Solly, I., Kruisz, C., Reischl, G., Fuzzi, S., Facchini, M. C., Hansson, H. C., Wiedensohler, A., & Svenningsson, I. B. (1992). Phase partitioning for different aerosol species in fog. *Tellus*, *44B*, 545–555.

Happo, M. S., Hirvonen, M. R., Hälinen, A. I., Jalava, P. I., Pennanen, A. S., Sillanpää, M., Hillamo, R., & Salonen, R. O. (2008). Chemical compositions responsible for inflammation and tissue damage in the mouse lung by coarse and fine particulate samples from contrasting air pollution in Europe. *Inhalation Toxicology*, *20*(14), 1215–1231. http://doi.org/10.1080/08958370802147282

Hegde, P., Kawamura, K., Joshi, H., & Naja, M. (2016). Organic and inorganic components of aerosols over the central Himalayas: Winter and summer variations in stable carbon and nitrogen isotopic composition. *Environmental Science and Pollution Research*, *23*(7), 6102–6118. http://doi.org/10.1007/s11356-015-5530-3

Herckes, P., Engling, G., Kreidenweis, S. M., & Collett, J. L. (2006). Particle Size Distributions of Organic Aerosol Constituents during the 2002 Yosemite Aerosol Characterization Study. *Environmental Science & Technology*, *40*(15), 4554–4562. http://doi.org/10.1021/es0515396

Herckes, P., Hannigan, M. P., Trenary, L., Lee, T., & Collett, J. L. (2002). Organic compounds in radiation fogs in Davis (California). *Atmospheric Research*, *64*(1–4), 99–108. http://doi.org/10.1016/S0169-8095(02)00083-2

Herckes, P., Lee, T., Trenary, L., Kang, G., Chang, H., & Collett, J. L. (2002). Organic matter in central California radiation fogs. *Environmental Science & Technology*, *36*(22), 4777–4782. http://doi.org/10.1021/es025889t

Herckes, P., Valsaraj, K. T., & Collett, J. L. (2013). A review of observations of organic matter in fogs and clouds: Origin, processing and fate. *Atmospheric Research*, *132–133*, 434–449. http://doi.org/10.1016/j.atmosres.2013.06.005

Herckes, P., Wortham, H., Mirabel, P., & Millet, M. (2002). Evolution of the fogwater composition in Strasbourg (France) from 1990 to 1999. *Atmospheric Research*, *64*(1–4), 53–62. http://doi.org/10.1016/S0169-8095(02)00079-0

Heyder, J., Gebhart, J., Rudolf, G., Schiller, C. F., & Stahlhofen, W. (1986). Deposition of particles in the human respiratory tract in the size range 0.005-15 μm. *Journal of Aerosol Science*, *17*(5), 811–825. http://doi.org/10.1016/0021-8502(86)90035-2

Hitzenberger, R., Berner, A., Giebl, H., Drobesch, K., Kasper-Giebl, A., Loeflund, M., Urbna, H., & Puxbaum, H. (2001). Black carbon (BC) in alpine aerosols and cloud water - Concentrations and scavenging efficiencies. *Atmospheric Environment*, *35*(30), 5135–5141. http://doi.org/10.1016/S1352-2310(01)00312-0

Hitzenberger, R., Berner, A., Kromp, R., Kasper-Giebl, A., Limbeck, A., Tscherwenka, W., & Puxbaum, H. (2000). Black carbon and other species at a high-elevation European site (Mount Sonnblick, 3106 m, Austria): Concentrations and scavenging efficiencies. *Journal of Geophysical Research-Atmospheres*, *105*(D20), 24637–24645. http://doi.org/Doi 10.1029/2000jd900349

Houghton, H. G. (1955). On the Chemical Composition of Fog and Cloud Water. *J. Meteorol.*, *14*, 355–357.

Huang, L., Brook, J. R., Zhang, W., Li, S. M., Graham, L., Ernst, D., Chivulescu, A., & Lu, G. (2006). Stable isotope measurements of carbon fractions (OC/EC) in airborne particulate: A new dimension for source characterization and apportionment. *Atmospheric Environment*, *40*(15), 2690–2705. http://doi.org/10.1016/j.atmosenv.2005.11.062

Huang, Y., Dupont, L., Sarnthein, M., Hayes, J. M., & Eglinton, G. (2000). Mapping of C4 plant input from North West Africa into North East Atlantic sediments. *Geochimica et Cosmochimica Acta*, *64*(20), 3505–3513.

Ingraham, N. L., & Matthews, R. A. (1988). Fog-Drip as a Source of Groundwater Recharge in Northern Kenya. *Water Resources Research*, *24*(8), 1406–1410.

Ingraham, N. L., & Matthews, R. A. (1990). A stable isotopic study of fog: The Point Reyes Peninsula, California, U.S.A. *Chemical Geology: Isotope Geoscience Section*, *80*(4), 281–290. http://doi.org/10.1016/0168-9622(90)90010-A

Jia, Y., & Fraser, M. (2011). Characterization of saccharides in size-fractionated ambient particulate matter and aerosol sources: The contribution of primary biological aerosol particles (PBAPs) and soil to ambient particulate matter. *Environmental Science and Technology*, *45*(3), 930–936. http://doi.org/10.1021/es103104e

Junge, C. (1972). Our Knowledge of the Physico-Chemistry of Aerosols in the Undisturbed Marine Environment. *Journal of Geophysical Research*, *77*(27), 5183–5200.

Karanasiou, A., Diapouli, E., Cavalli, F., Eleftheriadis, K., Viana, M., Alastuey, A., Querol, X., & Reche, C. (2011). On the quantification of atmospheric carbonate carbon by thermal/optical analysis protocols. *Atmospheric Measurement Techniques*, *4*(11), 2409–2419. http://doi.org/10.5194/amt-4-2409-2011

Kaseke, K. F., Tian, C., Wang, L., Seely, M., Vogt, R., Wassenaar, T., & Mushi, R. (2018). Fog Spatial Distributions over the Central Namib Desert - An Isotope Approach. *Aerosol and Air Quality Research*, *18*, 49–61. http://doi.org/10.4209/aaqr.2017.01.0062

Kaseke, K. F., Wang, L., & Seely, M. K. (2017). Nonrainfall water origins and formation mechanisms. *Science Advances*, *3*(3), e1603131. http://doi.org/10.1126/sciadv.1603131

Kasper-Giebl, A. (2002). Control of solute concentrations in cloud and fog water by liquid water content. *Atmospheric Environment, Discussion*(36), 1907–1908. http://doi.org/10.1016/S1352-2310(99)00351-9

Kaul, D. S., Gupta, T., Tripathi, S. N., Tare, V., & Collett, J. L. (2011). Secondary organic aerosol: a comparison between foggy and nonfoggy days. *Environmental Science & Technology*, *45*(17), 7307–13. http://doi.org/10.1021/es201081d

Keene, W. C., Pszenny, A. A. P., Galloway, J. N., & Hawley, M. E. (1986). Sea-salt corrections and interpretation of constituent ratios in marine precipitation. *Journal of Geophysical Research*, *91*(D6), 6647. http://doi.org/10.1029/JD091iD06p06647

Kirchstetter, T. W., Novakov, T., & Hobbs, P. V. (2004). Evidence that the spectral dependence of light absorption by aerosols is affected by organic carbon. *Journal of Geophysical Research D: Atmospheres*, *109*(21), 1–12. http://doi.org/10.1029/2004JD004999

Kirillova, E. N., Andersson, A., Sheesley, R. J., Krusa, M., Praveen, P. S., Budhavant, K., Safai, P. D., Rao, P. S. P., & Gustafsson, Ö. (2013). ^{13}C- And ^{14}C-based study of sources and atmospheric processing of water-soluble organic carbon (WSOC) in South Asian aerosols. *Journal of Geophysical Research Atmospheres*, *118*(2), 614–626. http://doi.org/10.1002/jgrd.50130

Laj, P., Fuzzi, S., Facchini, M. C., Lind, J. A., Orsi, G., Preiss, M., Maser, R., Jaeschke, W., Seyffer, E., Helas, G., Acker, K., Wieprecht, W., Möller, D., Arends, B. G., Möls, J. J., Colvile, R. N., Gallagher, M. W., Beswick, K. M., Hargreaves, K. J., Storeton-West, R. L., & Sutton, M. A. (1997). Cloud processing of soluble gases. *Atmospheric Environment*, *31*(16), 2589–2598. http://doi.org/10.1016/S1352-2310(97)00040-X

Lewis, C. W., Norris, G. A., Conner, T. L., & Henry, R. C. (2003). Source Apportionment of Phoenix $PM_{2.5}$ Aerosol with the Unmix Receptor Model. *Journal of the Air & Waste Management Association*, *53*(3), 325–338. http://doi.org/10.1080/10473289.2003.10466155

Li, M., Huang, Y., Obermajer, M., Jiang, C., Snowdon, L. R., & Fowler, M. G. (2001). Hydrogen isotopic compositions of individual alkanes as a new approach to petroleum correlation: Case studies from the Western Canada Sedimentary Basin. *Organic Geochemistry*, *32*(12), 1387–1399. http://doi.org/10.1016/S0146-6380(01)00116-4

Lim, B., Jickells, T. D., & Davies, T. D. (1991). Sequential sampling of particles, major ions and total trace metals in wet deposition. *Atmospheric Environment Part A, General Topics*, *25*(3–4), 745–762. http://doi.org/10.1016/0960-1686(91)90073-G

Lipsett, M. J., Tsai, F. C., Roger, L., Woo, M., & Ostro, B. D. (2006). Coarse particles and heart rate variability among older adults with coronary artery disease in the Coachella Valley, California. *Environmental Health Perspectives*, *114*(8), 1215–1220. http://doi.org/10.1289/ehp.8856

Löflund, M., Kasper-Giebl, A., Schuster, B., Giebl, H., Hitzenberger, R., & Puxbaum, H. (2002). Formic, acetic, oxalic, malonic and succinic acid concentrations and their contribution to organic carbon in cloud water. *Atmospheric Environment*, *36*(9), 1553–1558. http://doi.org/10.1016/S1352-2310(01)00573-8

López-Veneroni, D. (2009). The stable carbon isotope composition of $PM_{2.5}$ and PM_{10} in Mexico City Metropolitan Area air. *Atmospheric Environment*, *43*(29), 4491–4502. http://doi.org/10.1016/j.atmosenv.2009.06.036

MacNee, W., & Donaldson, K. (2003). Mechanism of lung injury caused by PM_{10} and ultrafine particles with special reference to COPD. *European Respiratory Journal*, *21*(Supplement 40), 47S–51s. http://doi.org/10.1183/09031936.03.00403203

Majestic, B. J., Anbar, A. D., & Herckes, P. (2009). Elemental and iron isotopic composition of aerosols collected in a parking structure. *Science of the Total Environment*, *407*(18), 5104–5109. http://doi.org/10.1016/j.scitotenv.2009.05.053

Malm, W. C., Day, D. E., Carrico, C., Kreidenweis, S. M., Collett, J. L., McMeeking, G., Lee., T., Carrillo, J., & Schichtel, B. (2005). Intercomparison and closure calculations using measurements of aerosol species and optical properties during the Yosemite aerosol characterization study. *Journal of Geophysical Research D: Atmospheres*, *110*(14), 1–21. http://doi.org/10.1029/2004JD005494

Mancilla, Y., Herckes, P., Fraser, M. P., & Mendoza, A. (2015). Secondary organic aerosol contributions to $PM_{2.5}$ in Monterrey, Mexico: Temporal and seasonal variation. *Atmospheric Research*, *153*, 348–359. http://doi.org/10.1016/j.atmosres.2014.09.009

Mancilla, Y., Mendoza, A., Fraser, M. P., & Herckes, P. (2016). Organic composition and source apportionment of fine aerosol at Monterrey, Mexico, based on organic markers. *Atmospheric Chemistry and Physics*, *16*(2), 953–970. http://doi.org/10.5194/acp-16-953-2016

Manoli, E., Voutsa, D., & Samara, C. (2002). Chemical characterization and source identification/apportionment of fine and coarse air particles in Thessaloniki, Greece. *Atmospheric Environment*, *36*(6), 949–961. http://doi.org/10.1016/S1352-2310(01)00486-1

Mar, T. F., Norris, G. A., Koenig, J. Q., & Larson, T. V. (2000). Associations between air pollution and mortality in Phoenix, 1995-1997. *Environmental Health Perspectives*, *108*(4), 347–353. http://doi.org/10.1289/ehp.00108347

Maricopa County Air Quality Department. (2018). Retrieved February 2, 2018, from http://www.maricopa.gov/1244/Air-Quality

Marley, N. A., Gaffney, J. S., Tackett, M., Sturchio, N. C., Heraty, L., Martinez, N., Hardy, K. D., Marchany-Rivera, A., Guilderson, T., MacMillan, A., & Steelman, K. (2009). The impact of biogenic carbon sources on aerosol absorption in Mexico City. *Atmospheric Chemistry and Physics*, *9*(5), 1537–1549. http://doi.org/10.5194/acp-9-1537-2009

Martinelli, L. A., Camargo, P. B., Lara, L. B. L. S., Victoria, R. L., & Artaxo, P. (2002). Stable carbon and nitrogen isotopic composition of bulk aerosol particles in a C4 plant landscape of southeast Brazil. *Atmospheric Environment*, *36*(14), 2427–2432. http://doi.org/10.1016/S1352-2310(01)00454-X

Masalaite, A., Remeikis, V., Garbaras, A., Dudoitis, V., Ulevicius, V., & Ceburnis, D. (2015). Elucidating carbonaceous aerosol sources by the stable carbon $\delta^{13}C_{TC}$ ratio in size-segregated particles. *Atmospheric Research*, *158–159*, 1–12. http://doi.org/10.1016/j.atmosres.2015.01.014

McCrea, J. M. (1950). On the Isotopic Chemistry of Carbonates and a Paleotemperature Scale. *The Journal of Chemical Physics*, *18*(6), 849–857. http://doi.org/10.1063/1.1747785

Michna, P., Werner, R. A., & Eugster, W. (2015). Does fog chemistry in Switzerland change with altitude? *Atmospheric Research*, *151*, 31–44. http://doi.org/10.1016/j.atmosres.2014.02.008

Millet, M., Sanusi, A., & Wortham, H. (1996). Chemical composition of fogwater in an urban area: Strasbourg (France). *Environmental Pollution*, *94*(3), 345–354. http://doi.org/10.1016/S0269-7491(96)00064-4

Millet, M., Wortham, H., & Mirabel, P. (1995). Solubility of polyvalent cations in fogwater at an urban site in Strasbourg (France). *Atmospheric Environment*, *29*(19), 2625–2631. http://doi.org/10.1016/1352-2310(95)00163-S

Millet, M., Wortham, H., Sanusi, A., & Mirabel, P. (1997). Low molecular weight organic acids in fogwater in an urban area: Strasbourg (France). *Science of The Total Environment*, *206*(1), 57–65. http://doi.org/10.1016/S0048-9697(97)00216-7

Miyazaki, Y., Fu, P. Q., Kawamura, K., Mizoguchi, Y., & Yamanoi, K. (2012). Seasonal variations of stable carbon isotopic composition and biogenic tracer compounds of water-soluble organic aerosols in a deciduous forest. *Atmospheric Chemistry and Physics*, *12*(3), 1367–1376. http://doi.org/10.5194/acp-12-1367-2012

Mladenov, N., Alados-Arboledas, L., Olmo, F. J., Lyamani, H., Delgado, A., Molina, A., & Reche, I. (2011). Applications of optical spectroscopy and stable isotope analyses to organic aerosol source discrimination in an urban area. *Atmospheric Environment*, *45*(11), 1960–1969. http://doi.org/10.1016/j.atmosenv.2011.01.029

Morawska, L., Bofinger, N. D., Kocis, L., & Nwankwoala, A. (1998). Submicrometer and supermicrometer particles from diesel vehicle emissions. *Environmental Science & Technology*, *32*(14), 2033–2042. http://doi.org/10.1021/es970826+

Moura, J. M. S., Martens, C. S., Moreira, M. Z., Lima, R. L., Sampaio, I. C. G., Mendlovitz, H. P., & Menton, M. C. (2008). Spatial and seasonal variations in the stable carbon isotopic composition of methane in stream sediments of eastern Amazonia. *Tellus*, *60B*(1), 21–31. http://doi.org/10.1111/j.1600-0889.2007.00322.x

Nguyen, D. L., Kawamura, K., Ono, K., Ram, S. S., Engling, G., Lee, C.-T., Lin, N. H., Chang, S. C., Chuang, M. T., Hsiao, T. C., Sheu, G. R., Yang, C. F. O., Chi, K. H., & Sun, S.-A. (2016). Comprehensive $PM_{2.5}$ Organic Molecular Composition and Stable Carbon Isotope Ratios at Sonla, Vietnam: Fingerprint of Biomass Burning Components. *Aerosol and Air Quality Research*, (June). http://doi.org/10.4209/aaqr.2015.07.0459

Noonan, K. (2012). Element Use and Acquisition Strategies in Biological Soil Crusts. *Available from Dissertations & Theses @ Arizona State University; ProQuest Dissertations & Theses Global.*

O'Leary, M. H. (1981). Carbon Isotope Fractionation in Plants. *Phytochemistry*, *20*(4), 553–567.

Oberdörster, G. (2001). Pulmonary effects of inhaled ultrafine particles. *International Archives of Occupational and Environmental Health*, *74*(1), 1–8. http://doi.org/10.1007/s004200000185

Park, R., & Epstein, S. (1960). Carbon isotope fractionation during photosynthesis. *Geochimica et Cosmochimica Acta*, *21*, 110–126.

Pichlmayer, F., Schoener, W., Seibert, P., Stichler, W., & Wagenbach, D. (1998). Stable Isotope Analysis for Characterization of Pollutants at High Elevation Alpine Sites. *Atmospheric Environment*, *32*(23), 4075–4085.

Raja, S., Raghunathan, R., Yu, X. Y., Lee, T., Chen, J., Kommalapati, R. R., Murugesan, K., Shen, X., Qingzhong, Y., Valsaraj, K. T., & Collett, J. L. (2008). Fog chemistry in the Texas-Louisiana Gulf Coast corridor. *Atmospheric Environment*, *42*(9), 2048–2061. http://doi.org/10.1016/j.atmosenv.2007.12.004

Ramadan, Z., Song, X. H., & Hopke, P. K. (2000). Identification of sources of Phoenix aerosol by positive matrix factorization. *Journal of the Air & Waste Management Association (1995)*, *50*(8), 1308–1320. http://doi.org/10.1080/10473289.2000.10464173

Raman, A., Arellano, A. F., & Brost, J. J. (2014). Revisiting haboobs in the southwestern United States: An observational case study of the 5 July 2011 Phoenix dust storm. *Atmospheric Environment*, *89*, 179–188. http://doi.org/10.1016/j.atmosenv.2014.02.026

Raman, A., Arellano, A., & Sorooshian, A. (2016). Decreasing Aerosol Loading in the North American Monsoon Region. *Atmosphere*, *7*(2), 24. http://doi.org/10.3390/atmos7020024

Reyes-Rodríguez, G. J., Gioda, A., Mayol-Bracero, O. L., & Collett, J. (2009). Organic carbon, total nitrogen, and water-soluble ions in clouds from a tropical montane cloud forest in Puerto Rico. *Atmospheric Environment*, *43*(27), 4171–4177. http://doi.org/10.1016/j.atmosenv.2009.05.049

Robinson, M. S., Anthony, T. R., Littau, S. R., Herckes, P., Nelson, X., Poplin, G. S., & Burgess, J. L. (2008). Occupational PAH exposures during prescribed pile burns. *Annals of Occupational Hygiene*, *52*(6), 497–508. http://doi.org/10.1093/annhyg/men027

Robinson, M. S., Zhao, M., Zack, L., Brindley, C., Portz, L., Quarterman, M., Long, X., & Herckes, P. (2011). Characterization of $PM_{2.5}$ collected during broadcast and slash-pile prescribed burns of predominately ponderosa pine forests in northern Arizona. *Atmospheric Environment*, *45*(12), 2087–2094. http://doi.org/10.1016/j.atmosenv.2011.01.051

Rolph, G. D., Stein, A. F., & Stunder, B. J. B. (2017). Real-time Environmental Applications and Display sYstem: READY. *Environmental Modelling & Software*, *95*, 210–228. http://doi.org/10.1016/j.envsoft.2017.06.025

Roth, E., Kehrli, D., Bonnot, K., & Trouvé, G. (2008). Size distributions of fine and ultrafine particles in the city of Strasbourg: Correlation between number of particles and concentrations of NO_x and SO_2 gases and some soluble ions concentration determination. *Journal of Environmental Management*, *86*(1), 282–290. http://doi.org/10.1016/j.jenvman.2006.12.022

Rudolph, J., Anderson, R. S., Czapiewski, K. V, & Czuba, E. (2003). The Stable Carbon Isotope Ratio of Biogenic Emissions of Isoprene and the Potential Use of Stable Isotope Ratio Measurements to Study Photochemical Processing of Isoprene in the Atmosphere. *Journal of Atmospheric Chemistry*, *44*, 39–55.

Rundel, P. W., Dillon, M. O., Palma, B., Mooney, H. A., Gulmon, S. L., & Ehleringer, J. R. (1991). The phytogeography and ecology of the coastal Atacama and Peruvian deserts. *Aliso*, *13*(1), 1–49. http://doi.org/10.5642/aliso.19911301.02

Sakugawa, H., & Kaplan, I. R. (1995). Stable Carbon Isotope Measurements of Atmospheric Organic Acids in Los Angeles, California. *Geophysical Research Letters*, *22*(12), 1509–1512. http://doi.org/10.1029/95GL01359

Salomons, W. (1975). Chemical and isotopic composition of carbonates in recent sediments and soils from Western Europe. *Journal of Sedimentary Petrology*, *45*(2), 440–449. http://doi.org/10.1306/212F6D84-2B24-11D7-8648000102C1865D

Samara, C., Voutsa, D., Kouras, A., Eleftheriadis, K., Maggos, T., Saraga, D., & Petrakakis, M. (2014). Organic and elemental carbon associated to PM_{10} and $PM_{2.5}$ at urban sites of northern Greece. *Environmental Science and Pollution Research*, *21*(3), 1769–1785. http://doi.org/10.1007/s11356-013-2052-8

Sander, R. (2015). Compilation of Henry's law constants (version 4.0) for water as solvent. *Atmospheric Chemistry and Physics*, *15*(8), 4399–4981. http://doi.org/10.5194/acp-15-4399-2015

Sang, X. F., Gensch, I., Laumer, W., Kammer, B., Chan, C. Y., Engling, G., Wahner, A., Wissel, H., & Kiendler-Scharr, A. (2012). Stable carbon isotope ratio analysis of anhydrosugars in biomass burning aerosol particles from source samples. *Environmental Science & Technology*, *46*(6), 3312–8. http://doi.org/10.1021/es204094v

Schefuß, E., Ratmeyer, V., Stuut, J.-B. W., Jansen, J. H. F., & Sinninghe Damsté, J. S. (2003). Carbon isotope analyses of *n*-alkanes in dust from the lower atmosphere over the central eastern Atlantic. *Geochimica et Cosmochimica Acta*, *67*(10), 1757–1767. http://doi.org/10.1016/S0016-7037(02)01414-X

Schipper, L. (2011). Automobile use, fuel economy and CO_2 emissions in industrialized countries: Encouraging trends through 2008? *Transport Policy*, *18*(2), 358–372. http://doi.org/10.1016/j.tranpol.2010.10.011

Schmid, S., Burkard, R., Frumau, K. F. A., Tobón, C., Bruijnzeel, L. A., Siegwolf, R., & Eugster, W. (2011). Using eddy covariance and stable isotope mass balance techniques to estimate fog water contributions to a Costa Rican cloud forest during the dry season. *Hydrological Processes*, *25*(3), 429–437. http://doi.org/10.1002/hyp.7739

Scholl, M. A., Giambelluca, T. W., Gingerich, S. B., Nullet, M. A., & Loope, L. L. (2007). Cloud water in windward and leeward mountain forests: The stable isotope signature of orographic cloud water. *Water Resources Research*, *43*(12), 1–13. http://doi.org/10.1029/2007WR006011

Scholl, M., Eugster, W., & Burkard, R. (2011). Understanding the role of fog in forest hydrology: Stable isotopes as tools for determining input and partitioning of cloud water in montane forests. *Hydrological Processes*, *25*(3), 353–366. http://doi.org/10.1002/hyp.7762

Seinfeld, J. H., & Pandis, S. N. (2016). *Atmospheric Chemistry and Physics: From Air Pollution to Climate Change* (3rd ed.). Hoboken, NJ: John Wiley& Sons, Inc.

Sellegri, K., Laj, P., Dupuy, R., Legrand, M., Preunkert, S., & Putaud, J.-P. (2003). Size-dependent scavenging efficiencies of multicomponent atmospheric aerosols in clouds. *Journal of Geophysical Research*, *108*(D11), 4334. http://doi.org/10.1029/2002JD002749

Shakya, K. M., Ziemba, L. D., & Griffin, R. J. (2010). Characteristics and Sources of Carbonaceous, Ionic, and Isotopic Species of Wintertime Atmospheric Aerosols in Kathmandu Valley, Nepal. *Aerosol and Air Quality Research*, *10*, 219–230.

Silverman, R. (1967). Carbon Isotopic Evidence for the Role of Lipids in Petroleum Formation. *Journal of the American Oil Chemists' Society*, *44*(12), 691–695.

Simoneit, B. R. T. (1989). Organic Matter of the Troposphere - V : Application of Molecular Marker Analysis to Biogenic Emissions into the Troposphere for Source Reconciliations. *Journal of Atmospheric Chemistry*, *8*, 251–275.

Simoneit, B. R. T. (1997). Compound-specific carbon isotope analyses of individual long-chain alkanes and alkanoic acids in Harmattan aerosols. *Atmospheric Environment*, *31*(15), 2225–2233. http://doi.org/10.1016/S1352-2310(97)00055-1

Solomon, P. A., & Moyers, J. L. (1986). A chemical characterization of wintertime haze in Phoenix, Arizona. *Atmospheric Environment (1967)*, *20*(1), 207–213. http://doi.org/10.1016/0004-6981(86)90221-0

Spiegel, J. K., Aemisegger, F., Scholl, M., Wienhold, F. G., Collett, J. L., Lee, T., van Pinxteren, D., Mertes, S., Tilgner, A., Herrmann, H., Werner, R. A., Buchmann, N., & Eugster, W. (2012a). Stable water isotopologue ratios in fog and cloud droplets of liquid clouds are not size-dependent. *Atmospheric Chemistry and Physics*, *12*(20), 9855–9863. http://doi.org/10.5194/acp-12-9855-2012

Spiegel, J. K., Aemisegger, F., Scholl, M., Wienhold, F. G., Collett, J. L., Lee, T., van Pinxteren, D., Mertes, S., Tilgner, A., Herrmann, H., Werner, R. A., Buchmann, N., & Eugster, W. (2012b). Temporal evolution of stable water isotopologues in cloud droplets in a hill cap cloud in central Europe (HCCT-2010). *Atmospheric Chemistry and Physics*, *12*(23), 11679–11694. http://doi.org/10.5194/acp-12-11679-2012

Stein, A. F., Draxler, R. R., Rolph, G. D., Stunder, B. J. B., Cohen, M. D., & Ngan, F. (2015). NOAA's hysplit atmospheric transport and dispersion modeling system. *Bulletin of the American Meteorological Society*, *96*(12), 2059–2077. http://doi.org/10.1175/BAMS-D-14-00110.1

Straub, D. J., Hutchings, J. W., & Herckes, P. (2012). Measurements of fog composition at a rural site. *Atmospheric Environment*, *47*, 195–205. http://doi.org/10.1016/j.atmosenv.2011.11.014

Sunset Laboratory Inc. (2018). Retrieved May 29, 2018, from http://www.sunlab.com/

Svenningsson, B., Hansson, H. C., Martinsson, B., Wiedensohler, A., Swietlicki, E., Cederfelt, S. I., Wendisch, M., Bower, K. N., Choularton, T. W., & Colvile, R. N. (1997). Cloud droplet nucleation scavenging in relation to the size and hygroscopic behaviour of aerosol particles. *Atmospheric Environment*, *31*(16), 2463–2475. http://doi.org/10.1016/S1352-2310(96)00179-3

Swineford, A., & Frye, J. C. (1955). Petrographic comparison of some loess samples from western Europe with Kansas loess. *Journal of Sedimentary Petrology*, *25*(1), 3–23. http://doi.org/10.1306/D42697E2-2B26-11D7-8648000102C1865D

Tanner, R. L., & Miguel, A. H. (1989). Carbonaceous Aerosol Sources in Rio de Janeiro. *Aerosol Science and Technology*, *10*(1), 213–223. http://doi.org/10.1080/02786828908959236

Taylor, S. R., McLennan, S. M., & McCulloch, M. T. (1983). Geochemistry of loess, continental crustal composition and crustal model ages. *Geochimica et Cosmochimica Acta*, *47*(11), 1897–1905. http://doi.org/10.1016/0016-7037(83)90206-5

Tsai, S.-S., Chang, C.-C., & Yang, C.-Y. (2013). Fine Particulate Air Pollution and Hospital Admissions for Chronic Obstructive Pulmonary Disease: A Case-Crossover Study in Taipei. *International Journal of Environmental Research and Public Health*, *10*(11), 6015–6026. http://doi.org/10.3390/ijerph10116015

Turner, J. R., Brown, S. G., & Minor, H. A. (2014). EPA's Pilot Study: Coarse PM Monitoring Program Results. *U. S. Environmental Protection Agency Office of Air Quality Planning and Standards.*

Upadhyay, N., Clements, A., Fraser, M., & Herckes, P. (2011). Chemical speciation of $PM_{2.5}$ and PM_{10} in South Phoenix, AZ, USA. *Journal of the Air and Waste Management Association*, *61*, 302–310. http://doi.org/10.3155/1047-3289.61.3.302

Upadhyay, N., Clements, A. L., Fraser, M. P., Sundblom, M., Solomon, P., & Herckes, P. (2015). Size-differentiated chemical composition of re-suspended soil dust from the Desert Southwest United States. *Aerosol and Air Quality Research*, *15*(2), 387–398. http://doi.org/10.4209/aaqr.2013.07.0253

Wang, G., Kawamura, K., Cheng, C., Li, J., Cao, J., Zhang, R., Zhang, T., Liu, S., & Zhao, Z. (2012). Molecular distribution and stable carbon isotopic composition of dicarboxylic acids, ketocarboxylic acids, and α-dicarbonyls in size-resolved atmospheric particles from Xi'an City, China. *Environmental Science & Technology*, *46*(9), 4783–91. http://doi.org/10.1021/es204322c

Wang, Y. (2014). Characterization of Atmospheric Organic Matter and its Processing by Fogs and Clouds. *Available from Dissertations & Theses @ Arizona State University; ProQuest Dissertations & Theses Global. (1640913556).*

Wang, Y., Guo, J., Wang, T., Ding, A., Gao, J., Zhou, Y., Collett, J. L., & Wang, W. (2011). Influence of regional pollution and sandstorms on the chemical composition of cloud/fog at the summit of Mt. Taishan in northern China. *Atmospheric Research*, *99*(3–4), 434–442. http://doi.org/10.1016/j.atmosres.2010.11.010

Wang, Y. Q., Zhang, X. Y., Arimoto, R., Cao, J. J., & Shen, Z. X. (2005). Characteristics of carbonate content and carbon and oxygen isotopic composition of northern China soil and dust aerosol and its application to tracing dust sources. *Atmospheric Environment*, *39*(14), 2631–2642. http://doi.org/10.1016/j.atmosenv.2005.01.015

Webb, T. L., & Kruger, J. E. (1970). Carbonates. In R. C. MacKenzie (Ed.), *Differential Thermal Analysis* (pp. 303–341). New York: Academic Press.

Whitford, W. G. (2002). *Ecology of Desert Systems* (1st ed.). San Diego, CA: Elsevier Science Ltd.

Widory, D. (2006). Combustibles, fuels and their combustion products: A view through carbon isotopes. *Combustion Theory and Modelling*, *10*(5), 831–841.

Widory, D., Roy, S., Le Moullec, Y., Goupil, G., Cocherie, A., & Guerrot, C. (2004). The origin of atmospheric particles in Paris: a view through carbon and lead isotopes. *Atmospheric Environment*, *38*(7), 953–961. http://doi.org/10.1016/j.atmosenv.2003.11.001

Willeke, K., & Whitby, K. T. (1975). Atmospheric Aerosols: Size Distribution Interpretation. *Journal of the Air Pollution Control Association*, *25*(5), 529–534. http://doi.org/10.1080/00022470.1975.10470110

Wozniak, A. S., Bauer, J. E., Dickhut, R. M., Xu, L., & McNichol, A. P. (2012). Isotopic characterization of aerosol organic carbon components over the eastern United States. *Journal of Geophysical Research*, *117*(D13), 1–14. http://doi.org/10.1029/2011JD017153

Yamamoto, S., & Kawamura, K. (2010). Compound-specific stable carbon and hydrogen isotopic compositions of *n*-alkanes in urban atmospheric aerosols from Tokyo. *Geochemical Journal*, *44*, 419–430.

Yin, J., Harrison, R. M., Chen, Q., Rutter, A., & Schauer, J. J. (2010). Source apportionment of fine particles at urban background and rural sites in the UK atmosphere. *Atmospheric Environment*, *44*(6), 841–851. http://doi.org/10.1016/j.atmosenv.2009.11.026

Zappoli, S., Andracchio, A., Fuzzi, S., Facchini, M. C., Gelencsér, A., Kiss, G., Krivácsy, Z., Molnár, Á., Mészáros, E., Hansson, H. -C., Rosman, K., & Zebühr, Y. (1999). Inorganic, organic and macromolecular components of fine aerosol in different areas of Europe in relation to their water solubility. *Atmospheric Environment*, *33*(17), 2733–2743. http://doi.org/10.1016/S1352-2310(98)00362-8

APPENDIX A

CARBONATE QUANTIFICATION: OPTIMIZATION OF EXPERIMENTAL PARAMETERS

Table A1

Experiments performed on three containers at 5, 15, and 25 minutes, and 4 hours after HCl addition, to determine a suitable incubation time.

Incubation Jar Number	Ambient Pressure (atm)	Ambient Temperature (K)	Amount of $NaHCO_3$ ($\times 10^{-7}$ mol)	Volume of Container (L)	Background CO_2 Concentration (ppmv)	Volume 1M HCl added (L)	5 Minute Incubation		
							CO_2 Pressure (ppmv)	Moles CO_2 Formed ($\times 10^{-7}$ mol)	Relative Error (%)
C	0.9891	294.5	3.70	0.1771	698	0.003	729	2.185	-40.94
J	0.9891	294.5	3.44	0.1776	562	0.003	592	2.122	-38.24
K	0.9891	294.5	4.23	0.1773	522	0.003	579	4.024	-4.82

Table A1 (continued)

Experiments performed on three containers at 5, 15, and 25 minutes, and 4 hours after HCl addition, to determine a suitable incubation time.

	15 Minute Incubation			25 Minute Incubation			4 Hour Incubation		
Incubation Jar Number	CO_2 Pressure (ppmv)	Moles CO_2 Formed ($\times 10^{-7}$ mol)	Relative Error (%)	CO_2 Pressure (ppmv)	Moles CO_2 Formed ($\times 10^{-7}$ mol)	Relative Error (%)	CO_2 Pressure (ppmv)	Moles CO_2 Formed ($\times 10^{-7}$ mol)	Relative Error (%)
C	723	1.774	-52.05	719	1.508	-59.25	630	-4.255	-215.00
J	590	1.984	-42.24	587	1.784	-48.08	577	1.134	-66.99
K	577	3.887	-8.06	575	3.754	-11.22	553	2.327	-44.97

Table A2

Experiments performed on three containers at 15, 20, and 25 minutes, and 3.5 hours after HCl addition, to determine a suitable incubation time.

Incubation Jar Number	Ambient Pressure (atm)	Ambient Temperature (K)	Amount of $NaHCO_3$ ($\times 10^{-7}$ mol)	Volume of Container (L)	Background CO_2 Concentration (ppmv)	Volume 1M HCl added (L)	15 Minute Incubation			
							CO_2 Pressure (ppmv)	Moles CO_2 Formed ($\times 10^{-7}$ mol)	Relative Error (%)	
C	0.9933	294.5	5.02	0.1771	453	0.003	512	4.176	-16.82	
J	0.9933	294.5	4.40	0.1776	461	0.003	509	3.409	-22.59	
K	0.9933	294.5	4.49	0.1773	468	0.003	519	3.616	-19.50	

Table A2 (continued)

Experiments performed on three containers at 15, 20, and 25 minutes, and 3.5 hours after HCl addition, to determine a suitable incubation time.

	20 Minute Incubation			25 Minute Incubation			3.5 Hour Incubation		
Incubation Jar Number	CO_2 Pressure (ppmv)	Moles CO_2 Formed ($\times 10^{-7}$ mol)	Relative Error (%)	CO_2 Pressure (ppmv)	Moles CO_2 Formed ($\times 10^{-7}$ mol)	Relative Error (%)	CO_2 Pressure (ppmv)	Moles CO_2 Formed ($\times 10^{-7}$ mol)	Relative Error (%)
C	509	3.970	-20.93	506	3.769	-24.93	496	3.119	-37.88
J	507	3.271	-25.73	505	3.137	-28.78	508	3.333	-24.33
K	515	3.340	-25.64	514	3.273	-27.13	504	2.622	-41.63

Table A3

Experiments performed on three containers to determine a suitable incubation time. The first measurement was taken 20 minutes after HCl addition, and subsequent measurements were taken every 30 minutes.

Incubation Jar Number	Ambient Pressure (atm)	Ambient Temperature (K)	Amount of $NaHCO_3$ ($\times 10^{-7}$ mol)	Volume of Container (L)	Background CO_2 Concentration (ppmv)	Volume 1M HCl added (L)	20 Minute Incubation		
							CO_2 Pressure (ppmv)	Moles CO_2 Formed ($\times 10^{-7}$ mol)	Relative Error (%)
C	0.9924	294.4	4.05	0.1771	458	0.003	511	3.749	-7.46
J	0.9924	294.4	3.52	0.1776	457	0.003	500	3.052	-13.37
K	0.9924	294.4	3.61	0.1773	459	0.003	505	3.260	-9.74

Table A3 (continued)

Experiments performed on three containers to determine a suitable incubation time. The first measurement was taken 20 minutes after HCl addition, and subsequent measurements were taken every 30 minutes.

	50 Minute Incubation			80 Minute Incubation			110 Minute Incubation		
Incubation Jar Number	CO_2 Pressure (ppmv)	Moles CO_2 Formed ($\times 10^{-7}$ mol)	Relative Error (%)	CO_2 Pressure (ppmv)	Moles CO_2 Formed ($\times 10^{-7}$ mol)	Relative Error (%)	CO_2 Pressure (ppmv)	Moles CO_2 Formed ($\times 10^{-7}$ mol)	Relative Error (%)
C	507	3.474	-14.25	502	3.140	-22.50	499	2.945	-27.31
J	499	2.983	-15.33	497	2.849	-19.14	495	2.719	-22.84
K	503	3.122	-13.56	499	2.854	-20.97	497	2.724	-24.58

Table A3 (continued)

Experiments performed on three containers to determine a suitable incubation time. The first measurement was taken 20 minutes after HCl addition, and subsequent measurements were taken every 30 minutes.

Incubation Jar Number	140 Minute Incubation			170 Minute Incubation		
	CO_2 Pressure (ppmv)	Moles CO_2 Formed ($\times 10^{-7}$ mol)	Relative Error (%)	CO_2 Pressure (ppmv)	Moles CO_2 Formed ($\times 10^{-7}$ mol)	Relative Error (%)
C	495	2.693	-33.55	491	2.447	-39.61
J	494	2.655	-24.64	492	2.532	-28.14
K	494	2.534	-29.83	492	2.411	-33.24

APPENDIX B

SAMPLING OF SOURCE MATERIALS IN TEMPE, AZ AND *N*-ALKANE LIMITS OF DETECTION

Sampling and Analysis of Local Source Materials

Potential local source materials of particulate matter were collected and analyzed. Since primary biogenic particles are known to directly comprise a portion of coarse particulate matter in Phoenix (Jia & Fraser, 2011), plant material was collected from the Arizona State University Tempe campus within 0.5 miles of the sampling site on April 1, 2016 (Table B1). Samples were dried at 100°C for 1 hour and homogenized to a fine powder with a mortar and pestle for analysis. Four additional plant material samples were collected in 2008 from the Herbarium at Arizona State University and were previously homogenized (Jia & Fraser, 2011).

Table B1

Plant material sampled on the ASU campus in Tempe, AZ and from the Herbarium at Arizona State University and results of isotopic analysis. The uncertainty in all $\delta^{13}C_{TC}$ results is 0.2‰.

Common Name	Scientific name	Photosynthetic Pathway	Sample Type	$\delta^{13}C_{TC}$ (‰)
Date Palm	*Phoenix dactylifera*	C_3	leaf	-26.2
Bottlebrush Tree	*Melaleuca viminalis*	C_3	leaf	-28.2
			flower	-24.6
Trumpetbush	*Tecoma stans*	C_3	leaf	-27.3
			flower	-26.1
Whitebark Acacia	*Acacia willardiana*	C_3	leaf	-23.9
Mexican Bird of Paradise	*Caesalpinia pulcherrima*	C_3	leaf	-26.3
Palo Brea	*Parkinsonia praecox*	C_3	leaf	-27.4
Blue Palo Verde	*Parkinsonia florida*	C_3	leaf	-27.8
			flower	-27.2
Grass family	Poaceae fam.	C_4	leaf	-13.6
Candelilla	*Euphorbia antisyphilitica*	C_4	leaf	-13.8
			flower	-14.1
Red Yucca	*Hesperaloe parviflora*	CAM	leaf	-18.4
			flower	-15.8
Texas Ranger	*Leucophyllum sp.*	C_3	leaf	-25.8
			flower	-25.6
Prickly Pear	*Opuntia sp. (hybrid cultivar)*	CAM	cactus	-13.2
			flower	-13.3
Fern-of-the-Desert	*Lysiloma thornberi*	C_3	leaf	-29.2
Seville Sour Orange	*Citrus aurantium*	C_3	leaf	-29.1
Alkalai Goldenbush	*Isocoma Acradenia*	C_3	homogenized powder	-28.8
Hummingbird Bush	*Justicia Californica*	C_3	homogenized powder	-29.2
Mesquite	*Prosopis Juliflora*	C_3	homogenized powder	-27.2
Desertbroom	*Baccharis Sarothroides*	C_3	homogenized powder	-30.9

Tailpipe emissions were scraped from vehicles parked on the ASU campus in Tempe in the spring and summer of 2016 (Table B2).

Table B2

Tailpipe scrapings from vehicles parked on the ASU campus in Tempe, AZ. The uncertainty in all $\delta^{13}C_{TC}$ results is 0.2‰.

Sample Date	Fuel Type	$\delta^{13}C_{TC}$ (‰)
4/19/2016	diesel	-25.6
6/21/2016	diesel	-25.5
6/21/2016	diesel	-24.0
7/10/2016	gasoline	-26.4
7/10/2016	gasoline	-26.3
7/10/2016	gasoline	-25.8

Aerosol sampling of emissions in a parking structure (Tyler Street Garage, Arizona State University, Tempe, AZ) was performed in May 2010 using a Tisch high-volume aerosol sampler (1.13 m^3/min) equipped with a $PM_{2.5}$ impaction stage using prebaked quartz fiber filters (Table B3). The sampler location and structure details are identical to previous studies (Benn et al., 2012; Majestic et al., 2009).

Table B3

Parking structure emissions sampled at the Tyler Street Garage on the ASU campus in Tempe, AZ. The uncertainty in all $\delta^{13}C_{TC}$ results is 0.2‰.

Sampling Start Date	Sampling End Date	Sampling Start Time	Sampling End Time	$\delta^{13}C_{TC}$ (‰)
5/4/2010	5/6/2010	9:15 AM	9:09 AM	-24.3
5/6/2010	5/10/2010	9:17 AM	8:47 AM	-24.2
5/10/2010	5/12/2010	8:51 AM	8:58 AM	-24.5
5/12/2010	5/14/2010	9:04 AM	3:18 PM	-24.4
5/14/2010	5/17/2010	3:25 PM	9:30 AM	-24.4
5/17/2010	5/18/2010	9:35 AM	2:45 PM	-24.5

Fireplace emissions were collected by performing a controlled burn in June 2016 of several common fireplace materials. A firewood bundle, two Duraflame logs (standard and Earth Fire), and a Clean Flame compressed recycled paper log were purchased from a local supermarket. A controlled burn site was set up in an empty lot north of the Arizona State University Tempe campus. A ceramic tile was placed on the ground and surrounded by cinderblocks. A ventilation duct placed on top of the cinderblocks was attached on the opposite side to a Tisch high-volume aerosol sampler (1.13 m^3/min). Each material was ignited, and total suspended particulate (TSP) emissions were collected onto prebaked quartz fiber filters in both flaming and smoldering conditions (Table B4). Samples were stored in aluminum foil at -20°C.

Table B4

Fireplace emissions collection details and carbon isotope analysis results. The uncertainty in all $\delta^{13}C_{TC}$ results is 0.2‰.

Sample Name	Sample Type	Burn Type	$\delta^{13}C_{TC}$ (‰)
A1	Firewood	Flame	-21.4
A2	Firewood	Smolder	-21.7
B1	Clean Flame compressed recycled paper log	Flame	-29.7
B2	Clean Flame compressed recycled paper log	Smolder	-29.5
C1	Duraflame Hearth Fire log	Flame	-27.5
D1	Duraflame log	Flame	-27.4

Aerosol samples collected during campaigns studying the health and environmental effects of biomass burning were analyzed. $PM_{2.5}$ of prescribed pile burns

was sampled in 2006 on the White Mountain Apache Tribe reservation in eastern Arizona (Robinson et al., 2008). $PM_{2.5}$ of prescribed pile burns and broadcast burns was sampled between 2001 and 2007 in the Coconino and Apache – Sitgreaves National Forests in northern Arizona (Robinson et al., 2011). $PM_{2.5}$ and TSP ambient air samples from a forest fire in Ft. Collins, CO were provided by Colorado State University (Table B5).

Table B5

Biomass burning sample details and carbon isotope analysis results. The uncertainty in all $\delta^{13}C_{TC}$ results is 0.2‰.

Sample Name	Sample Details	Reference	$\delta^{13}C_{TC}$ (‰)
2007QSm1B	Slash-Pile Prescribed Burn	Robinson et al., 2011	-25.4
2007Qlg1A	Slash-Pile Prescribed Burn	Robinson et al., 2011	-24.6
FC PM2.5 062502 GE	Slash-Pile Prescribed Burn	This Study	-23.9
FC TSP 062502 GE	Slash-Pile Prescribed Burn	This Study	-23.3
A31S2Q5	Broadcast Prescribed Burn	Robinson et al., 2011	-24.3
A32S1Q4	Broadcast Prescribed Burn	Robinson et al., 2011	-24.6
A33S1Q4	Broadcast Prescribed Burn	Robinson et al., 2011	-24.3
QS 1.2	Broadcast Prescribed Burn	Robinson et al., 2011	-24.4
QS 1.3	Broadcast Prescribed Burn	Robinson et al., 2011	-24.0
QS 1.4 110205	Broadcast Prescribed Burn	Robinson et al., 2011	-24.1
QS1A 042006	Pinyon Pine Wood Mock Burn	Robinson et al., 2011	-22.7
QS1B 042006	Ponderosa Pine Wood Mock Burn	Robinson et al., 2011	-24.9
QS1 102005	Kiwanis Pine Needles Mock Burn	Robinson et al., 2011	-25.8
Q402	Slash-Pile Prescribed Burn	Robinson et al., 2008	-24.3
Q301	Slash-Pile Prescribed Burn	Robinson et al., 2008	-24.3
Q202	Slash-Pile Prescribed Burn	Robinson et al., 2008	-23.0
Q101	Slash-Pile Prescribed Burn	Robinson et al., 2008	-24.2

Soil samples collected in 2009 and 2010 as part of the Desert Southwest Coarse Particulate Matter Study in Pinal County, AZ (Clements et al., 2014; Upadhyay et al., 2015) were analyzed. Agricultural soil, native soil, and unpaved dirt road dust from an

agricultural area collected in the spring, fall and winter were selected for analysis (Table B6); see references for further details on sample collection. The samples, which had been stored at -20°C, were heated at 100°C for 24h and were then gently compressed to break up large soil aggregates, taking care to avoid mechanical abrasion of small particles. The samples were added to a clean 1L vacuum flask, and HEPA-filtered air was blown over the sample to resuspend small particles. The particles passed through a size-selective cyclone (URG Corporation) at 28L/min (the operating flow rate for PM_{10} sampling) and collected onto three parallel prebaked 47mm quartz fiber filters (Upadhyay et al., 2015). Filters were stored in aluminum foil at -20°C.

Table B6

Resuspended soil (PM_{10}) sample details and carbon isotope analysis results. nss = available amount of sample not sufficient for analysis. The uncertainty in all $\delta_{13}C_{TC}$ results is 0.2‰.The uncertainty in all $\delta^{13}C_{CC}$ results is 0.3‰.

Sample Category	Season	$\delta^{13}C_{TC}$ (‰)	$\delta^{13}C_{CC}$ (‰)
Native	Spring	-15.8	-0.9
	Fall	-15.9	-1.7
	Winter	-16.7	-1.6
Agricultural	Spring	-13.4	-3.3
	Fall	-15.9	nss
	Winter	-14.7	nss
Unpaved Dirt Road Dust from an Agricultural Area	Spring	-5.0	-1.6
	Fall	-4.0	-0.6
	Winter	-4.7	0.0

All source materials collected onto quartz fiber filters were analyzed by thermal optical transmittance (TOT) for TC concentration using a Sunset Lab OC-EC Aerosol

Analyzer (Birch & Cary, 1996) using a variation of Sunset's "Quartz" TOT method. Variable time steps of 60-200 seconds were used during OC evolution, with temperature plateaus at 310°C, 475°C, 615°C, and 870°C. During EC evolution, the temperature was held at 550°C, 625°C, 700°C, 775°C, and 850°C for 45 seconds each, with a final hold at 870°C for 120 seconds. Quality control included the analysis of lab blanks, field blanks, replicate samples, and a sucrose standard, which was routinely within 10% of the known concentration.

Isotopic measurements for $\delta^{13}C_{VPDB}$ of TC in all source materials were performed using a Costech Elemental Analyzer coupled to a Thermo Delta Plus Advantage Isotope Ratio Mass Spectrometer (EA-IRMS). The analytical uncertainty of samples analyzed on this method is reported at 0.2‰, unless the standard deviation of replicate standards is greater than 0.2‰. NIST 2710 (Montana soil) was used as a linearity standard for burn samples and soil samples. NIST 1573a (tomato leaves) was used as a linearity standard for biogenic samples. Three in-house glycine standards were used to perform and verify a two-point calibration from -39.6‰ to 15.7‰.

Limits of Detection of n-Alkanes Analyzed by GC/MS

Table B7

Limits of detection of n*-alkanes.*

n -Alkane LOD (ng/m^3)	January						April					
	<0.49 µm	0.49µm - 0.95µm	0.95µm - 1.5µm	1.5µm - 3µm	3µm - 7.2µm	>7.2µm	<0.49 µm	0.49µm - 0.95µm	0.95µm - 1.5µm	1.5µm - 3µm	3µm - 7.2µm	>7.2µm
$C_{14}H_{30}$	0.004	0.0003	0.0004	0.0004	0.0007	0.001	0.004	0.0003	0.0005	0.0004	0.0001	0.0003
$C_{15}H_{32}$	0.003	0.0003	0.0003	0.0003	0.0006	0.0009	0.004	0.0002	0.0004	0.0003	0.0001	0.0003
$C_{16}H_{34}$	0.003	0.0002	0.0003	0.0003	0.0005	0.0009	0.003	0.0002	0.0004	0.0003	0.0001	0.0002
$C_{17}H_{36}$	0.003	0.0002	0.0003	0.0003	0.0005	0.0008	0.003	0.0002	0.0004	0.0003	0.0001	0.0002
$C_{18}H_{38}$	0.003	0.0002	0.0003	0.0003	0.0005	0.0008	0.003	0.0002	0.0004	0.0003	0.0001	0.0002
$C_{19}H_{40}$	0.002	0.0002	0.0002	0.0002	0.0004	0.0005	0.002	0.0001	0.0003	0.0002	0.00008	0.0002
$C_{20}H_{42}$	0.002	0.0002	0.0002	0.0002	0.0003	0.0005	0.002	0.0001	0.0003	0.0002	0.00008	0.0002
$C_{21}H_{44}$	0.002	0.0002	0.0002	0.0002	0.0003	0.0005	0.002	0.0001	0.0003	0.0002	0.00008	0.0002
$C_{22}H_{46}$	0.002	0.0002	0.0002	0.0002	0.0003	0.0005	0.002	0.0001	0.0003	0.0002	0.00008	0.0002
$C_{23}H_{48}$	0.002	0.0001	0.0002	0.0002	0.0003	0.0005	0.002	0.0001	0.0002	0.0002	0.00007	0.0001
$C_{24}H_{50}$	0.002	0.0001	0.0002	0.0002	0.0003	0.0005	0.002	0.0001	0.0002	0.0002	0.00007	0.0001
$C_{25}H_{52}$	0.002	0.0002	0.0002	0.0002	0.0003	0.0005	0.002	0.0001	0.0003	0.0002	0.00008	0.0002
$C_{26}H_{54}$	0.002	0.0002	0.0002	0.0002	0.0003	0.0005	0.002	0.0001	0.0002	0.0002	0.00007	0.0002
$C_{27}H_{56}$	0.002	0.0002	0.0002	0.0002	0.0004	0.0006	0.002	0.0001	0.0003	0.0002	0.00008	0.0002
$C_{28}H_{58}$	0.002	0.0001	0.0002	0.0002	0.0003	0.0005	0.001	0.00009	0.0002	0.0002	0.00006	0.0001
$C_{29}H_{60}$	0.002	0.0002	0.0002	0.0002	0.0003	0.0005	0.001	0.0001	0.0002	0.0002	0.00007	0.0001
$C_{30}H_{62}$	0.002	0.0002	0.0002	0.0002	0.0003	0.0005	0.002	0.0001	0.0002	0.0002	0.00007	0.0001
$C_{31}H_{64}$	0.002	0.0002	0.0002	0.0002	0.0003	0.0005	0.002	0.0001	0.0002	0.0002	0.00007	0.0001
$C_{32}H_{66}$	0.002	0.0002	0.0002	0.0002	0.0003	0.0005	0.002	0.0001	0.0002	0.0002	0.00007	0.0001
$C_{33}H_{68}$	0.002	0.0002	0.0002	0.0002	0.0003	0.0005	0.002	0.0001	0.0002	0.0002	0.00007	0.0001
$C_{34}H_{70}$	0.003	0.0004	0.0005	0.0007	0.001	0.002	0.003	0.0002	0.0004	0.0005	0.0002	0.0003
$C_{35}H_{72}$	0.003	0.0004	0.0005	0.0007	0.001	0.002	0.003	0.0002	0.0004	0.0005	0.0002	0.0003
$C_{36}H_{74}$	0.003	0.0004	0.0005	0.0007	0.001	0.002	0.003	0.0002	0.0004	0.0005	0.0002	0.0003
$C_{37}H_{76}$	0.004	0.0005	0.0006	0.0008	0.001	0.002	0.004	0.0003	0.0004	0.0006	0.0002	0.0004

Table B7 (continued)

Limits of detection of n-*alkanes.*

n -Alkane LOD (ng/m^3)	June						October					
	<0.49 µm	0.49µm - 0.95µm	0.95µm - 1.5µm	1.5µm - 3µm	3µm - 7.2µm	>7.2µm	<0.49 µm	0.49µm - 0.95µm	0.95µm - 1.5µm	1.5µm - 3µm	3µm - 7.2µm	>7.2µm
$C_{14}H_{30}$	0.002	0.0004	0.0003	0.0002	0.0003	0.0002	0.003	0.0003	0.0003	0.0003	0.0007	0.0006
$C_{15}H_{32}$	0.002	0.0004	0.0003	0.0002	0.0003	0.0002	0.003	0.0003	0.0002	0.0003	0.0006	0.0006
$C_{16}H_{34}$	0.002	0.0004	0.0003	0.0001	0.0003	0.0002	0.002	0.0003	0.0002	0.0003	0.0006	0.0005
$C_{17}H_{36}$	0.002	0.0003	0.0003	0.0001	0.0003	0.0002	0.002	0.0003	0.0002	0.0002	0.0006	0.0005
$C_{18}H_{38}$	0.002	0.0003	0.0003	0.0001	0.0002	0.0002	0.002	0.0002	0.0002	0.0002	0.0005	0.0005
$C_{19}H_{40}$	0.001	0.0003	0.0002	0.0001	0.0002	0.0001	0.002	0.0002	0.0001	0.0002	0.0003	0.0004
$C_{20}H_{42}$	0.001	0.0003	0.0002	0.0001	0.0002	0.0001	0.002	0.0002	0.0001	0.0002	0.0003	0.0004
$C_{21}H_{44}$	0.001	0.0002	0.0002	0.0001	0.0002	0.0001	0.002	0.0002	0.0001	0.0002	0.0003	0.0003
$C_{22}H_{46}$	0.001	0.0002	0.0002	0.00009	0.0002	0.0001	0.002	0.0002	0.0001	0.0002	0.0003	0.0003
$C_{23}H_{48}$	0.001	0.0002	0.0002	0.00008	0.0002	0.0001	0.001	0.0002	0.0001	0.0001	0.0003	0.0003
$C_{24}H_{50}$	0.001	0.0002	0.0002	0.00009	0.0002	0.0001	0.001	0.0002	0.0001	0.0002	0.0003	0.0003
$C_{25}H_{52}$	0.001	0.0002	0.0002	0.00009	0.0002	0.0001	0.002	0.0002	0.0001	0.0002	0.0003	0.0003
$C_{26}H_{54}$	0.001	0.0002	0.0002	0.00009	0.0002	0.0001	0.001	0.0002	0.0001	0.0002	0.0003	0.0003
$C_{27}H_{56}$	0.001	0.0003	0.0002	0.0001	0.0002	0.0001	0.002	0.0002	0.0001	0.0002	0.0003	0.0003
$C_{28}H_{58}$	0.001	0.0002	0.0001	0.00007	0.0001	0.0001	0.001	0.0001	0.0001	0.0001	0.0002	0.0002
$C_{29}H_{60}$	0.001	0.0002	0.0001	0.00007	0.0001	0.0001	0.001	0.0001	0.0001	0.0001	0.0002	0.0002
$C_{30}H_{62}$	0.001	0.0002	0.0001	0.00008	0.0001	0.0001	0.001	0.0001	0.0001	0.0001	0.0002	0.0003
$C_{31}H_{64}$	0.001	0.0002	0.0001	0.00008	0.0001	0.0001	0.001	0.0001	0.0001	0.0001	0.0002	0.0003
$C_{32}H_{66}$	0.001	0.0002	0.0001	0.00008	0.0001	0.0001	0.001	0.0001	0.0001	0.0001	0.0002	0.0003
$C_{33}H_{68}$	0.001	0.0002	0.0001	0.00008	0.0001	0.0001	0.001	0.0001	0.0001	0.0001	0.0002	0.0003
$C_{34}H_{70}$	0.002	0.0004	0.0003	0.0001	0.0002	0.0003	0.002	0.0002	0.0002	0.0002	0.0005	0.0005
$C_{35}H_{72}$	0.002	0.0004	0.0003	0.0001	0.0002	0.0003	0.002	0.0002	0.0002	0.0002	0.0005	0.0005
$C_{36}H_{74}$	0.002	0.0004	0.0003	0.0001	0.0002	0.0003	0.002	0.0002	0.0002	0.0002	0.0005	0.0005
$C_{37}H_{76}$	0.002	0.0004	0.0003	0.0002	0.0003	0.0003	0.003	0.0003	0.0002	0.0003	0.0005	0.0006

APPENDIX C

SAMPLING INFORMATION AND ANALYSIS RESULTS FOR PARTICULATE MATTER SAMPLES COLLECTED IN STRASBOURG AND GEISPOLSHEIM

Table C1

*Sampling details and analysis results for $PM_{2.5}$ samples collected in Strasbourg. $\delta^{13}C_{VPDB}$ results are for total carbon; the uncertainty for all values is 0.2‰. * = [TC] below the calibration curve and could not be isotopically characterized.*

					Air Mass Concentrations						
Sample ID	**Start Date/Time**	**End Date/Time**	**Sampling Time (h)**	**Air Volume (m^3)**	**OC ($\mu g/m^3$)**	**OC unc ($\mu g/m^3$)**	**EC ($\mu g/m^3$)**	**EC unc ($\mu g/m^3$)**	**TC ($\mu g/m^3$)**	**TC unc ($\mu g/m^3$)**	**$\delta^{13}C_{VPDB}$ (‰)**
Field Blanks:											
SA01	10/27/16 12:43 PM	10/27/16 12:44 PM	0.02	0.04	178.7	41.7	0.09	32.79	178.74	74.50	*
SA73	12/8/16 9:56 AM	12/8/16 9:57 AM	0.02	0.04	546.7	60.1	-0.06	32.78	546.67	92.90	*
SA87	12/15/16 12:07 PM	12/15/16 12:08 PM	0.02	0.04	160.1	40.8	0.79	32.82	160.84	73.61	*
Samples:											
SA02	10/27/16 12:56 PM	10/28/16 7:38 AM	18.7	43.0	4.8	0.3	0.87	0.07	5.7	0.3	-27.1
SA03	10/28/16 7:51 AM	10/28/16 10:51 AM	3.0	6.9	6.2	0.5	2.1	0.3	8.2	0.8	-27.6
SA04	10/28/16 11:08 AM	10/29/16 9:05 AM	21.9	50.5	4.9	0.3	0.86	0.07	5.7	0.3	-26.7
SA05	10/29/16 9:14 AM	10/30/16 4:30 AM	20.3	46.6	5.0	0.3	0.95	0.07	5.9	0.3	-26.8
SA06	10/30/16 4:46 AM	10/30/16 11:42 AM	6.9	15.9	4.3	0.3	1.1	0.1	5.3	0.4	-27.6
SA07	10/30/16 11:51 AM	10/31/16 7:43 AM	19.9	45.7	3.5	0.2	0.86	0.07	4.3	0.3	-26.6
SA08	10/31/16 7:53 AM	10/31/16 11:19 PM	15.4	35.5	4.2	0.2	0.86	0.08	5.0	0.3	-26.7
SA09	10/31/16 11:27 PM	11/1/16 7:33 AM	8.1	18.6	4.3	0.3	0.9	0.1	5.2	0.4	-27.1
SA10	11/1/16 8:43 AM	11/1/16 9:48 AM	1.1	2.5	7.9	0.9	0.00	0.50	8	1	*
SA11	11/1/16 9:58 AM	11/2/16 10:17 AM	24.3	55.9	5.4	0.3	0.82	0.06	6.3	0.4	-26.4
SA12	11/2/16 10:31 AM	11/3/16 8:52 AM	22.3	51.4	3.1	0.2	0.87	0.07	3.9	0.2	-27.0
SA13	11/3/16 9:02 AM	11/4/16 3:34 AM	18.5	42.6	5.6	0.3	1.3	0.1	6.9	0.4	-26.8
SA14	11/4/16 7:32 AM	11/5/16 9:34 AM	26.0	59.9	6.4	0.3	1.15	0.08	7.5	0.4	-26.6
SA15	11/5/16 9:47 AM	11/6/16 9:30 AM	23.7	54.5	3.0	0.2	0.55	0.05	3.5	0.2	-26.8
SA16	11/6/16 9:38 AM	11/7/16 12:01 PM	26.4	60.7	2.8	0.2	0.53	0.05	3.3	0.2	-26.5
SA17	11/7/16 12:12 PM	11/8/16 7:32 AM	19.3	44.5	3.6	0.2	0.73	0.06	4.4	0.3	-26.3
SA18	11/8/16 7:42 AM	11/9/16 11:49 AM	28.1	64.7	3.5	0.2	0.70	0.05	4.2	0.3	-26.6
SA19	11/9/16 11:58 AM	11/10/16 9:46 AM	21.8	50.1	1.3	0.1	0.34	0.04	1.6	0.1	-27.3
SA20	11/10/16 9:58 AM	11/11/16 7:21 AM	21.4	49.2	1.4	0.1	0.44	0.05	1.9	0.1	-27.2
SA21	11/11/16 7:33 AM	11/11/16 5:26 PM	9.9	22.7	1.5	0.1	0.32	0.07	1.8	0.2	-27.2
SA22	11/11/16 5:36 PM	11/12/16 7:32 AM	13.9	32.0	3.3	0.2	0.43	0.06	3.7	0.3	-26.5
SA23	11/12/16 7:43 AM	11/12/16 5:29 PM	9.8	22.5	4.9	0.3	0.77	0.09	5.7	0.4	-26.4
SA24	11/12/16 5:37 PM	11/13/16 7:06 AM	13.5	31.0	5.9	0.3	1.1	0.1	7.0	0.4	-26.2
SA25	11/13/16 7:18 AM	11/13/16 5:17 PM	10.0	23.0	6.0	0.4	0.78	0.09	6.8	0.5	-26.5
SA26	11/13/16 5:25 PM	11/14/16 7:04 AM	13.6	31.4	4.6	0.3	0.90	0.08	5.5	0.4	-25.9
SA27	11/14/16 7:12 AM	11/14/16 5:11 PM	10.0	23.0	4.6	0.3	0.75	0.09	5.4	0.4	-26.1
SA28	11/14/16 5:19 PM	11/15/16 7:10 AM	13.8	31.9	4.7	0.3	0.71	0.07	5.4	0.3	-26.2
SA29	11/15/16 7:20 AM	11/15/16 5:07 PM	9.8	22.5	5.2	0.3	0.77	0.09	6.0	0.4	-26.4
SA30	11/15/16 5:19 PM	11/16/16 7:14 AM	13.9	32.0	3.3	0.2	0.63	0.07	3.9	0.3	-26.4
SA31	11/16/16 7:31 AM	11/17/16 8:39 AM	25.1	57.8	1.7	0.1	0.47	0.04	2.2	0.1	-26.8
SA32	11/17/16 8:52 AM	11/18/16 9:12 AM	24.3	56.0	1.6	0.1	0.31	0.04	1.9	0.1	-26.6
SA33	11/18/16 9:24 AM	11/19/16 10:30 AM	25.1	57.7	1.3	0.1	0.28	0.03	1.6	0.1	-27.0
SA34	11/19/16 10:46 AM	11/19/16 8:14 PM	9.5	21.8	1.7	0.1	0.47	0.08	2.1	0.2	-26.9
SA35	11/19/16 8:25 PM	11/20/16 10:16 AM	13.8	31.9	3.0	0.2	0.49	0.06	3.5	0.2	-26.5
SA36	11/20/16 10:24 AM	11/20/16 8:23 PM	10.0	23.0	2.9	0.2	0.31	0.07	3.2	0.3	-26.6
SA37	11/20/16 8:31 PM	11/21/16 10:09 AM	13.6	31.4	4.5	0.3	0.84	0.08	5.3	0.3	-26.7
SA38	11/21/16 10:19 AM	11/21/16 8:24 PM	10.1	23.2	7.6	0.4	2.0	0.2	9.6	0.6	-26.6
SA39	11/21/16 8:33 PM	11/22/16 10:10 AM	13.6	31.3	7.2	0.4	2.2	0.1	9.5	0.5	-26.7

Table C1 (continued)

*Sampling details and analysis results for $PM_{2.5}$ samples collected in Strasbourg. $\delta^{13}C_{VPDB}$ results are for total carbon; the uncertainty for all values is 0.2‰. * = [TC] below the calibration curve and could not be isotopically characterized.*

Sample ID	Start Date/Time	End Date/Time	Sampling Time (h)	Air Volume (m^3)	Air Mass Concentrations						$\delta^{13}C_{VPDB}$ (‰)
					OC ($\mu g/m^3$)	OC unc ($\mu g/m^3$)	EC ($\mu g/m^3$)	EC unc ($\mu g/m^3$)	TC ($\mu g/m^3$)	TC unc ($\mu g/m^3$)	
SA40	11/22/16 10:20 AM	11/22/16 8:17 PM	9.9	22.9	9.0	0.5	2.3	0.2	11.3	0.7	-26.7
SA41	11/22/16 8:27 PM	11/23/16 10:09 AM	13.7	31.5	6.5	0.4	1.8	0.1	8.2	0.5	-26.9
SA42	11/23/16 10:17 AM	11/23/16 8:15 PM	10.0	22.9	7.8	0.4	2.7	0.2	10.5	0.6	-26.9
SA43	11/23/16 8:24 PM	11/24/16 10:15 AM	13.9	31.9	6.5	0.4	1.7	0.1	8.2	0.5	-26.6
SA44	11/24/16 10:26 AM	11/24/16 8:17 PM	9.8	22.7	4.7	0.3	1.2	0.1	5.8	0.4	-26.8
SA45	11/24/16 8:26 PM	11/25/16 10:06 AM	13.7	31.4	3.7	0.2	0.60	0.07	4.3	0.3	-26.4
SA46	11/25/16 10:16 AM	11/25/16 8:16 PM	10.0	23.0	4.3	0.3	0.61	0.09	4.9	0.4	-26.6
SA47	11/25/16 8:24 PM	11/26/16 10:10 AM	13.8	31.7	5.1	0.3	0.91	0.09	6.0	0.4	-26.3
SA48	11/26/16 10:18 AM	11/26/16 8:18 PM	10.0	23.0	6.0	0.4	1.5	0.1	7.5	0.5	-26.6
SA49	11/26/16 8:25 PM	11/27/16 10:09 AM	13.7	31.6	5.4	0.3	0.97	0.09	6.4	0.4	-26.3
SA50	11/27/16 10:19 AM	11/27/16 8:16 PM	10.0	22.9	4.5	0.3	0.58	0.08	5.1	0.4	-26.5
SA51	11/27/16 8:26 PM	11/28/16 10:00 AM	13.6	31.2	2.7	0.2	0.36	0.06	3.1	0.2	-26.9
SA52	11/28/16 10:09 AM	11/28/16 8:23 PM	10.2	23.5	2.7	0.2	0.35	0.07	3.1	0.3	-27.2
SA53	11/28/16 8:32 PM	11/29/16 10:07 AM	13.6	31.2	2.5	0.2	0.47	0.06	3.0	0.2	-26.8
SA54	11/29/16 10:14 AM	11/29/16 8:20 PM	10.1	23.2	4.1	0.3	0.9	0.1	5.0	0.4	-26.6
SA55	11/29/16 8:28 PM	11/30/16 10:02 AM	13.6	31.2	8.1	0.4	1.5	0.1	9.6	0.6	-26.5
SA56	11/30/16 10:10 AM	11/30/16 8:19 PM	10.2	23.3	9.4	0.5	2.1	0.2	11.5	0.7	-26.7
SA57	11/30/16 8:26 PM	12/1/16 10:03 AM	13.6	31.3	18	1	2.6	0.2	21	1	-26.5
SA58	12/1/16 10:11 AM	12/1/16 8:19 PM	10.1	23.3	8.8	0.5	1.5	0.1	10.3	0.6	-26.5
SA59	12/1/16 8:26 PM	12/2/16 10:04 AM	13.6	31.4	8.4	0.5	1.3	0.1	9.7	0.6	-26.6
SA60	12/2/16 10:12 AM	12/2/16 8:19 PM	10.1	23.3	10.3	0.6	2.1	0.2	12.4	0.7	-26.7
SA61	12/2/16 8:26 PM	12/3/16 7:54 AM	11.5	26.4	6.2	0.4	1.0	0.1	7.2	0.5	-26.7
SA62	12/3/16 8:02 AM	12/3/16 10:08 AM	2.1	4.8	3.5	0.4	1.0	0.3	4.5	0.7	*
SA63	12/3/16 10:15 AM	12/3/16 8:14 PM	10.0	23.0	4.0	0.3	0.56	0.08	4.6	0.3	-26.8
SA64	12/3/16 8:21 PM	12/4/16 9:31 AM	13.2	30.3	5.0	0.3	0.83	0.08	5.9	0.4	-26.4
SA65	12/4/16 9:38 AM	12/4/16 8:06 PM	10.5	24.1	5.8	0.3	0.84	0.09	6.7	0.4	-26.3
SA66	12/4/16 8:14 PM	12/5/16 4:45 AM	8.5	19.6	7.2	0.4	1.4	0.1	8.6	0.6	-26.2
SA67	12/5/16 4:52 AM	12/5/16 10:38 AM	5.8	13.3	10.3	0.6	1.9	0.2	12.2	0.8	-26.5
SA68	12/5/16 10:45 AM	12/6/16 10:13 AM	23.5	54.0	7.5	0.4	0.96	0.07	8.4	0.5	-26.7
SA69	12/6/16 10:27 AM	12/6/16 6:36 PM	8.2	18.7	7.2	0.4	1.2	0.1	8.4	0.6	-26.8
SA70	12/6/16 6:43 PM	12/7/16 10:37 AM	15.9	36.6	5.3	0.3	0.95	0.08	6.2	0.4	-26.7
SA71	12/7/16 10:45 AM	12/7/16 5:06 PM	6.4	14.6	7.7	0.5	1.2	0.1	9.0	0.6	-27.0
SA72	12/7/16 5:14 PM	12/8/16 9:47 AM	16.5	38.1	6.3	0.3	1.06	0.09	7.4	0.4	-26.8
SA74	12/8/16 10:03 AM	12/8/16 5:27 PM	7.4	17.0	11.4	0.6	2.2	0.2	13.6	0.8	-26.8
SA75	12/8/16 5:35 PM	12/9/16 9:41 AM	16.1	37.0	12.9	0.7	2.0	0.1	14.9	0.8	-26.7
SA76	12/9/16 9:50 AM	12/9/16 5:23 PM	7.6	17.4	10.0	0.6	2.6	0.2	12.7	0.8	-26.8
SA77	12/9/16 5:31 PM	12/10/16 9:40 AM	16.2	37.1	18.0	0.9	3.7	0.2	22	1	-26.7
SA78	12/10/16 9:49 AM	12/10/16 7:37 PM	9.8	22.5	10.7	0.6	2.2	0.2	12.9	0.8	-26.7
SA79	12/10/16 7:46 PM	12/11/16 9:55 AM	14.2	32.5	11.9	0.6	1.6	0.1	13.5	0.7	-26.4
SA80	12/11/16 10:08 AM	12/11/16 8:31 PM	10.4	23.9	5.9	0.3	1.1	0.1	7.1	0.5	-26.5
SA81	12/11/16 8:40 PM	12/12/16 9:27 AM	12.8	29.4	8.6	0.5	1.2	0.1	9.7	0.6	-26.3
SA82	12/12/16 9:36 AM	12/13/16 2:24 AM	16.8	38.6	7.1	0.4	1.5	0.1	8.7	0.5	-26.5
SA83	12/13/16 2:33 AM	12/13/16 10:19 AM	7.8	17.9	5.6	0.4	1.5	0.1	7.1	0.5	-26.8
SA84	12/13/16 10:25 AM	12/14/16 10:02 AM	23.6	54.3	7.5	0.4	1.20	0.08	8.7	0.5	-26.7
SA85	12/14/16 10:11 AM	12/15/16 1:29 AM	15.3	35.2	11.2	0.6	1.7	0.1	12.9	0.7	-26.6
SA86	12/15/16 1:36 AM	12/15/16 12:00 PM	10.4	23.9	8.3	0.5	2.0	0.2	10.4	0.6	-26.9

Table C2

Sampling details and analysis results for PM_{10} samples collected in Geispolsheim. $\delta^{13}C_{VPDB}$ results are for total carbon; the uncertainty for all values is 0.2‰.

Sample ID	Start Date/Time	End Date/Time	Sampling Time (h)	Air Volume (m^3)	Air Mass Concentrations						$\delta^{13}C_{VPDB}$ (‰)
					OC ($\mu g/m^3$)	OC unc ($\mu g/m^3$)	EC ($\mu g/m^3$)	EC unc ($\mu g/m^3$)	TC ($\mu g/m^3$)	TC unc ($\mu g/m^3$)	
GPM01	10/28/2016 18:30	10/28/2016 23:30	5.0	11.5	9.7	0.6	1.8	0.2	11.5	0.8	-26.6
GPM02	10/28/2016 23:30	10/29/2016 7:50	8.3	19.2	8.3	0.5	1.2	0.1	9.4	0.6	-26.5
GPM03	10/29/2016 10:30	10/30/2016 0:05	13.6	31.2	6.6	0.4	2.0	0.1	8.5	0.5	-26.5
GPM04	10/30/2016 0:05	10/30/2016 12:10	12.1	27.8	6.4	0.4	1.0	0.1	7.4	0.5	-26.6
GPM05	10/30/2016 12:10	10/31/2016 0:35	12.4	28.6	7.5	0.4	1.4	0.1	8.8	0.5	-26.3
GPM06	10/31/2016 0:35	10/31/2016 9:55	9.3	21.5	5.3	0.3	0.8	0.1	6.1	0.4	-26.3
GPM07	10/31/2016 9:55	10/31/2016 23:35	13.7	31.4	6.3	0.4	1.5	0.1	7.8	0.5	-26.3
GPM08	11/1/2016 0:00	11/1/2016 10:35	10.6	24.3	4.3	0.3	1.0	0.1	5.3	0.4	-27.3
GPM09	11/1/2016 12:00	11/2/2016 13:15	25.3	58.1	8.0	0.4	1.10	0.08	9.1	0.5	-26.2
GPM10	11/2/2016 13:15	11/3/2016 11:25	22.2	51.0	6.6	0.4	1.28	0.09	7.9	0.5	-26.1